European Commission

EU harmonised accelerated stress testing protocols for low-temperature water electrolyser

A proposal for assessing performance degradation in water electrolyser stacks

Malkow, T., Pilenga, A.

2024

Joint Research Centre

Contents

Abstract

This document proposes accelerated stress testing (AST) protocols for assessing the performance degradation of low-temperature water electrolyser (LTWE) stacks. Water electrolyser (WE) stacks generate bulk amount of clean hydrogen by the electrolysis of water using electricity mainly from renewable energy sources (RESs).

By applying these protocols, it is generally possible to evaluate the performance degradation of different stacks. It is then possible to adequately compare the three low-temperature water electrolysis (LTWEL) technologies, namely alkaline water electrolysis (AEL) in an alkaline water electrolyser (AWE), anion exchange membrane water electrolysis (AEMEL) in an anion exchange polymer membrane water electrolyser (AEMWE) and proton exchange membrane water electrolysis (PEMEL) in a proton exchange polymer membrane water electrolyser (PEMWE).

These protocols are to be used by the research community and industry alike. For example, to evaluate research and development (R&D) progress, set research and innovation (R&I) priorities with the inclusion of cost targets, development milestones, and technological benchmarks while also making informed decisions regarding technology selection.

Foreword

This report was prepared under the framework contract between the Directorate-General JRC of the European Commission (EC) and the Clean Hydrogen Joint Undertaking (Clean H_2 JU), the successor to the Fuel Cells and Hydrogen second Joint Undertaking (FCH2JU) [1]. The JRC contractual activities are stated in the strategic research and innovation agenda 2021-2027 of the Clean Hydrogen Partnership for Europe (SRIA) [2]. This report constitutes part two of the deliverable B.1 entitled "Report summarising the workshop findings on electrolyser lifetime degradation phenomena SoA and a preliminary proposal for setting up harmonised protocols for accelerated stress testing of low temperature electrolysers" of the Rolling Plan 2023 contained in the Clean H_2 JU work programme 2023 [3]. It is the result of a collaborative effort between partners from research and technology organisations (RTOs) in industry and academia participating to European Union (EU) funded R&D projects [4] in power-to-hydrogen (P-to-H_2) and hydrogen-to-industry (H_2-to-I) applications involving LTWE for demonstration and eventually, industrial deployment.

---

[1] According to Article 3(1)(c) of Council Regulation (EU) No 2021/2085 of 19/11/2021 (EU OJ L 427, 30.11.2021, p. 17), the Clean H_2 JU succeeds the FCH2JU as of 30 November 2021.

[2] See p. 103 at https://www.clean-hydrogen.europa.eu/about-us/key-documents/strategic-research-and-innovation-agenda_en

[3] See p. 163 at https://www.clean-hydrogen.europa.eu/about-us/key-documents/annual-work-programmes_en

[4] For a list of projects, see online at https://www.clean-hydrogen.europa.eu/projects-repository_en. More comprehensive information is searchable at the Community Research and Development Information Service (CORDIS) under https://cordis.europa.eu.

Acknowledgements

Note: Contributors are listed in alphabetical order according to the name of their participating organisation.

	Organisation	Contributor(s)
	accelera by Cummins	Sebastiaan Herregods
	Commissariat à l'énergie atomique et aux énergies alternatives	Julie Mougin Frédéric Fouda-Onana
	The Chemours Company	Patrick Redon
	Consiglio Nazionale delle Ricerche	Antonino Salvatore Aricò Stefania Siracusano
	Deutsches Zentrum für Luft- und Raumfahrt e. V.	Aldo Saul Gago Rodriguez

	Elogen SAS	Pierre Millet [a]
	Forschungszentrum Jülich GmbH	Felix Lohmann-Richters
	Fraunhofer Institut für Chemische Technologie	Felix Dittmar Carsten Cremers Julia Melke
	Fundación para el Desarrollo de las Tecnologías del Hidrógeno en Aragón	Lidia Martínez Izquierdo
	ITM Power plc	Daniel A Greenhalgh
	Johnson Matthey plc	Colleen Jackson Chris Zalitis
	ProPuls GmbH	Ulrich Wilhelm Rost
	Schaeffler AG	Peter Bouwman
	Shell Global Solutions International BV	Jeffrey (Jeff) B Martin
	Stiftelsen for industriell og teknisk forskning	Luis Colmenares-Rausseo
	Nederlandse Organisatie voor Toegepast Natuurwetenschappelijk Onderzoek	Johan Buurma Jordi Creus Casanovas Eduardo Da Rosa Silva
	Technische Universiteit Eindhoven	Matheus T (Thijs) de Groot
	Technische Universität Graz	Merit Bodner

104   [a]   co-affiliated to Université Paris-Saclay

1 Introduction

Water electrolyser (WE) stacks (**4.2.78**) ([13]) used in water electrolyser systems (WE systems) (**4.2.79**) are at the core of generating clean hydrogen (H_2) in bulk amounts in addition to oxygen (O_2) by the electrolysis (**4.2.35**) of water (H_2O) using fluctuating electricity particularly from sources of variable renewable energy (VRE). Most industrial WE systems (Figure 1.1) employing commercial WE stacks use low-temperature water electrolysis (LTWEL) technologies, namely alkaline water electrolysis (AEL) (**4.2.7**) in an alkaline water electrolyser (AWE) (**4.2.6**) and proton exchange membrane water electrolysis (PEMEL) (**4.2.63**) in a proton exchange polymer membrane water electrolyser (PEMWE) (**4.2.62**) (Chatenet *et al.*, 2022, Shih *et al.*, 2022).

Figure 1.1: Schematic of a WE system comprising one or more WE stacks (WE 1 to WE N), common balance of plant (BoP) and instrumentation & control devices including safety sensors and software.
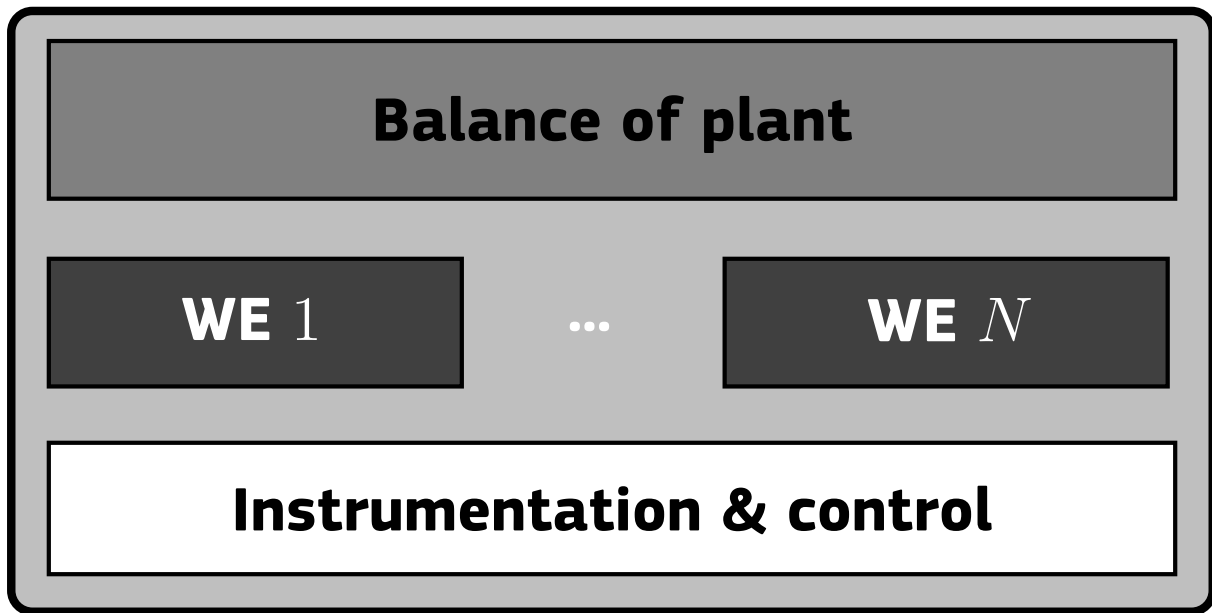
AWE have the advantage of being least reliant on the use of critical raw materials (CRM) (**4.2.21**). CRM are a serious concern for the European Union (EU) with regard to up-scaling and large-scale deployment of low-temperature water electrolyser (LTWE) technologies (Carrara *et al.*, 2023). PEMWE use CRM in catalysts (**4.2.15**), namely platinum (Pt) at the cathode (negative electrode) and platinum-group metals (PGM) (**4.2.60**) oxides such as iridium oxide (IrO_x) or iridium-ruthenium oxide (IrO_x-RuO_y) at the anode (positive electrode) to facilitate the water electrolysis (WEL) reactions in the electrodes of the proton exchange polymer membrane water electrolysis cells (PEMECs), see equation (3.1.4).

PEMWE have the benefits of high hydrogen output pressure and of more flexible operation especially relevant for delivering grid balancing services (Allidières *et al.*, 2019). Note, electricity grids (**4.2.29**) will exceedingly rely on balancing services in the future compared to the present situation with increasing use of diverse sources of VRE (solar, tidal, wave, wind, etc) in the grid.

Today, WE stacks using anion exchange membrane water electrolysis (AEMEL) (**4.2.10**) in an anion exchange polymer membrane water electrolyser (AEMWE) (**4.2.9**) are less common. AEMWE potentially combine the advantages of AEL and PEMEL (see Table 3.1) in a single device (Du *et al.*, 2022, Santoro *et al.*, 2022). In the future, they use de-mineralised liquid water (**4.2.24**) as in PEMWE while a current variant, namely an alkaline anion exchange polymer membrane water electrolyser (AAEMWE) uses dilute alkaline solution similar to AWE.

Commonly, the manufacturer of the WE system specifies the system boundaries while considering the BoP components (**4.2.12**) which form part of the system ([14]). Besides common hardware (piping, valves, actuators, sensors, wiring/cabling, etc), BoP usually consists of

---

([13]) This number refers to the term defined in section 4.2.

([14]) The immediate use of the hydrogen generated may require compression equipment (Sdanghi *et al.*, 2020, Durmuş *et al.*, 2021, Tahan, 2022, Marciuš *et al.*, 2022) as part of the BoP especially in power-to-gas (P-to-G) applications and in industrial processes requiring high pressure hydrogen. In applications of energy storage (ES) (**4.2.39**) including hydrogen-to-power (H_2-to-P) with hydrogen stored as compressed gaseous hydrogen (CGH_2) (**4.2.18**) in vessels or large (seasonal) underground storage facilities, compression equipment may be part of the BoP of a particular WE system (Ausfelder *et al.*, 2017). In power-to-mobility (P-to-M) applications with hydrogen stored either as CGH_2 or as liquid hydrogen (LH_2) (**4.2.46**) in vessels, liquefaction equipment may be part of the BoP of a particular WE system in the latter case.

- **electric power supply** (**4.2.30**) such as AC-to-DC (AC/DC) converter when grid-connected, or DC-to-DC (DC/DC) converter when directly coupled (off-grid) to one or another renewable energy source (RES) (**4.2.66**), for example, photovoltaic (PV) array (**4.2.58**) and/or wind turbine (**4.2.81**),

- **conditioning unit** including pumps, ion exchanger and heat exchanger for feeding de-mineralised water to PEMWE and AEMWE stack(s) and alkaline solution to AWE and AAEMWE stack(s) and

- **hydrogen purifier** (**4.2.42**) including liquid/gas separators, cooler(s), dryer(s) and de-oxidiser.

Where systems jointly use points of connection (PoCs) for electricity and/or fluid supply and for conveying exiting hydrogen and oxygen as part of a plant, the system boundary as the delineation between system interior and system exterior is to be defined by the manufacturer with the user's agreement.

Before their wider deployment in significantly large numbers and at scales ranging from a few hundred megawatts to several tens of gigawatt in capacity for use in ES and industrial applications across the EU and worldwide, stacks used in WE systems have to overcome a number of serious challenges (see section 3.4) by research and development (R&D) efforts and exceedingly, in real-world demonstrations accompanied with capital investment in the said LTWE technologies ([15]).

([15]) For EU policy measures taken, see, for example, at `https://energy.ec.europa.eu/topics/energy-systems-integration/hydrogen_en`.

2 Objective and scope of this document

The objective of this document is to propose accelerated stress testing (AST) (**4.2.2**) protocols (**4.2.3**) for establishing the performance degradation (**4.2.56**) of WE stacks used for generating bulk amounts of hydrogen by LTWEL at temperatures usually below 100 °C (373,15 K). Note, seawater electrolysis (Khan *et al.*, 2021), wastewater electrolysis (Cartaxo *et al.*, 2022) and bipolar polymer membrane water electrolysis (BPMEL) (Mayerhöfer *et al.*, 2020) are not considered herein ([16]). This also applies to hybrid redox flow batteries (HRFBs) where in addition to their use as ordinary redox flow batteries (RFBs), electrolysis to generate hydrogen is intended (Schmucker *et al.*, 2021).

WE stacks which can be rectangular, square or circular in geometry, use electricity preferably from least dispatchable sources of VRE. A WE stack used in a WE system can be deployed in various applications where hydrogen is used as an energy carrier (**4.2.37**) (fuel or commodity) among others in ES such as P-to-G, P-to-M (road, rail, maritime) and power-to-X (P-to-X) including power-to-chemical (P-to-C), power-to-liquid (P-to-L) and power-to-fuel (P-to-F), as well as for direct use as feedstock or reducing agent in hydrogen-to-industry (H_2-to-I) processes. By applying the AST protocols (section 6) along with a test plan (**4.2.76**) to execute a test programme in a test campaign, the performance degradation of WE stacks are established under given test conditions (section 6.3), for example,

- To evaluate R&D progress made,

- To set research and innovation (R&I) priorities for development milestones and technological benchmarks to improve technology and assess impact on cost and

- To make well-informed business decisions regarding the selection of a particular WE stack technology.

The test methods suggested are mainly those contained in standards of the International Organization for Standardization (ISO) and the International Electrotechnical Commission (IEC). Readers are advised to sufficiently familiarise with the referred standards and the test methods described or cited therein ([17]).

In addition, we also consider testing procedures previously developed as part of the EU water electrolysis harmonisation activities (Malkow *et al.*, 2018b, Malkow *et al.*, 2018a, Malkow and Pilenga, 2023a). Note, it is not intended to exclude any other suitable testing procedure or test method. The operation profiles (**4.2.51**) presented (section 6.8.2) serve as examples to establish the durability (**4.2.27**) of WE stacks by performing accelerated lifetime testing (ALT) (**4.2.1**) under reference test and operating conditions (section 6.4) as well as AST under stressing operating conditions (**4.2.70**) (section 6.5). They can be complemented by duty cycles, for example, to reflect realistic RES power generation profiles (section 6.8.2) for on-demand stack operation including the performance of services especially to balance variable loads of renewable energy (**4.2.65**) on the electricity grid known as balancing services ([18]).

The use of RES-derived power profiles for stack testing distinguish these test protocols (**4.2.72**) from those developed in EU-funded research projects (Enhanced performance and cost-effective materials for long-term operation of PEM water electrolysers coupled to renewable power sources (ELECTROHYPEM), Hydrogen meeting FUTURE needs of low carbon manufacturing value chains (H2FUTURE), High Performance PEM Electrolyzer for Cost-effective Grid Balancing Applications (HPEM2GAS), Next Generation PEM Electrolyser under New Extremes (NEPTUNE), Novel modular stack design for high pressure PEM water electrolyzer technology with wide operation range and reduced cost (PRETZEL), Cost-effective PROton Exchange MEmbrane WaTer Electrolyser for Efficient and Sustainable Power-to-H2 Technology (PROMETH2), Next Generation Alkaline Membrane Water Electrolysers with Improved Components and Materials (NEWELY) and Anion Exchange Membrane Electrolysis for Renewable Hydrogen Production on a Wide-Scale (ANIONE)) (Aricò *et al.*, 2013, Aricò *et al.*, 2016, Aricò *et al.*, 2018, Strataki, 2018, Stiber *et al.*, 2020, Fouda-Onana, 2020, Aricò *et al.*, 2020).

These protocols constitute testing guidance including mandatory requirements and agreed reference operating conditions for WE stacks to establish their performance degradation in a given power-to-hydrogen (P-to-H_2) application. They allow for sufficient flexibility when the test plan (section 6.6) of a scheduled test campaign is drawn up for a specific test programme addressing the use of the test item (**4.2.74**) in the target application. Thus, the test plan is to provide further details on

- test execution including

    - setting of test input parameters (TIPs) (**4.2.73**) with permissible variations,

---

([16])   Bipolar polymer membrane water electrolyser (BPMWE) composed of bipolar polymer membrane water electrolysis cells (BPMWECs) perform BPMEL without gas evolution at the AEM-PEM bipolar junction.

([17])   Standards, Technical Specification (TS) and Technical Reports (TRs) are not open access but they can be purchased from ISO and IEC directly or their constituting national committees (NCs).

([18])   Currently, working group (WG) 32 of ISO Technical Committee (TC) 197 prepares the approved working item (AWI) entitled "ISO 22734-2 Hydrogen generators using water electrolysis - Industrial, commercial, and residential applications - Part 2: Testing guidance for performing electricity grid service".

- test criteria for acceptance, failure and emergency stop, and
- operation profiles (section 6.8)

based on the stated purpose(s) and objective(s) of the tests and

- where necessary, provide more specific details on

  - test set-up (*e. g.* sensor positions, stack compression, etc) including specification and requirements of test equipments,
  - testing procedures including start-up and shut-down including emergency stop,
  - instrumentation, test and measurement methods (section 6.2),
  - data acquisition (DAQ) (**4.2.23**) and post-processing of test results including an agreed set of test output parameters (TOPs) (**4.2.75**).

Importantly, the application of these AST protocols to WE stacks does not require the specification of the type and characteristics of the tested stack. Also users may selectively execute tests that are suitable for the objective(s) and purpose(s) of their test campaign from among those described herein.

3 Overview of low-temperature water electrolysis technologies

3.1 WEL electrode reactions

The generation of one mole of gaseous hydrogen, $H_{2\,(g)}$ (subscript $_{(g)}$ denotes gaseous phase), along with half a mole of gaseous oxygen, $O_{2\,(g)}$, by the electrolysis of one mole of liquid water, $H_2O_{(l)}$ (subscript $_{(l)}$ denotes liquid phase), as shown in the overall reaction

$$H_2O_{(l)} \rightarrow \frac{1}{2}O_{2\,(g)} + H_{2\,(g)} \tag{3.1.1}$$

is performed in a water electrolyser. The three LTWEL technologies considered are

- **Alkaline water electrolysis**: Gaseous oxygen is formed by oxidising hydroxide ions (OH^-) in the aqueous phase (denoted by subscript $_{(aq)}$) of the alkaline solution, typically 20-40 wt-% KOH (potassium hydroxide or lye), as electrolyte (**4.2.36**) at the anode or oxygen electrode in the oxygen evolution reaction (OER):

$$\text{Anode: } 2\,OH^-_{(aq)} \xrightarrow{\text{OER}} \frac{1}{2}O_{2\,(g)} + H_2O_{(l)} + 2e^-_{(ed)} \tag{3.1.2a}$$
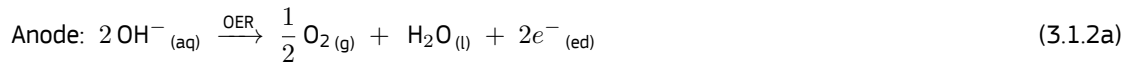
under an applied positive difference in potential (voltage) in excess of the open circuit potential (OCP) (U_{OCP}) sometimes called open circuit voltage (OCV) (U_{OCV}) resulting from the supplied direct current (DC) (I_{dc}). Simultaneously, at the cathode or hydrogen electrode, gaseous hydrogen is formed by reducing liquid water in the hydrogen evolution reaction (HER):

$$\text{Cathode: } 2\,H_2O_{(l)} + 2e^-_{(ed)} \xrightarrow{\text{HER}} H_{2\,(g)} + 2\,OH^-_{(aq)}. \tag{3.1.2b}$$
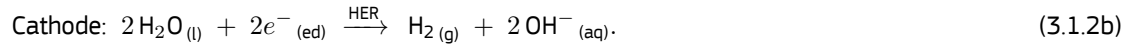
The electrons (e^-) are conducted via the electrodes (subscript $_{(ed)}$ denotes electrode) connected to an external circuit (DC power supply) entailing an ohmic resistance. The hydroxide ions diffuse along the potential-induced concentration gradient within the electrolyte of the alkaline water electrolysis cell (AEC) in the AWE stack from cathode to anode via a diaphragm.

- **Anion exchange membrane water electrolysis**: Gaseous oxygen is formed by oxidising hydroxide ions at the anode in the OER:
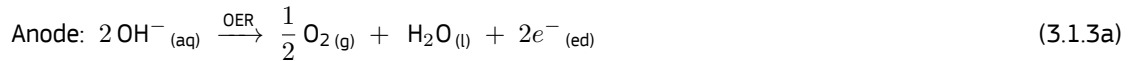
$$\text{Anode: } 2\,OH^-_{(aq)} \xrightarrow{\text{OER}} \frac{1}{2}O_{2\,(g)} + H_2O_{(l)} + 2e^-_{(ed)} \tag{3.1.3a}$$

under an applied potential in excess of OCV. Gaseous hydrogen is formed simultaneously by reducing liquid water at the cathode in the HER:
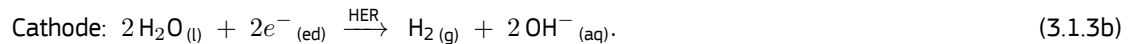
$$\text{Cathode: } 2\,H_2O_{(l)} + 2e^-_{(ed)} \xrightarrow{\text{HER}} H_{2\,(g)} + 2\,OH^-_{(aq)}. \tag{3.1.3b}$$

Whereas electrons are conducted via the electrodes connected to an external circuit, hydrated hydroxide ions are conducted by the vehicular mechanism (standard diffusion) and the Grotthuss (proton hopping) mechanism (Dong *et al.*, 2018, Chen *et al.*, 2016) through the anion exchange polymer membrane (AEM) electrolyte of the anion exchange polymer membrane water electrolysis cell (AEMEC) in the AEMWE stack. In the case of an alkaline anion exchange polymer membrane electrolysis cell (AAEMEC), water is substituted by a dilute lye solution. Note, the identical electrode reactions (3.1.2) and (3.1.3) proceed in different media, namely alkaline solution in AWE according to reactions (3.1.2) and liquid water in AEMWE according to reactions (3.1.3).

- **Proton exchange membrane water electrolysis**: Gaseous oxygen is formed by oxidising water at the anode in the OER:
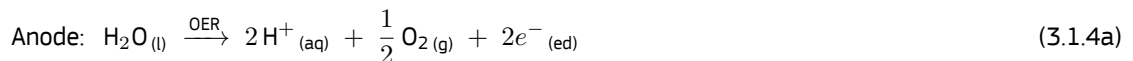
$$\text{Anode: } H_2O_{(l)} \xrightarrow{\text{OER}} 2\,H^+_{(aq)} + \frac{1}{2}O_{2\,(g)} + 2e^-_{(ed)} \tag{3.1.4a}$$

under an applied potential in excess of OCV. Gaseous hydrogen is formed simultaneously by reducing protons (H^+) at the cathode in the HER:

$$\text{Cathode: } 2\,H^+_{(aq)} + 2e^-_{(ed)} \xrightarrow{\text{HER}} H_{2\,(g)}. \tag{3.1.4b}$$

Whereas electrons are conducted via the electrodes connected to an external circuit, hydrated protons (H_3O^+) are conducted by the vehicular and Grotthuss mechanisms through the proton exchange polymer membrane (PEM) electrolyte of the PEMEC in the PEMWE stack. That is, water is also yielded on the cathode due to electro-osmosis (**4.2.31**).

3.2 Materials, operating conditions and technology readiness levels

Whereas AWEs with technology readiness level (TRL) 9 at the MW scale are mature as they benefit from many decades of operational experience in the chlor-alkali electrolysis process, PEMWEs with PEMECs as constituting units having TRL 8 to 9 at the kW to MW scale are most mature among the polymer membrane based WEs. The least mature with TRL 6 at the kW scale are AEMWEs using AEMECs as constituting units employing dilute alkaline solution. In the future, AEMWEs may be fed by pure water.

Most common in AWEs are Zirfon®, a porous composite made of zirconia-polysulfone coated open mesh polyphenylene sulfide (PPS) polymer fabric, as porous separator membrane, nickel (Ni) or Ni/Ni Fe alloys (on steel core) as anode and nickel or Ni alloy coated stainless steel as cathode. Current collectors (**4.2.22**) are made of nickel plates or Ni-coated steel. Typically, AWEs operate at temperatures between 60 to 90 °C (333,15 K to 363,15 K), current densities of between 0,2 A/cm^2 and 0,9 A/cm^2 and atmospheric pressure or pressures up to 30 bar (3 MPa) (Ehlers *et al.*, 2023, Brauns and Turek, 2020).

AEMWEs often use permeable fluorine-free hydrocarbon polymers as electrolyte membranes, non-PGM especially Co, Ni or Fe, their alloys and (mixed) oxides as anodes and Ni and its alloys as cathodes besides Pt. Typically, AEMWEs operate at temperatures between 40 to 80 °C (313,15 K to 353,15 K), current densities of between 0,5 A/cm^2 and 2 A/cm^2 and atmospheric pressure or at pressure from 8 to 35 bar (800 kPa to 3,5 MPa). The gas diffusion layer (GDL) (**4.2.40**) are made of carbon paper or cloth, titanium sheets, stainless steel felts or Ni foam (Miller *et al.*, 2020, Du *et al.*, 2022). They provide for electronic conductivity between the catalyst layer (CL) (**4.2.16**) and the bipolar plates (biPs) (**4.2.13**) and remove gaseous products (hydrogen and oxygen).

Most often, PEMWEs use perfluoro sulfonic acid (PFSA) (**4.2.54**) as electrolyte membrane, PGM oxides such as IrO$_x$ and IrO$_x$- RuO$_y$ as anode catalysts and PGM such as Pt as cathode catalyst. Typically, PEMWEs operate at temperatures between 50 to 90 °C (323,15 K to 363,15 K), current densities of 1 A/cm^2 to 4 A/cm^2 and atmospheric pressure or at differential pressures of up to 50 bar (5 MPa). Their biPs are made of titanium (Ti) or graphite (Kumar and Lim, 2023, Carmo *et al.*, 2013).

3.3 Stack operation modes

Under galvanostatic conditions, direct current provided to a WE stack results in a DC voltage (U_{dc}) across each cell. Adding the voltage of all series-connected water electrolysis cells (WECs) results in the stack voltage. Under potentiostatic conditions, a DC voltage applied to a WE stack results in a current flowing through the stack perpendicular to the active electrode area (A_{act}) (**4.2.5**) of all in-series WECs of the stack. DC electricity is in the form of electric energy (E_{el}):

$$E_{el} \ (\text{kWh}) \ = \ P_{el} \ (\text{kW}) \cdot t \ (\text{h}) \ \text{ where} \tag{3.3.1a}$$

P_{el} is electric power and t is the duration of applied electric power. Specifically, the electric power of a stack is DC power:

$$P_{el,dc} \ (\text{kW}) \ = \ U_{dc} \ (\text{kV}) \cdot I_{dc} \ (\text{A}). \tag{3.3.1b}$$

The electric power density of a stack ($P_{el,d,stack}$) is calculated as

$$P_{el,d,stack} \ (\text{kW/cm}^2) \ = \ U_{dc} \ (\text{kV}) \cdot J_{stack} \ (\text{A/cm}^2) \ \text{ where} \tag{3.3.1c}$$

$$J_{stack} \ (\text{A/cm}^2) \ = \ \frac{I_{dc} \ (\text{A})}{A_{act} \ (\text{cm}^2)} \tag{3.3.1d}$$

is the stack current density. Depending on temperature (T), the three operation modes of a WE stack are

- *Endothermic operation*: The water temperature decreases from input to output of the stack with its voltage below the thermal-neutral voltage ([19]) but above the reversible potential ([20]). Among the three modes of stack operation, this mode corresponds to the highest energy efficiency (η_e) (**4.2.38**) of the stack (section 6.7.13). But, it comes at the expense of a low hydrogen output rate (section 6.7.8). The heat required for the WEL reactions (3.1.2), (3.1.3) and (3.1.4) to proceed as desired stems under presumed adiabatic conditions from the supplied water rather than from Joule (ohmic) heating (**4.2.44**) due to an insufficient supply of electricity.

---

[19] At standard ambient pressure and standard ambient temperature (**4.2.69**) of liquid water (pH = 0), the thermal-neutral voltage (U_{tn}) is 1,481 V while this voltage is 1,473 V at 80 °C (353,15 K). However, the thermal-neutral voltage decreases with increasing temperature and higher pH value.

[20] At standard ambient pressure and standard ambient temperature of liquid water (pH = 0), the reversible potential (U_{rev}) is 1,229 V vs SHE while this potential is 1,184 V vs SHE at 80 °C (353,15 K). However, the reversible potential decreases with increasing temperature and higher pH value while it slightly increases with increasing pressure.

- *Isothermal (thermal-neutral) operation*: The water temperature is virtually the same at both input and output of the WE stack. The stack voltage is basically the thermal-neutral voltage. The additional heat required to sustain the equilibrium of the WEL reactions (3.1.2), (3.1.3) and (3.1.4) usually stems from Joule heating due to the externally supplied electricity required to establish the reversible potential.

- *Exothermic operation*: The water temperature increases from input to output of the WE stack with its voltage above the thermal-neutral voltage. As a result, heat is formed by Joule heating due to the supplied excess electricity. In this mode, the heat generated is more than that required to sustain the WEL reactions (3.1.2), (3.1.3) and (3.1.4). An advantage of this mode is that more supplied electricity means a higher hydrogen output. It comes at the expense of high overvoltages (overpotentials) (**4.2.52**) or voltage gains and an increase in performance degradation upon prolonged operation at high current densities (> 1 A/cm^2). Hence, voltage limits not exceeding 3,0 V for AEC, 2,0 V for AEMEC and 2,5 V for PEMEC are common (Kumar and Lim, 2022) to prevent excessive stack degradation. At WE system level, any recovered heat boosts the overall energy efficiency of the system.

3.4 Advantages, disadvantages and challenges

Table 3.1 lists common advantages, disadvantages and main challenges of the three LTWE technologies.

Table 3.1: Common advantages, disadvantages and main challenges of three major LTWEL technologies (AWE, AEMWE and PEMWE)

	AWE	AEMWE	PEMWE
Advantages	relatively high energy efficiency [a]	use of less expensive non-PGM catalyst [b]	high energy efficiency [c]
	use of less expensive non-PGM catalysts materials [d]	low water impurity sensitivity	fast response time including rapid start-up and shut-down [e]
		relatively low capital expenditure (CAPEX)	small footprint, compact, light-weight and simpler BoP
Disadvantages	use of corrosive alkaline electrolyte	limited response time	use of expensive cell materials [g]
	limited tolerance to lye impurities [f]	low ionic conductivity	limited tolerance to impurities [f]
	low current density, pressure and gas purity and limited operational flexibility		sensitive to feed water quality
		safety risk due to species (hydrogen and/or oxygen) crossover [h]	
Challenges	PTLs free of PGM coatings with integrated MPLs and catalysts operating at higher temperatures (enabling higher efficiencies)	AEM improvement in chemical and thermo-mechanical stability	reduction and eventual replacement of PGM oxide as catalysts [i] counteracting corrosion and low conductivity in passive layers on current collectors
	improvement of (micro-porous) membranes to reach higher ionic conductivities (enabling higher current densities) with better mechanical properties (enabling thinner membranes) and reduced gas crossover (enabling lower power operation without compromising safety)		substitution of fluoropolymers especially perfluoroalkyl and polyfluoroalkyl substances (PFAS) (**4.2.53**) by PEM with lower gas diffusivity [j]

Note: This table does not claim to present an exhaustive list of advantages and disadvantages.
[a] Typically, the energy efficiency of AWE stacks is 70-80 % (higher heating value (HHV)).
[b] for example, nickel or cobalt
[c] Typically, the energy efficiency of PEMWE stacks is above 70 % (HHV).
[d] Often, Ni and Ni alloys are used.
[e] Relevant to ensure rapid responses to fluctuating power from variable RES.
[f] Typically, these impurities are dissolved minerals and other contaminants.
[g] These include ion exchange membranes (IEMs) (**4.2.43**) as electrolyte, Pt-based catalysts at the cathode and iridium oxides based catalysts at the anode with high CAPEX.
[h] Crossover of hydrogen to the oxygen electrode and oxygen to the hydrogen electrode can lead to the formation of explosive atmospheres.
[i] Especially, IrO_x and IrO_x-RuO_y as OER catalysts in the anode and Pt as HER catalyst in the cathode.
[j] In PEMECs, the PEM electrolyte, ionomer, gaskets and sealants frequently use fluoropolymers.
Source: Joint Research Centre (JRC), 2023

The most mature among these three technologies is the AWE technology. AWEs are initially prime candidates for reliable hydrogen generation in bulk amounts. In the midterm, they will likely be increasingly replaced or complemented by more versatile PEMWEs. In the more distant future, less mature AEMWE technology could become the dominant LTWE technology. Often, AEMWEs are portrayed as beneficially uniting the advantages of AWEs and PEMWEs without necessarily sharing their drawbacks.

However, the two most demanding challenges encountered today by the three LTWE technologies are:

- Upon completion of the ongoing REACH restriction process ([21]), the possibility of a future ban by the EU on the use of PFAS-containing materials (EC, 2020b) in products placed on the single market ([22]) and

- Without realising high iridium (Ir) recycling rates, the scarcity of iridium on earth threatening the scale-up of PEMEL technology to the terrawatt-scale globally (Clapp *et al.*, 2023, Kibsgaard and Chorkendorff, 2019, Kiemel *et al.*, 2021).

As a result, some WEC materials used in stacks will inevitably be different to those used presently once these challenges are met progressively in the future ([23]). Ideally, this happens without changing too many key performance indicator (KPI) (**4.2.45**) targets. Also, the operating conditions of WE stacks and their mode(s) of operation may require adaptation since new WEC materials may have different properties and stack design could change. In addition, WEC materials and their morphologies integrated into WE stacks and interfaces within WE stacks may undergo iterative optimisation, including possible modifications in configuration and design suitable for high-throughput processing and mass manufacture of WE stacks.

Also, the generation and consumption patterns of electricity will change. Future electricity supply will be more variable as more and more RES installations of increasingly larger size are connected and their type and scale variety increases. Most probable, future smart grids (**4.2.68**) will exceedingly rely on autonomous distributed energy resources (DER) (**4.2.26**) managed by continuously improving artificial intelligence (AI)-based software. It includes automated on-demand deployment and disengaging of one or another WE system as part of a grid with fluctuating electricity.

Further, a WE system directly coupled to a large-scale RES installation as part of solar or wind energy farm will increasingly use AI-based supervisory control and data acquisition (SCADA) (**4.2.71**) software with predictive energy and weather forecasting and monitoring so that the supply of electricity to such a system or WE plant will not only be dependent on weather conditions and actual energy demand but also revenue considerations as regards the sale of renewable electricity versus clean hydrogen.

As a result, the mechanisms of material degradation in individual WECs (*e.g.* iridium dissolution and re-deposition, carbon catalyst support corrosion with agglomeration of platinum nano-particles, membrane thinning with fluoride release, and blocking of ion exchange sites by foreign cations in lye/liquid water feed) and thus of the performance degradation of WE stacks (*e.g.* passivation by titanium oxide formation on Ti-based PTL and biP) as currently known are likely to differ in their significance and extent. New degradation phenomena could emerge while degradation phenomena of little relevance today, could become more dominant.

Along with future material developments and stack optimisation, ongoing research into degradation phenomena of WEC materials and stack components and the mechanisms for their explanation will need to address the set-up of AST protocols for assessing the performance degradation of WE stacks in real-world applications dominated by fluctuating RES-derived electricity for the production of hydrogen. Developed AST protocols therefore need to consider the mentioned challenges and must provide for the necessary user flexibility.

([21]) See at https://echa.europa.eu/regulations/reach/restrictions/restriction-procedure

([22]) Due to risks (toxic and bio-accumulative effects) for human health, animals and the environment owing primarily to the strength of the carbon-fluorine (C-F) covalent bond in fluoropolymers, which makes them water-, oil- and grease-repellent and highly resistant to chemical and thermo-mechanical attacks, actions proposed by the European Commission (EC) aim at phasing out PFAS use in the EU unless proven essential for society (EC, 2020a); see also https://www.eea.europa.eu/publications/emerging-chemical-risks-in-europe and https://echa.europa.eu/hot-topics/perfluoroalkyl-chemicals-pfas. PFAS containing materials are also used in several BoPs components of WE systems, for example, in pumps, valves, cables, and electronics. In addition, fluoropolymers (PFAS membranes) are used in the electrolysis of potassium chloride (KCl) to create KOH, to be used in AEL technologies.

([23]) The manufacture and use of PFAS substitute materials in stacks may pose other challenges and could have risks to human health and the environment, too.

4 Terminology

4.1 General

Terms and definitions used in this document are given below and in two JRC EUR reports (Tsotridis and Pilenga, 2018, Malkow *et al.*, 2021). In addition, ISO and IEC maintain terminological databases at the following websites:

- ISO Online browsing platform available at `https://www.iso.org/obp`.

- IEC Electropedia available at `http://www.electropedia.org`.

The verbal forms used have the following meaning:

- "shall" indicates a requirement,

- "should" indicates a recommendation,

- "may" indicates a permission and

- "can" indicates a possibility or a capability.

Reference to Système International d'Unités (SI) coherent (derived) units includes, as appropriate, metric prefixes. Following clause 9.1 of ISO/IEC Directives, Part 2 (ISO and IEC, 2021), decimal fractions are denoted by comma. Alongside SI units, non-SI units may be used as customary. For example, we use degree Celsius (°C) as unit of temperature (T) alongside Kelvin (K) and kilo Watt hours (kWh) as unit of energy (E) instead of kilo Joule (kJ).

4.2 Terms and definitions

4.2.1 accelerated lifetime testing (ALT)
destructive testing of a test item (**4.2.74**) by subjecting it to aggravated conditions (*e. g.* current, pressure, temperature, voltage, etc) in excess of nominal conditions of real-life use, in an attempt to reveal likely faults and modes of failure in a short amount of time by increasing their frequency of occurrence, magnitude, duration, or any combination thereof and thereby, to assess the reliability of the item mainly for commercial purposes

Note 1 to entry: ALT may help to predict the remaining useful life and required maintenance intervals of the test item. It shall not alter the basic failure modes and mechanisms, or their relative prevalence.

4.2.2 accelerated stress testing (AST)
testing of a test item (**4.2.74**) by applying high levels of stress (*e. g.* current, pressure, temperature, voltage, etc) in excess of those under normal conditions of use to shorten the test duration in an attempt to trigger the same performance degradation mechanism(s) as would presumably occur for a longer exposure of the test item when tested under normal conditions of use mainly to advance the maturity of the test item

Note 1 to entry: AST is intentionally non-destructive and mainly for identifying potentially detrimental operating conditions and modes of operation as well as unsuitable designs and ineffective materials and components. It may also be performed to identify and to characterise performance degradation (**4.2.56**) and their mechanisms(s) occurring in the test item. Design of experiment (DoE) (**4.2.25**) along with physics-based modelling and post-mortem characterisation of the test item may help to gain insight into and to understand the relationship between the applied stress and performance degradation and their mechanism(s).

4.2.3 AST protocol
test protocol (**4.2.72**) specific for accelerated stress testing (**4.2.2**)

4.2.4 activation polarisation
part of the electrode polarisation (**4.2.33**) arising from a charge-transfer step of the electrode reaction

[*Source*: IEV 482-03-05]

4.2.5 active electrode area (A_{act})
geometric area of the electrode perpendicular to the direction of the current flow

[`Source`: IEV 485-02-08]

Note 1 to entry: Active electrode area is expressed in cm^2.

4.2.6 alkaline water electrolyser (AWE)
water electrolyser using alkaline solution as electrolyte (**4.2.36**)

[Source: JRC EUR 30324 EN report, term 680 (Malkow *et al.*, 2021)]

4.2.7 alkaline water electrolysis (AEL)
electrolyis (**4.2.35**) that employs an alkaline solution as electrolyte (**4.2.36**)

[Source: JRC EUR 30324 EN report, term 678 (Malkow *et al.*, 2021)]

4.2.8 anion exchange polymer membrane (AEM)
polymer based membrane with an anion conductivity, which acts as an electrolyte (**4.2.36**) and a separator
between anode and cathode

[Source: JRC EUR 30324 EN report, term 681 (Malkow *et al.*, 2021)]

4.2.9 anion exchange polymer membrane water electrolyser (AEMWE)
electrolyser (**4.2.34**) that employs a polymer with (hydroxide) ion exchange capability as the electrolyte
(**4.2.36**)

[Source: JRC EUR 30324 EN report, term 684 (Malkow *et al.*, 2021)]

4.2.10 anion exchange membrane water electrolysis (AEMEL)
electrolysis (**4.2.35**) that employs an anion exchange polymer membrane (**4.2.8**) as electrolyte (**4.2.36**)

[Source: JRC EUR 30324 EN report, term 682 (Malkow *et al.*, 2021)]

4.2.11 artificial intelligence (AI)
set of methods or automated entities that together build, optimize and apply a model so that the system
can, for a given set of predefined tasks, compute predictions, recommendations, or decisions

[Source: ISO/TR 6026:2022, 3.3 (ISO, 2022b)]

4.2.12 balance of plant (BoP)
supporting and auxiliary components, associated subsystems and structures based on the source of
electricity and site-specific requirements and integrated into a comprehensive water electrolyser system
(**4.2.79**) necessary to generate hydrogen

4.2.13 bipolar plate (biP)
conductive plate separating individual cells in a water electrolyser stack (**4.2.78**), acting as current collector
(**4.2.22**) and providing mechanical support for the electrodes

4.2.14 Bode plot
combined graphical representation of impedance modulus (absolute value) and phase angle (argument)
as functions of frequency on a logarithmic scale

Note 1 to entry: This plot is named after Hendrik Wade Bode (1905-1982).

4.2.15 catalyst
substance that accelerates an electrochemical reaction without being consumed itself

Note 1 to entry: The catalyst lowers the activation energy of the reaction, allowing for an increase
in the reaction rate.

[*Source*: IEV 485-01-01]

4.2.16 catalyst layer (CL)
porous region adjacent to either side of the electrolyte (**4.2.36**), containing the electro-catalyst, typically
with ionic and electronic conductivity

Note 1 to entry: The catalyst layer comprises the spatial region where the electrochemical reactions
take place.

[*Source*: IEV 485-02-06]

4.2.17 cold start
start-up when the test item (**4.2.74**) is at ambient temperature

4.2.18 compressed gaseous hydrogen (CGH$_2$)
gaseous hydrogen which has been compressed and stored for later use

4.2.19 compression factor (f_{compr})
positive multiplier of less than unity used to shorten the original duration of an operation profile (**4.2.51**)

4.2.20 concentration polarisation
part of the electrode polarisation (**4.2.33**) arising from concentration gradients of electrode reactants and products

[*Source*: IEV 482-03-08]

Note 1 to entry: Concentration polarisation is most relevant at high current densities. In water electrolysis cells, concentration polarisation can result in a non-proportional increase in voltage.

4.2.21 critical raw materials (CRM)
materials that, according to a defined classification methodology, are economically important and have a high-risk associated with their supply

[Source: ISO 14009:2020, 3.2.14 (ISO, 2020c)]

4.2.22 current collector
conductive material in a water electrolyser stack (**4.2.78**) that collects electrons from the anode side or conducts electrons to the cathode side

4.2.23 data acquisition (DAQ)
process of collecting and entering data

[Source: ISO 15143-1:2010, 3.1.4 (ISO, 2010a)]

4.2.24 de-mineralised water
water of which the mineral matter or salts have been removed by de-ionisation

[Source: ISO 23321:2019, 3.1 (ISO, 2019b)]

4.2.25 design of experiment (DoE)
systematic methodology for collecting information to guide improvement of any process

Note 1 to entry: Statistical models are developed to represent the process under analysis.
Note 2 to entry: Simulation tools and optimisation can be applied to test and confirm specific improvements.

[Source: ISO 13053-2:2011, 2.12 (ISO, 2011a)]

4.2.26 distributed energy resources (DER)
generators (with their auxiliaries, protection and connection equipment), including loads having a generating mode (such as electrical energy storage systems), connected to a low-voltage or a medium-voltage network

[Source: IEV 617-04-20]

4.2.27 durability
ability of a test item (**4.2.74**) to maintain its performance characteristics (**4.2.55**) as required, under given conditions of use and maintenance

4.2.28 durability test
test intended to verify whether or to evaluate to which degree a test item (**4.2.74**) is able to maintain its performance characteristics (**4.2.55**) over a period of use

4.2.29 electricity grid
public electricity network

[Source: ISO 52000-1:2017, 3.4.8 (ISO, 2017a)]

4.2.30 electric power supply
provision of electric energy from a source

[Source: IEV 151-13-75]

4.2.31 electro-osmosis
flow of water induced by a direct electric current applied across a membrane separating two electrolytes

[Source: IEV 891-02-84]

Note 1 to entry: The membrane can also be a diaphragm.

4.2.32 electrochemical cell
composite system in which the supplied electric energy mainly produces chemical reactions or, conversely, in which the energy released by chemical reactions is mainly delivered by the system as electric energy

[Source: IEV 114-03-01]

Note 1 to entry: In the first case, an electrochemical cell is also known as an electrolytic cell.

4.2.33 electrode polarisation
accumulation or depletion of electric charges at an electrode, resulting in a difference between the electrode potential with current flow, and the potential without current flow or equilibrium electrode potential

[*Source*: IEV 114-02-15]

4.2.34 electrolyser
device that performs electrolysis (**4.2.35**)

[Source: ISO/TR 15916:2015, 3.33 (ISO, 2015)]

4.2.35 electrolysis
method of separating and neutralising ions by an electric current in an electrolytic cell

[Source: IEV 114-04-09]

4.2.36 electrolyte
liquid or solid substance containing mobile ions that render it ionically conductive

[Source: IEV 485-03-01]

Note 1 to entry: The electrolyte is the main distinctive feature of the different LTWEL technologies.

4.2.37 energy carrier
substance or phenomenon that can be used to produce mechanical work or heat or to operate chemical or physical processes

[Source: ISO 52000-1:2017, 3.4.9 (ISO, 2017a)]

4.2.38 energy efficiency (η_e)
ratio of useful energy output to the total energy input including all parasitic and auxiliary energy needed to operate the system

Note 1 to entry: Energy efficiency is expressed in % on the basis either of lower heating value (LHV) or higher heating value (HHV) which should be stated.

4.2.39 energy storage (ES)
action or method used to accumulate, retain and release energy for later use in an energy using system

[Source: ISO/IEC 13273-1:2015, 3.1.5 (ISO and IEC, 2015a)]

4.2.40 gas diffusion layer (GDL)

porous substrate placed between the catalyst layer (**4.2.16**) and the bipolar plate (**4.2.13**) to serve as an electric contact and allow the access of reactants to the catalyst layer and the removal of reaction products

[Source: IEV 485-04-05]

4.2.41 hot start

start-up when the item test (**4.2.74**) is within its normal operating temperature range

4.2.42 hydrogen purifier

equipment to remove undesired constituents from the hydrogen

Note 1 to entry: Hydrogen purifiers can comprise purification vessels, dryers, filters and separators.

[Source: ISO 19880-1:2020, 3.41 (ISO, 2020d)]

4.2.43 ion exchange membrane (IEM)

polymer sheet that contain negatively or positively charged functional groups in its polymer matrix designed to conduct cations or anions while blocking opposite charged ions

[Source: ISO 20468-6:2021, 3.1.18 (ISO, 2021a)]

4.2.44 Joule heating (ohmic heating)

heating caused by an electric current through a resistive material

[*Source*: IEV 815-15-41]

Note 1 to entry: It is named after James Prescott Joule (1818-1889).

4.2.45 key performance indicator (KPI)

quantifiable level of achieving a critical objective

Note 1 to entry: The KPIs are derived directly from, or through an aggregation function of, physical measurements, data and/or other KPIs.

[Source: ISO 22400-1:2014, 2.1.5 (ISO, 2014)]

4.2.46 liquid hydrogen (LH$_2$)

hydrogen that has been liquefied, i.e. brought to a liquid state

[Source: ISO 13984:1999, 3.4 (ISO, 1999)]

4.2.47 machine learning (ML)

process using algorithms rather than procedural coding that enables learning from existing data in order to predict future outcomes

[Source: ISO/TR 22100-5:2021, 3.2 (ISO, 2021b)]

4.2.48 Nyquist plot

graphical representation of the real component of impedance versus the negative of the imaginary component of impedance in rectangular coordinates

Note 1 to entry: This plot is named after Harry Nyquist (1889-1976).

4.2.49 ohmic polarisation

polarisation caused by the resistance to the flow of ions in the electrolyte (**4.2.36**) and of electrons in the electrodes, bipolar plates (**4.2.13**), and current collectors (**4.2.22**)

Note 1 to entry: The term "ohmic" refers to the fact that the voltage drop follows Ohm's law proportional to the current with an ohmic resistance (called "internal resistance" of the cell) as the proportionality constant.

[*Source*: IEV 485-15-03]

4.2.50 operating (working) point
point on a characteristic performance curve representing the values of variable quantities at which usual operation is expected and optimum efficiency is desired

Note 1 to entry: Characteristic performance curves of a water electrolyser stack (**4.2.78**) are direct current-DC voltage curves and energy efficiency(electrical efficiency)-electric power curves.

4.2.51 operation profile
curve representing electric power, current or voltage against time used to illustrate the variance in electric power, current or voltage during a given time interval

4.2.52 overvoltage (overpotential)
voltage difference between the measured electrode potential and the equilibrium potential

[*Source*: ISO 8044:2020, 7.1.30 (ISO, 2020a)]

Note 1 to entry: In WE stacks, overvoltage relates to a given current density under specified conditions.

4.2.53 perfluoroalkyl and polyfluoroalkyl substances (PFAS)
commonly used international abbreviation for organic compounds with replacement of most or all hydrogen atoms by fluorine in the aliphatic chain structure

Note 1 to entry: The term is used in the broader sense for per- and polyfluoroalkyl substances (PFAS), and per- and polyfluorinated compounds (PFC) as well.

[*Source*: ISO 21675:2019, 3.1 (ISO, 2019c)]

4.2.54 perfluoro sulfonic acid (PFSA)
chemical compounds of the formula $C_nF_{(2n+1)}SO_3H$ and thus belong to the family of perfluorinated and polyfluorinated alkyl compounds

4.2.55 performance characteristics
characteristics defining the ability of a test item (**4.2.74**) to operate as intended under given conditions of use and maintenance

4.2.56 performance degradation
process leading to a significant change in the performance of the test item (**4.2.74**), typically characterised by a change of properties, whether reversible or irreversible, or by a decay affected by environmental and test conditions, proceeding over a period of time and comprising one or several steps that effect the test item (**4.2.74**) to operate as intended, under given conditions of use

4.2.57 performance test
test intended to verify whether or to evaluate to which degree a test item (**4.2.74**) is able to accomplish its performance characteristics (**4.2.55**)

4.2.58 photovoltaic (PV) array
two or more photovoltaic modules at one location that together provide a photovoltaic solar energy system

[*Source*: ISO 6707-3:2022, 3.3.7 (ISO, 2022a)]

4.2.59 photovoltaic (PV) power
technology that turns sunlight directly into electricity

[*Source*: ISO/IEC TR 15067-3-8:2020, 3.19 (ISO, 2020e)]

4.2.60 platinum-group metals (PGM)
group of six noble, precious metallic elements (ruthenium, rhodium, palladium, osmium, iridium, and platinum) clustered together in the periodic table

Note 1 to entry: These transition metals are located in the d-block of the periodic table. They have similar physical and chemical properties.

4.2.61 proton exchange polymer membrane (PEM)
polymer based membrane with cation (proton) conductivity which acts as an electrolyte (**4.2.36**) and a separator between anode and cathode

Note 1 to entry: PEM is a cation exchange membrane exclusively in the acidic H^+ form.

[Source: JRC EUR 30324 EN report, term 695 (Malkow *et al.*, 2021)]

4.2.62 proton exchange membrane water electrolysis (PEMEL)
electrolyser that employs a polymer with (proton) ion exchange capability as the electrolyte (**4.2.36**)

[Source: IEC 62282-8-102:2019, 3.1.26 (IEC, 2019b)]

4.2.63 proton exchange membrane water electrolysis (PEMEL)
electrolysis (**4.2.35**) that employs a proton exchange polymer membrane (**4.2.61**) as electrolyte (**4.2.36**)

[Source: JRC EUR 30324 EN report, term 696 (Malkow *et al.*, 2021)]

4.2.64 principle of superposition
principle that the time response to the sum of several input variables is the same as the sum of the time responses caused by the individual input variables

Note 1 to entry: The principle of superposition includes the special case, that at multiplication of an input variable by a constant factor the accompanying time response is multiplied by the same factor (often called "principle of amplification").

[Source: IEV 351-45-01]

Note 2 to entry: In electrochemical impedance spectroscopy (EIS) measurements, input variables are current and voltage under galvanostatic conditions and potentiostatic conditions, respectively. Under these conditions, the time responses are the resulting voltage and current.

Note 3 to entry: This principle is attributed to Ludwig Boltzmann (1844-1906) and John Hopkinson (1849-1898).

4.2.65 renewable energy
energy obtained from a renewable energy source (**4.2.66**)

[Source: ISO/IEC 13273-2:2015, 3.1.6 (ISO and IEC, 2015b)]

4.2.66 renewable energy source (RES)
energy source not depleted by extraction as it is naturally replenished at a rate faster than it is extracted

[Source: ISO/IEC 30134-3:2016, 3.1.4 (ISO, 2016a)]

4.2.67 reverse current
flow of induced current in a commissioned AWE (**4.2.6**) stack during OCV operation (zero supply current) given the electrical connections of a closed circuit made of the bipolar plates (**4.2.13**) with electronic conduction and ionic conduction of the electrolyte (lye) solution in the manifolds of the stack

4.2.68 smart grid
electric power system that utilises information exchange and control technologies, distributed computing and associated sensors and actuators for purposes such as:

- to integrate the behaviour and actions of the network users and other stakeholders,
- to efficiently deliver sustainable, economic and secure electricity supplies

[Source: IEV 617-04-13]

Note 1 to entry: Smart grids enable enhanced and automated monitoring and control of electricity generation, transmission and distribution for added availability, reliability, efficiency, and cost-effective operations.

4.2.69 standard ambient temperature and pressure (SATP) conditions
conditions of standard ambient pressure (p^0 = 100 kPa) and standard ambient temperature (T^0 = 298,15 K)

4.2.70 stressing operating conditions

operating conditions intentionally in excess of normal operating conditions exerted onto a test item (**4.2.74**) which are likely to cause performance degradation (**4.2.56**) of the item during its operation

4.2.71 supervisory control and data acquisition (SCADA)

process control system generally used to control dispersed assets using centralised data acquisition (**4.2.23**) and supervisory controls

[*Source*: ISO/IEC 27019:2017, 3.15 (ISO and IEC, 2017)]

Note 1 to entry: Systems operate with coded signals over communication channels with remote equipment to acquire information about the status for display or recording functions and accessing process control set points and current and historical online data.

4.2.72 test protocol

list of the steps to be followed in the test

[*Source*: ISO/IEC/IEEE 26513:2017, 3.141 (ISO *et al.*, 2017)]

Note 1 to entry: Typically, test protocols describe the specific testing including TIPs (**4.2.73**) to be set, monitored and reported in accordance with a test plan (**4.2.76**) which details their actual values and TOPs (**4.2.75**) to be measured or calculated, analysed and reported as well as test cases and test profiles to be executed employing test and measurement methods.

4.2.73 test input parameter (TIP)

parameter whose values can be set in order to define the test conditions of the test system including the operating conditions of the test object

Note 1 to entry: TIPs have to be controllable and measurable. Values of TIPs are known before conducting the test. TIPs can be either static or variable. Static TIPs stay constant and variable TIPs are varied during the test.

[*Source*: IEC 62282-8-101, 3.1.33 (IEC, 2020c)]

4.2.74 test item

electrolyser (**4.2.34**) stack of type AWE (**4.2.6**), AEMWE (**4.2.9**) including AAEMWE, or PEMWE (**4.2.62**)

4.2.75 test output parameter (TOP)

parameter that indicates the response of the test system/test object as a result of variation of test input parameters (**4.2.73**)

[*Source*: IEC 62282-8-101, 3.1.34 (IEC, 2020c)]

Note 1 to entry: Values of TOPs are unknown before conducting the test and are measured during the test or calculated subsequently.

4.2.76 test plan

planning document detailing the principles, test methods, conditions, procedures and data quality required to carry out testing and to produce test data

[*Source*: ISO 14050:2020, 3.4.19 (ISO, 2020b)]

Note 1 to entry: The test plan outlines the objective(s), purpose(s), requirements and strategy for testing including the type of test(s), descriptions of test environments and conditions including TIP (**4.2.73**) set point values, responsibility for the testing, the equipment and instrumentation for use in the testing as well as the process for performing (work flow of testing) and documenting the test(s) (recording, analysing and reporting of test results) and for handling test failure(s).

4.2.77 uncertainty

parameter, associated with the result of a measurement, that characterises the dispersion of the values that could reasonably be attributed to the measurand

[*Source*: International Electrotechnical Vocabulary (IEV) 415-05-13]

4.2.78 water electrolyser (WE) stack

assembly of two or more electrochemical cells (**4.2.32**), separators, manifolds and a supporting structure using DC electricity to generate hydrogen and heat by the electrolysis (**4.2.35**) of liquid water

Note 1 to entry: Alkaline water electrolyser (**4.2.6**) stacks and alkaline anion exchange polymer membrane water electrolyser stacks employ alkaline solution rather than liquid water.

4.2.79 water electrolyser (WE) system

assembly of interrelated components of defined configuration with one or more water electrolyser stacks (**4.2.78**) at its core, which delivers hydrogen

Note 1 to entry: A water electrolyser system can include components such as power supply terminals, fluid connectors, compressors, storage vessels, piping, valves, pressure-relief devices, pumps, expansion joints, gauges, cabling, and control, monitoring and safety subsystems including communication interfaces.
Note 2 to entry: A water electrolyser system can refer to a site, a facility at a site, or an installation at a facility. A water electrolyser plant may contain multiple water electrolyser systems.

4.2.80 wind power

use of wind to provide mechanical power through wind turbines (**4.2.81**) to turn electric generators

[*Source*: ISO 6707-3:2022, 3.6.19 (ISO, 2022a)]

4.2.81 wind turbine (WT)

device that converts kinetic energy from the wind into electricity

[*Source*: ISO 6707-3:2022, 3.2.5 (ISO, 2022a)]

4.3   Abbreviations and acronyms used

A list of abbreviations and acronyms used in this report is appended, see page 65.

4.4   Symbols used

A list of symbols used in this report is appended, see page 69.

5 Description of test items

5.1 AWE stack

Figure 5.1 shows schematically the input and output streams of energy forms and substances of an AWE stack.

Figure 5.1: Schematic of the input and output streams (directional arrows) of energy forms (diamond shape) and substances (circular shape) of an AWE stack (rectangular shape); q and p represent flow rate and pressure, respectively. The thick line around the grey-shaded box denotes the stack boundary. The use of the grey colour indicates streams of secondary relevance in the context of accelerated stress testing.
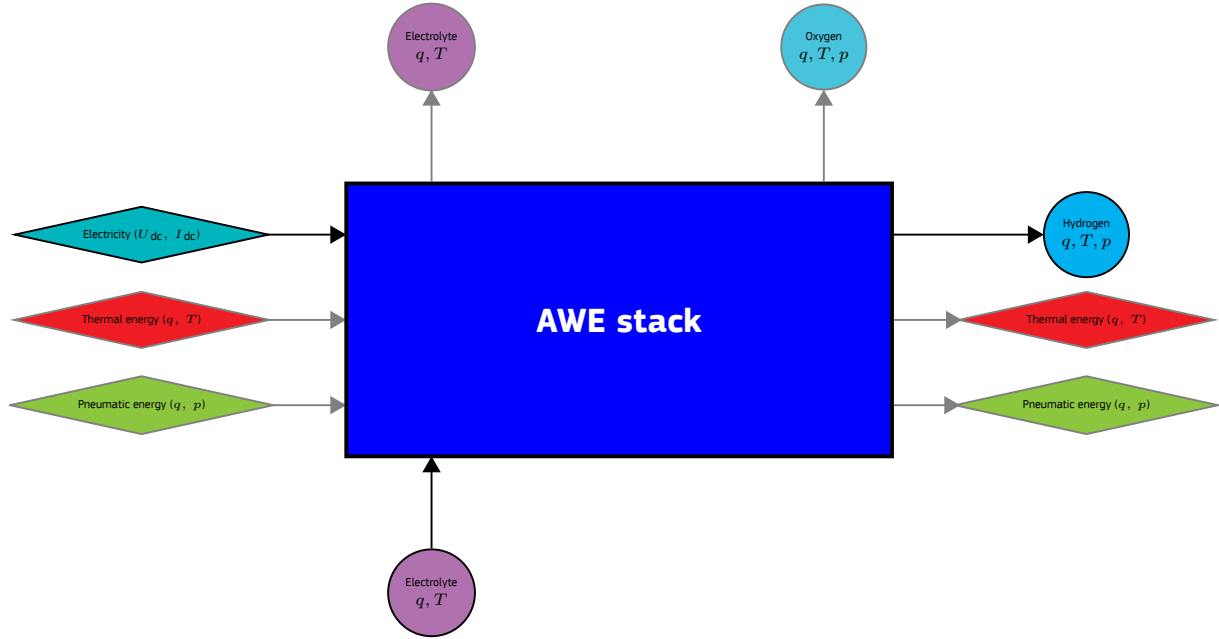
At its PoCs (current/voltage terminals and fluid inlets), the input energy streams to an AWE stack are

- **Electricity** in the form of electric energy, see equation (3.3.1a), by supplying DC power, see equation (3.3.1b),

- **Thermal energy** (E_{th}), if any, in the form of heat/cold:

$$E_{th} \text{ (kWh)} = P_{th} \text{ (kW)} \cdot t \text{ (h)} \text{ where} \tag{5.1.1a}$$

P_{th} is thermal power given by equation (5.1.1b) and t is the duration of heat/cold supply.

$$P_{th} \text{ (kW)} = \sum_i q_m^i \text{ (kg/s)} \cdot c_p^i \text{ (kJ/(kg K))} \cdot (T^i \text{ (K)} - T^0 \text{ (K))}; \tag{5.1.1b}$$

q_m^i, c_p^i and T^i are mass flow rate, specific heat capacity at constant pressure and temperature of fluid i, respectively. On input, the heat transfer fluid i (input substance stream) is the aqueous electrolyte.

- **Pneumatic energy** (E_{compr}) is only relevant for pressurised stacks:

$$E_{compr} \text{ (kWh)} = P_{compr} \text{ (kW)} \cdot t \text{ (h)} \text{ where} \tag{5.1.2a}$$

P_{compr} is the power of compression given by equation (5.1.2b) and t is the duration of pressurised stack operation.

$$P_{compr} \text{ (kW)} = \sum_j \left(\frac{\gamma^j}{\gamma^j - 1} \right) \frac{\bar{Z}^j \cdot R_g \text{ (kJ/(mol K))} \cdot T^0 \text{ (K)} \cdot q_n^j \text{ (mol/h)}}{3600 \text{ (s/h)}} \left(\left(\frac{p^j \text{ (kPa)}}{p^0 \text{ (kPa)}} \right)^{\frac{\gamma^j - 1}{\gamma^j}} - 1 \right); \tag{5.1.2b}$$

22

R_g, $\bar{Z}^j$, q_n^j and p^j are universal gas constant, average compressibility factor, molar flow rate and pressure of fluid j, respectively. The isentropic expansion factor of fluid j is calculated as follows

$$\gamma^j \;=\; \frac{c_p^j \;(\text{kJ/(kg K)})}{c_V^j \;(\text{kJ/(kg K)})}; \tag{5.1.2c}$$

c_p^j and c_V^j are specific heat capacity at constant pressure and constant volume of fluid j, respectively. For a pressurised stack, the pneumatic fluids j (output substance streams) are hydrogen and oxygen.

At fluid outlets, the output energy and substance streams from an AWE stack are

- Thermal energy carried by heat transfer fluids:
    - aqueous electrolyte,
    - hydrogen and
    - oxygen,
- Pneumatic energy carried by compressible fluids:
    - hydrogen and
    - oxygen,
- Hydrogen at the cathode and
- Oxygen and water at the anode.

5.2   AEMWE stack

Figure 5.2 shows schematically the input and output streams of energy forms and substances of an AEMWE stack.

Figure 5.2: Schematic of the input and output streams (directional arrows) of energy forms (diamond shape) and substances (circular shape) of an AEMWE stack (rectangular shape). The thick line around the grey-shaded box denotes the stack boundary. The use of the grey colour indicates streams of secondary relevance in the context of accelerated stress testing.
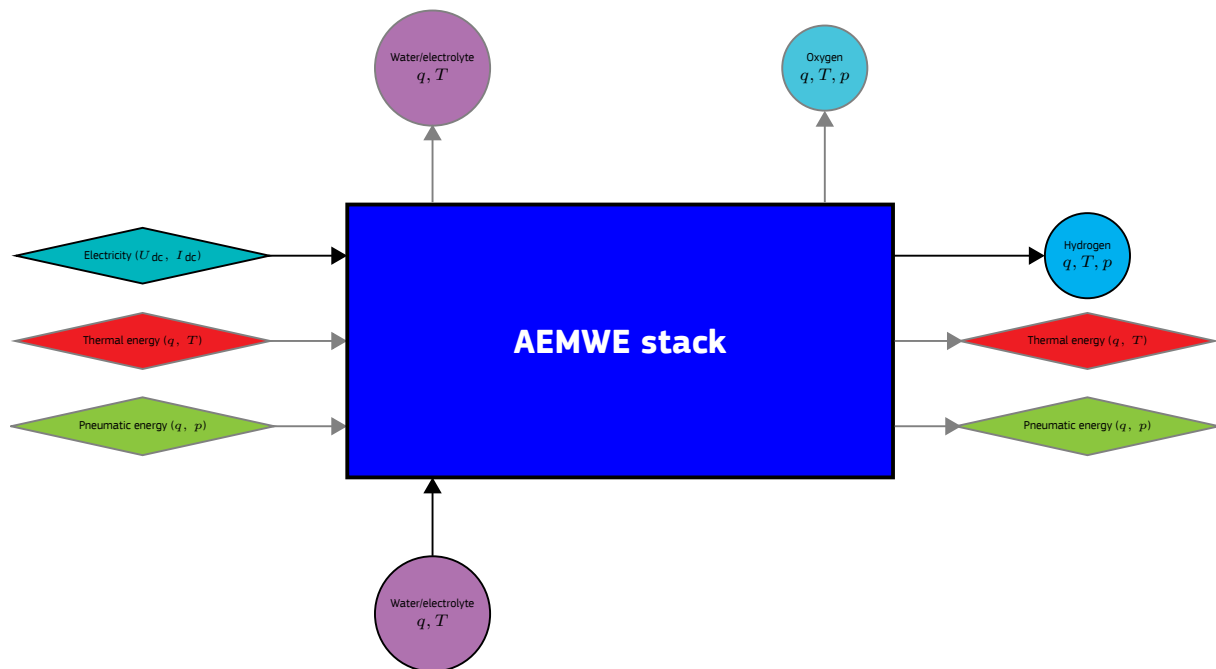
Source: JRC, 2023.

At its PoCs (current/voltage terminals and fluid inlets), the input energy streams to an AEMWE stack are

- **Electricity** in the form of electric energy, see equation (3.3.1a), by supplying DC power, see equation (3.3.1b),

- **Thermal energy**, see equation (5.1.1a), if any, in the form of heat/cold where on input the heat transfer fluid i (input substance stream) is liquid water for AEMECs and aqueous electrolyte for AAEMECs.

- **Pneumatic energy**, see equation (5.1.2a), which is only relevant for pressurised stacks where the pneumatic fluids j (output substance streams) are hydrogen and oxygen.

At fluid outlets, the output energy and substance streams from an AEMWE stack are

- Thermal energy carried by heat transfer fluids:
    - liquid water for AEMECs and aqueous electrolyte (lye) for AAEMECs,
    - hydrogen and
    - oxygen,

- Pneumatic energy carried by compressible fluids:
    - hydrogen and
    - oxygen,

- Hydrogen at the cathode and

- Oxygen and water/lye at the anode.

5.3 PEMWE stack

Figure 5.3 shows schematically the input and output streams of energy forms and substances of a PEMWE stack.

Figure 5.3: Schematic of the input and output streams (directional arrows) of energy forms (diamond shape) and substances (circular shape) of a PEMWE stack (rectangular shape). The thick line around the grey-shaded box denotes the stack boundary. The use of the grey colour indicates streams of secondary relevance in the context of accelerated stress testing.
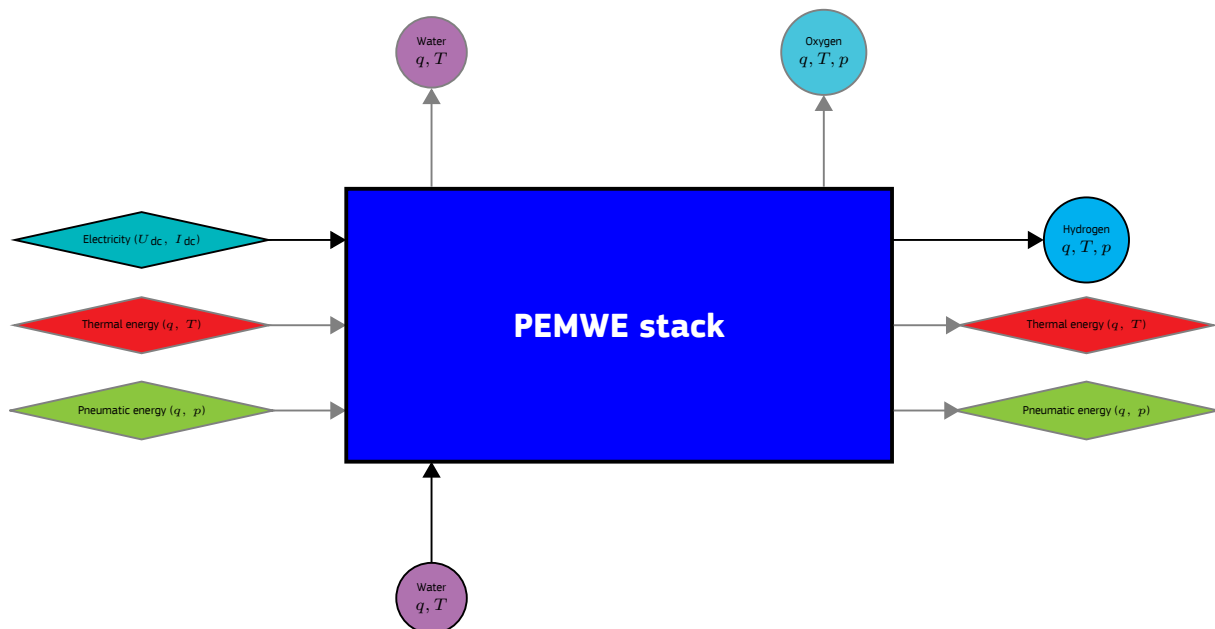
Source: JRC, 2023.

At its PoCs (current/voltage terminals and fluid inlets), the input energy streams to a PEMWE stack are

- **Electricity** in the form of electric energy, see equation (3.3.1a), by supplying DC power, see equation (3.3.1b),

- **Thermal energy**, see equation (5.1.1a), if any, in the form of heat/cold where on input the heat transfer fluid i (input substance stream) is liquid water.

- **Pneumatic energy**, see equation (5.1.2a), which is only relevant for pressurised stacks where the pneumatic fluids j (output substance streams) are hydrogen and oxygen.

At fluid outlets, the output energy and substance streams from a PEMWE stack are

- Thermal energy carried by heat transfer fluids:
    - liquid water,
    - hydrogen and
    - oxygen,
- Pneumatic energy carried by compressible fluids:
    - hydrogen and
    - oxygen,
- Hydrogen and water due to electro-osmosis (see section 3.1) at the cathode and
- Oxygen at the anode.

6 Proposal for AST protocols

6.1 General

A test campaign for assessing the performance degradation of WE stacks under specified test and operating conditions may have different objectives such as

- Determining qualitatively and/or quantitatively one or another identified degradation phenomenon including interactions (coupling) among different and possibly simultaneously occurring phenomena for a given set of WEC materials in a particular stack configuration of known design,

- Identifying or verifying hypothesised degradation mechanisms associated with one or more known phenomena occurring for a set of WEC materials in given stack,

- Evaluating the performance and durability of improved or newly developed materials for WEC components deployed in a representative stack design and configuration,

- Checking on suitable stack designs and configurations as well as

- Identifying potentially detrimental operating conditions and modes of operation as well as optimising operation modes of a stack in a given WE system deployed in a particular application.

As for any test campaign, an AST campaign on WE stacks follows a test programme with a test plan (section 6.6) and schedule to conduct tests according to protocols describing precisely what type of tests, whether performance tests (**4.2.57**) or durability tests (**4.2.28**), should be carried out under which test and operating conditions (section 6.3) and how tests should be performed, in which order, when and for how long or how often. It includes post-processing and presentation of the test results (section 7) as well as their reporting (Annex B).

What makes an AST campaign different from a test campaign testing the durability of WE stacks, is that the former test campaign aims to significantly shorten the time required for stack testing in order to save cost on R&D of WE stacks. Alternatively, it is to test a greater variety of WEC materials and stacks in the same amount of time using the available test hardware and equipments more effectively. It seeks at an earlier demonstration and market entry of the developed WE stacks and eventually accelerates their commercialisation. For this reason, WE stacks are operated for a short time under operating conditions different to their normal operating conditions in an attempt to trigger similar performance degradation mechanism(s) as occur for longer stack exposures. It leads inevitably to more and higher transient operation of WE stacks primarily supplied by fluctuating RES electricity with a higher number of and more frequent changes in current or voltage (including start/stop (ON/OFF) operation) as would occur under real-life operating conditions.

In an AST campaign, available real-world operation profiles of RES-derived power (section 6.8.2) may be compressed in duration by a compression factor (f_{compr}) (**4.2.19**) and combined to obtain simulated duty cycles for dynamic operation of a WE stack undergoing accelerated stress testing. Additional stress is by setting other operating parameters especially stack operating temperature (T_{stack}) and differential (anode-to-cathode) pressure to their extreme values but not out of the range specified by the stack manufacturer to avoid dysfunction or destruction of the WE stack. As well, additional stress can be applied to a WE stack when deliberately adding known contaminants in sufficient quantities to the lye solution in AWE and AAEMWE and to liquid water in AEMWE and PEMWE but not too high in amount and combination to risk dysfunction or destruction of the stack.

However, the operation of the WE stacks (section 5) shall be in accordance with applicable safety requirements (Annex A) and the manufacturer's instructions. WE stacks should not be subjected to test and operating conditions jeopardising safety or risk the dysfunction or destruction of the stack. Then, the selection of the stressing operating conditions (section 6.5) and of their values and ranges shall be within the specification of the stack manufacturer. Also, the test equipment used shall be suitable to apply the stressing operating conditions to the WE stack.

When an aspect of performance degradation of a WE stack is initially not or insufficiently known, an iterative and possibly step-wise approach may be applied where one condition and mode of operation is varied within a reasonable parameter range considering the limiting operating conditions specified by the stack manufacturer. Progressively, more than one such condition or operation mode may be changed in order to arrive on a set of suitable stressing operating conditions and mode of operation of a WE stack. The established conditions and operating mode are for use in subsequent AST campaigns.

Note, in comparison to presently identified stressing operating conditions and mode of operation suggested in available testing protocols (Aricò *et al.*, 2013, Aricò *et al.*, 2016, Aricò *et al.*, 2018, Strataki, 2018, Stiber *et al.*, 2020, Mennemann *et al.*, 2021, Aricò *et al.*, 2020, Fouda-Onana, 2020), the various challenges experienced by WE stacks (section 3.4) will likely entail seeking to re-establish such conditions and modes of operation when testing improved or newly developed materials in one or another WEC component of a WE stack. Also, the design and configuration of stacks may adapt to changes in the set-up and operation of WE system in response

26

to these challenges. An ever increasing share of VRE in the electricity grid across Europe and ongoing market developments in exceedingly and diverse P-to-H$_2$ and H$_2$-to-I applications worldwide may also lead to stack adaptations.

The testing of WE stacks under given test conditions (section 6.3) consists of executing, usually at their beginning-of-life (BoL), all or selected types of tests according to a defined test plan (section 6.6). BoL of a stack shall be the start of its first-time operation following complete conditioning according to manufacturer instructions. Performance tests (section 6.7) of a stack at BoL are followed by durability tests (section 6.9) conducted for a prescribed period of use of the stack (section 6.9.2) employing application-oriented operation profiles of power, current or voltage (section 6.8.2) as appropriate for the intended use of the stack (section 6.9.3).

Optionally, performance tests can be executed intermittently at specified intervals to assess how the stack has maintained or altered its performance characteristics [24]. Performance tests are mandatory at the end of the test campaign to evaluate the final degree of stack degradation using suitable KPIs (section 6.10). Changes in the performance characteristics of stacks are usually also presented graphically versus the total test duration or the number of performed operation profiles or sequence(s) of operation profiles (section 7).

The test plan (section 6.6) may require to intermittently perform safety checks (Annex A) on the stack. Testing shall not continue for stacks unsafe to operate.

6.2 Measurement techniques

The test equipment, measuring instruments and measurement methods shall conform to relevant standards (*e.g.* IEC 61010-1:2010+AMD1:2016 CSV (IEC, 2016)), test methods and procedures or best testing practices. Instruments shall be calibrated in accordance with applicable standard(s), measurement method(s) or procedure(s) as recommended by the manufacturer of the stack to meet the targeted uncertainty (**4.2.77**) of the concerned test parameter, whether TIP (**4.2.73**) or TOP (**4.2.75**). The measurement set-up shall be documented. Calibration records and certificates of the measuring instruments should be available. Guidance on how to carry out an uncertainty analysis of the test results is provided by the Guide to the expression of uncertainty in measurement (GUM) (JCGM, 2008, JCGM, 2009, JCGM, 2020).

6.3 Test conditions

The test conditions with permissible variations are

- environmental conditions of the immediate surrounding (ambient) of the item under test: air (composition, velocity, pressure, temperature, humidity), salinity, ultraviolet (UV) radiation and other (weather) conditions, see clause 4.4 of IEC 60204-1:2016+AMD1:2021 CSV (IEC, 2021a).

- actual operating conditions and modes of WE stack operation: start-up (hot and cold), shut-down, emergency stop and quiescence (standby).

They shall be defined prior to testing in accordance with the purpose(s) and objective(s) of the test campaign and be in conformity with the specification of the stack as provided by the manufacturer.

However, the TIPs used in the various performance and durability tests constitute the operating conditions of the stack. In the test plan (section 6.6), the individual set point values of these TIPs shall be listed per test to be performed. The test plan should also list and name the TOPs (test results) to be measured or calculated per each test.

Further, while the inlet flow rates, temperatures and compositions of liquid feeds (lye and water) are TIPs set (operating conditions), the electrode gas pressures and outlet temperatures are TOPs needing regulation. Other set of operating conditions to be set are stack power (P_{stack}), stack current (I_{stack}) or stack voltage (U_{stack}).

In the first case, stack power is the TIP set, the stack current and DC voltage are measured TOPs. In the second case, stack current is the TIP set. The stack voltage is a TOP measured. In the third case, stack voltage is the TIP set. The stack current is the TOP measured. In both latter cases, the stack power is a derived TOP to be calculated.

6.4 Reference test conditions

Reference test conditions are agreed prior to testing to facilitate comparison of test results [25]. That is, reference test conditions are defined in agreement with manufacturer specification to assess the performance degradation

---

[24] The operation regime applied to the stack during a performance test can affect its degradation rate.

[25] For the three WEL technologies (AEL, AEMEL and PEMEL), the strategic research and innovation agenda 2021-2027 of the Clean Hydrogen Partnership for Europe (SRIA) states 2024 and 2030 KPI targets for current density and hydrogen pressure but not for stack operating temperature (lye/water output temperature); see online at `https://www.clean-hydrogen.europa.eu/knowledge-management/sria-key-performance-indicators-kpis_en`.

of WE stacks upon durability tests (section 6.9) conducted under stressing operating conditions (section 6.5) as appropriate, by means of polarisation curve measurements (section 6.7.11) and EIS measurements (section 6.7.12). Table 6.1 provides reference operating conditions recommended for typical WE stacks of type AWE, AEMWE and PEMWE. For a test campaign aiming at a direct comparison of the three LTWE technologies or at a comparison of one stack technology versus another stack technology, the reference values of stack current density and stack operating temperature may be chosen to be the same.

Table 6.1: Recommended reference operating conditions for typical WE stacks (AWE, AEMWE and PEMWE)

Description	Unit	Symbol	AWE	AEMWE	PEMWE
Stack current density ([1])	A/cm^2	J_{stack}	0,4 ($\pm$ 2,5 %)	1,0 ($\pm$ 1 %)	2,0 ($\pm$ 0,5 %)
Stack operating temperature ([2])	K	T_{stack}	353,15 ($\pm$2 K)	333,15 ($\pm$2 K)	353,15 ($\pm$2 K)
Hydrogen pressure ([3])	kPa(g)	p_{H_2}	100 ($\pm$2 %) ([4])	100 ($\pm$2 %)	100 ($\pm$2 %) ([4])

Note: The test plan (section 6.6) may list other conditions including ambient environmental conditions of the WE stack other than standard ambient temperature and pressure (SATP) conditions (**4.2.69**); see, for example, clause 5.2.3.1 of ISO 22734:2019 (ISO, 2019a).
([1])   This value should correspond to the maximum current density at BoL.
([2])   Unless otherwise agreed or specified by the manufacturer, the sensor (*e.g.* thermocouple) position to determine the stack operating temperature should be at the center of the tubing where lye/water is put out by the WE stack close to its outlet.
([3])   The gauge pressure of hydrogen is measured at the outlet of the WE stack, preferably upon removal of residual liquid (lye or water). Gauge pressure is chosen to allow comparison when testing is conducted at sites having different atmospheric pressure levels. Balanced pressure or differential pressure operation of the stack shall be reported.
([4])   The SRIA anticipates a pressure of hydrogen of 3 MPa for the AEL and PEMEL technologies, see footnote 25. This pressure level is not selected as not all test equipment may allow testing at such pressure.
Source: JRC, 2023

A WE stack should first be subjected to testing at reference test conditions before proceeding to testing under other specified test conditions including stressing operating conditions (section 6.5). Particularly, this regards polarisation curve measurements (section 6.7.11) and EIS measurements (section 6.7.12) at beginning-of-test (BoT) and at end-of-test (EoT) when WE stacks should again be tested under these reference test conditions to assess their overall performance degradation in the test campaign.

6.5   Stressing operating conditions

Major stressing operating conditions for WE stacks are (Tsotridis and Pilenga, 2021)

- *High current density operation*: This concerns operation at stack current densities in excess of the recommended value (see Table 6.1), for example, at up to 200 % of the recommended value.

- *Dynamic electric operation*: This concerns variable electric power, direct current or DC voltage (including frequent ON/OFF operation) (Sayed-Ahmed *et al.*, 2024) employing simulated operation profiles (Alia *et al.*, 2019, Allidières *et al.*, 2019, Aßmann *et al.*, 2020, Tsotridis and Pilenga, 2021, Malkow and Pilenga, 2023b, Reissner *et al.*, 2020), or RES-derived "real-world" operation profiles (section 6.8.2). For AWE stacks, OFF operation (zero supply current or OCV conditions), the phenomenon of the flow of a reverse current (**4.2.67**) occurs which leads to materials oxidation at the negatively charged cathode and materials reduction at the positively charged anode on the respective biP side (Haleem *et al.*, 2021).

- *AC ripple*: This concerns current (or voltage) fluctuations due to non-optimum AC/DC conversion, which are inevitable in real converters, superimposed onto DC (or DC voltage) supplied to the stack (Parache *et al.*, 2022).

- *Stack operating temperature*: The stack operating temperature influences the thermal-neutral voltage of the stack and the overvoltages as well as temperature-activated reaction kinetics at the electrodes.

- *Pressure*: This concerns especially anode-to-cathode differential pressure of the stack. For example, pressure cycling can be performed within the range of 60 % and 100 % of the nominal pressure (as specified by the manufacturer) or beyond nominal pressure to test the mechanical integrity of the stack. For operational safety, the stack may intermittently be subject to leak testing to identify significant external and internal leaks.

- *Lye/water inlet flow rate*: Too low lye/water inlet flow rates may result in insufficient wetting, risking dry active area and a reduction in gas bubble removal which could result in hotspots and overvoltage increases. Too high lye/water inlet flow rates could accelerate catalyst loss due to dissolution/erosion effects.

- *Lye/water impurities*: This concerns deliberate additions of calcium, copper, iron, potassium, magnesium, sodium, nickel, zinc, chloride and carbonate ions (dissolved CO_2) to mainly affect IEM capability and catalyst activity (Becker *et al.*, 2023). Also, organics stemming from BoP components or products of in-stack materials deterioration, which are introduced to the stack by re-circulated lye/water, may deliberately be added.

Considering the specification of the stack and the test equipment capabilities, the test plan (section 6.6) shall specify the values and ranges of these stressing operating conditions including the compression factor applied to the original operation profile. The compression factor is the ratio of the duration of the compressed operation profile (t_{compr}) to the duration of the original operation profile (t_{origin}) calculated as follows

$$f_{compr} = \frac{t_{compr}\text{ (h)}}{t_{origin}\text{ (h)}}, \ 0 < f_{compr} < 1. \tag{6.5.1}$$

The actual choice of a compression factor shall be such that the test equipment used can readily apply the intended dynamic operation of the stack and the ramp rates resulting from the simulated duty cycle(s) do not exceed those specified by the stack manufacturer, if any.

In addition to accelerated stress testing of WE stacks, accelerated lifetime testing of the same type of stack may be conducted employing the original operation profile (section 6.8.2) while applying the same stack operating temperature and differential pressure without deliberately adding lye/water impurities. Note, performing accelerated lifetime testing of stacks as part of a test campaign using a suitable DoE (**4.2.25**) methodology along with physics-based modelling will assist in

- Identifying ranges of aggravated test conditions (stressing operating conditions) representative of the targeted application and duty cycle in real-world stack operation which do not significantly alter the interdependency or eminence of intrinsic degradation mechanisms and

- Deriving robust AST transfer functions to correlate accelerating factors (stressing operating conditions) with the occurrence or amplification of performance degradation in stacks and eventually, to reliably quantify rates of performance degradation allowing to predict durability under real-world conditions which can contemporaneously or sequentially be combined for evaluating various relevant stack operation modes.

This is especially useful to lower overall R&D cost of WE stacks as test durations could significantly be reduced.

6.6 Test plan

The test plan shall take into account

(a) the manufacturer specification and instructions (*e.g.* maximum voltage, pressure and anode-to-cathode differential pressure, stack operating temperature, range of heating/cooling rates and electrode gas compositions, etc),

(b) an activation/conditioning procedure for initial stack operation upon manufacture, refurbishment or prolonged non-operation (Lickert *et al.*, 2023, Tomić *et al.*, 2023),

(c) the test conditions: reference test conditions (section 6.4) and stressing operating conditions (section 6.5),

(d) the measurement techniques and instrumentation (section 6.2),

(e) the test type (section 6.7 and section 6.9), sequence, frequency, duration and operation profiles,

(f) the DAQ with number and logging rates of the data points ([26]),

(g) re-start procedure upon unintended test interruptions other than pre-mature stack failure (*i. e.* test equipment break down, emergency stops, power supply failure, etc),

(h) one or more KPIs, whether measured or derived TOPs, as a result of performance tests,

(i) one or more test stop criteria to end testing to prevent unintended failure or destruction of the stack and

(j) the post-processing of test results, data reduction and uncertainty analysis (coverage factor of 2) (JCGM, 2008) according to GUM (JCGM, 2009).

One or more KPIs shall be defined to assess the performance and durability of the test item. For this purpose, TIPs and TOPs should be specified to obtain KPIs as functions of such parameters; for example,

---

[26] Considering the duration of the individual tests and the expected standard uncertainty in the measurements, different numbers, ranges and data logging rates may apply to performance tests (section 6.7) and durability tests (section 6.9).

- TIPs:
  - input electric power ($P_{\text{el, in}}$) (section 6.7.1), input current (I_{in}) (section 6.7.2) or input voltage (U_{in}) (section 6.7.3) to the stack,
  - input temperature of lye ($T_{\text{in}}^{\text{lye}}$) to AWE and AAEMWE stacks and
  - input water temperature (T_{in}^{w}) to PEMWE and AEMWE stacks.
- TOPs:
  - stack operating temperature (T_{stack}),
  - output pressure of hydrogen (p_{H_2}) and
  - temperature of hydrogen (T_{H_2}) generated by the stack.

Environmental conditions other than SATP conditions may also be considered; for example, conditions likely to be experienced at intended installation sites of WE systems.

Consistent with the test campaign purpose(s) and objective(s), the test plan should specify the test methods and measurement techniques employed where standards, testing procedures and manufacturer's instructions provide different possibilities. The test plan may also list (micro-structural) characterisation methods, for example, to perform post-test analysis of stack materials to gain more insight into the obtained test results.

6.7 Performance tests

6.7.1 Input electric power

The input electric power to a WE stack shall be determined in accordance with clause 5.2.1 of ISO 16110-2:2010 (ISO, 2010b).

6.7.2 Input direct current

For a specified DC voltage set, the input direct current to a WE stack shall be determined from electric power measurements (section 6.7.1). The input direct current is the measured input electric power divided by the specified DC voltage.

6.7.3 Input DC voltage

For a specified direct current set, the input DC voltage applied to a WE stack shall be determined from electric power measurements (section 6.7.1). The input DC voltage is the measured input electric power divided by the specified direct current.

6.7.4 Input thermal power

The input thermal power ($P_{\text{th, in}}$) to a WE stack conveyed by heat transfer fluid(s), if any, shall be determined in accordance with clause 5.2.2 of ISO 16110-2:2010 (ISO, 2010b).

6.7.5 Input power of compression

The input power of compression ($P_{\text{compr, in}}$) to a WE stack conveyed by pneumatic fluid(s), if any, shall be determined in accordance with clause 5.2.2 of ISO 16110-2:2010 (ISO, 2010b).

6.7.6 Response time and ramp energy

Especially for delivering grid balancing services by electrolysers (Allidières *et al.*, 2019), the response time (t_{resp}) of a WE stack to a given positive or negative ramp rate of input electric power, input direct current or input DC voltage (section 6.6) should be determined in accordance with clause 5.6.1 of IEC 62282-8-201:2020 (IEC, 2020d). Ramp rates shall be consistent with the manufacturer's instructions. In addition to response time, the ramp energy (E_{ramp}) should be determined in accordance with clause 14.6.3.2 of IEC 62282-3-201:2017+AMD1:2022 CSV (IEC, 2022) where by analogy, reference to fuel cell (FC) is replaced by water electrolyser.

The response time and ramp energy shall be recorded separately for positive and negative ramps in the test report (Annex B). The test plan shall specify appropriate indices to be added to t_{resp} and E_{ramp} to distinguish between different ramps, whether positive and negative. The state prior to ramping may include cold start (**4.2.17**) and hot start (**4.2.41**).

1152   The determination of response time and ramp energy should at least be at BoT and EoT. It is for assessing
1153 whether or not changes in the ability of a WE stack to respond as intended to variations in input electric power
1154 (input direct current or input DC voltage) occurred due to durability testing of the stack (section 6.9).

6.7.7   Measurements of fluid feeds

1156 For AWE and AAEMWE stacks, the pH value and the electrical conductivity (σ_{el}) of the alkaline solution (KOH
1157 electrolyte) entering the stack shall, by analogy to water, be determined in accordance with clauses 7.1 and 7.2
1158 of ISO 3696:1987 (ISO, 1987), respectively.
1159   For AEMWE and PEMWE stacks, the pH value and the electrical conductivity of the feed water to the stack shall
1160 be determined in accordance with ISO 10523:2008 (ISO, 2008) and ISO 7888:1985 (ISO, 1985), respectively.

6.7.8   Hydrogen output rate and quality

1162 The product gas output rate, also known as product gas molar flow rate ($q_{n,out}$) of the WE stack, shall be
1163 determined in accordance with clause 5.2.11.1 of ISO 22734:2019 (ISO, 2019a). From the product gas molar
1164 flow rate, the hydrogen output rate, also known as molar flow rate of hydrogen (q_{n,H_2}), shall be calculated as
1165 follows

$$1166 \qquad q_{n,H_2} \text{ (mol/h)} \ = \ x_{n,H_2} \text{ (mol/mol)} \cdot q_{n,out} \text{ (mol/h)}; \tag{6.7.1}$$

1167 x_{n,H_2} is the molar concentration of hydrogen in the product gas to be determined by gas analysis in accordance
1168 with clause 5.2.2.2 of ISO 16110-2:2010 (ISO, 2010b). From the molar flow rate of hydrogen, the volumetric
1169 flow rate of hydrogen (q_{V,H_2}) generated under SATP conditions is calculated as follows

$$1170 \qquad q_{V,H_2} \text{ (m}^3\text{/h)} \ = \ q_{n,H_2} \text{ (mol/h)} \cdot V_{m,H_2} \text{ (m}^3\text{/mol)}; \tag{6.7.2}$$

1171 $V_{m,H_2} \approx 24,79 \cdot 10^{-3}$ m³/mol is the molar volume of hydrogen under SATP conditions ([27]). The hydrogen output
1172 quality of a WE stack other than the molar concentration of hydrogen in the product gas, in particular, humidity,
1173 shall be determined in accordance with clause 5.2.11.2 of ISO 22734:2019 (ISO, 2019a).
1174   Note, neglecting gas crossover and leakages in the stack, the theoretical volumetric flow rate of hydrogen
1175 generated under SATP conditions can be calculated as follows

$$1176 \qquad q_{V,H_2}^{theo} \text{ (m}^3\text{/h)} \ = \ \frac{V_{m,H_2} \text{ (m}^3\text{/mol)} \cdot I_{dc} \text{ (A)}}{z \cdot F \text{ (C/mol)}} \cdot 3600 \text{ s/h}; \tag{6.7.3}$$

1177 F = 96485,3321 C/mol is Faraday constant and z is the number of electrons exchanged in the WEC reactions
1178 (3.1.2), (3.1.3) or (3.1.4). The mass flow rate of hydrogen (q_{m,H_2}) generated by a WE stack related to SATP
1179 conditions is calculated as follows

$$1180 \qquad q_{m,H_2} \text{ (kg/h)} \ = \ q_{n,H_2} \text{ (mol/h)} \cdot m_{H_2} \text{ (kg/mol)}; \tag{6.7.4}$$

1181 $m_{H_2} \approx 2,02 \cdot 10^{-3}$ kg/mol is the molar mass of hydrogen under SATP conditions ([28]).

6.7.9   Oxygen output rate and concentration

1183 The oxygen output rate, also known as molar flow rate of oxygen (q_{n,O_2}) of the WE stack, shall be determined in
1184 accordance with clause 5.2.11.1 of ISO 22734:2019 (ISO, 2019a). The molar concentration of oxygen (x_{n,O_2}),
1185 shall be determined in accordance with clause 5.2.11.2 of ISO 22734:2019 (ISO, 2019a).

6.7.10   Water quality measurements

1187 For AEMWE and PEMWE stacks with materials containing fluorine (F), PFAS and polycyclic aromatic hydrocarbons
1188 (PAH) such as membranes, coatings, sealants, etc , the quality of the water entering and exiting the stack should
1189 be determined regarding

1190   (a) fluoride concentration (c_F) in accordance with ISO 10359-1:1992 (ISO, 1992), ISO 10359-2:1994 (ISO,
1191   1994), ISO 10304-1:2007 (ISO, 2007), ISO/TS 17951-1:2016 (ISO, 2016b), ISO/TS 17951-2:2016 (ISO,
1192   2016b) or ISO/TS 15923-2:2017 (ISO, 2017b), as appropriate.

---

[27]   At a temperature of 273,15 K and a pressure of 101,3 kPa, the molar volume of hydrogen is $V_{m,H_2} \approx 22,41 \cdot 10^{-3}$ m³/mol.
[28]   The mass of deuterium and tritium as hydrogen isotopes are not considered due to their negligible natural abundance.

(b) PFAS concentration (c_{PFAS}) in accordance with ISO 21675:2019 (ISO, 2019c) or any other suitable analysis technique ([29]), as feasible.

(c) PAH concentration (c_{PAH}) in accordance with ISO 17993:2002 (ISO, 2002), ISO 7981-1:2005 (ISO, 2005a), ISO 7981-2:2005 (ISO, 2005b) or ISO 28540:2011 (ISO, 2011b), as appropriate.

The content of fluoride, PFAS and PAH in the water on stack inlet shall be substracted from the respective content at stack outlet ([30]). Upon substracting any fluoride inlet content from that at stack outlet, the occurrence of fluoride in the water exiting the stack as an end product of the decomposition of fluoropolymers is conclusive evidence for the performance degradation of the stack by materials deterioration. Also, upon applying a similar substraction procedure, the occurrence of PFAS and PAH in the exit water of a stack as fragments of partially decomposed polymers is likewise conclusive evidence for the performance degradation of the stack by materials deterioration. The identified type of fragments along with their analysed quantities may assist in determining the pathways of material deterioration to gain useful insight into the performance degradation of stacks.

Especially for WE stacks tested using ion impurities in water as stressing operating conditions (section 6.5), the quality of the water entering and exiting the stack shall be determined regarding

- calcium concentration (c_{Ca}) in accordance with ISO 6058:1984 (ISO, 1984a), ISO 7980:1986 (ISO, 1986a), ISO 14911:1998 (ISO, 1998) or ISO/TS 15923-2:2017 (ISO, 2017b), as appropriate,

- chloride concentration (c_{Cl}) in accordance with ISO 9297:1989 (ISO, 1989), ISO 10304-4:1997 (ISO, 1997), ISO 15682:2000 (ISO, 2000), ISO 10304-1:2007 (ISO, 2007), ISO 15923-1:2013 (ISO, 2013) or ISO 10304-4:2022 (ISO, 2022c), as appropriate,

- copper concentration (c_{Cu}) in accordance with ISO 8288:1986 (ISO, 1986b),

- iron concentration (c_{Fe}) in accordance with ISO 6332:1988 (ISO, 1988) or ISO/TS 15923-2:2017 (ISO, 2017b), as appropriate,

- potassium concentration (c_K) in accordance with ISO 9964-2:1993 (ISO, 1993b), ISO 9964-3:1993 (ISO, 1993c) or ISO 14911:1998 (ISO, 1998), as appropriate,

- magnesium concentration (c_{Mg}) in accordance with ISO/TS 15923-2:2017 (ISO, 2017b) or ISO 6059:1984 (ISO, 1984b), as appropriate,

- sodium concentration (c_{Na}) in accordance with ISO 9964-1:1993 (ISO, 1993a), ISO 9964-3:1993 (ISO, 1993c) or ISO 14911:1998 (ISO, 1998), as appropriate,

- nickel concentration (c_{Ni}) in accordance with ISO 8288:1986 (ISO, 1986b) and

- zinc concentration (c_{Zn}) in accordance with ISO 8288:1986 (ISO, 1986b).

The content of calcium (Ca), chloride (Cl⁻), copper (Cu), iron (Fe), potassium (K), magnesium (Mg), sodium (Na), nickel (Ni) and zinc (Zn) in the water on the inlet of the stack shall be substracted from those at the stack outlet.

6.7.11   Polarisation curve measurements

The measurement of the current-voltage (I_{dc}-U_{dc}) characteristics or polarisation curves of WE stacks shall be determined by applying the EU harmonised polarisation curve test method for LTWEL (Malkow *et al.*, 2018b). Polarisation curve measurements are commonly performed under reference test conditions (section 6.4) at a minimum of three different set points to be specified in the test plan (section 6.6).

Polarisation curve measurements under reference test conditions may act as an operation phase for *in-situ* stack regeneration to recover reversible degradation (Tsotridis and Pilenga, 2021). The test plan (section 6.6) may also foresee another type of procedure for stack regeneration to be applied prior to polarisation curve measurements.

In case the cell voltage difference in galvanostatic polarisation measurements is negligible (*i. e.* less than 10 mV for all data points) when starting from (near) zero current to proceed to maximum current (I_{max}) (ascending polarisation curve) compared to starting from maximum current to proceed to (near) zero current (descending polarisation curve), subsequent measurements may be conducted unidirectional with respect to changes in current while maintaining a steady stack operating temperature (Lettenmeier *et al.*, 2016).

---

[29]   Note, the appendix to annex E.4 of the Annex XV Restriction Report on the manufacture, placing on the market and use of PFAS contains an overview on analytical methods for the analysis of PFAS in different matrices; see at `https://echa.europa.eu/restrictions-under-consideration/-/substance-rev/72301/term`.

[30]   For sampling water and subsequent analysis, materials free of fluoride, PFAS and PAH shall be used.

The maximum current is the current at which the voltage of any one cell in the stack is for three consecutive samplings equal to the cut-off voltage ($U_{\text{cut-off}}$) defined prior to testing as part of the test plan (section 6.6) or following manufacturer recommendations. As a voltage limit, the cut-off voltage is to prevent excessive stack degradation. Thus, polarisation curve measurements are preferably conducted under galvanostatic conditions.

For AWE stacks, no OCV (zero supply current) shall be used as a set point in the polarisation curve measurement to prevent the flow of a reverse current in the stack leading to materials deterioration (see section 6.5).

From the I_{dc}-U_{dc} curve, the current-electric power (I_{dc}-P_{el}) curve is calculated, see equation (3.3.1b). The energy efficiency (η_{e}) given by equation (6.7.16) versus the electric power density given by equation (3.3.1c) and the electrical efficiency (η_{el}) given by equation (6.7.16) versus the electric power density are also plotted to assess the optimum operating (working) point (**4.2.50**) of the WE stack under the test conditions.

The distribution of the cell voltage is a measure of voltage homogeneity in the stack. The mean absolute error of average cell voltage ($\text{MAE}_{\overline{U_{\text{cell}}}}$) and standard deviation of average cell voltage ($\text{SD}_{\overline{U_{\text{cell}}}}$) are two complementary statistical indicators of cell voltage distribution calculated as follows

$$\text{MAE}_{\overline{U_{\text{cell}}}} \text{ (mV)} \;=\; \frac{1}{N_{\text{cell}}} \sum_n \left| U_{\text{cell},n} \text{ (V)} - \overline{U_{\text{cell}}} \text{ (V)} \right| \cdot 10^3 \text{ mV/V} \tag{6.7.5a}$$

$$\text{SD}_{\overline{U_{\text{cell}}}} \text{ (mV)} \;=\; \sqrt{\frac{1}{N_{\text{cell}}-1} \sum_n \left(U_{\text{cell},n} \text{ (V)} - \overline{U_{\text{cell}}} \text{ (V)} \right)^2} \cdot 10^3 \text{ mV/V} \tag{6.7.5b}$$

where

$$\overline{U_{\text{cell}}} \text{ (V)} \;=\; \frac{1}{N_{\text{cell}}} \sum_n U_{\text{cell},n} \text{ (V)} \tag{6.7.5c}$$

is the average cell voltage of all series-connected WECs in the stack; $U_{\text{cell},n}$ is the voltage of cell number n and N_{cell} is the number of cells in the stack. A significant deviation of the average cell voltage times the number of cells from the measured stack voltage, $U_{\text{stack}} \not\approx N_{\text{cell}} \cdot \overline{U_{\text{cell}}}$, indicates ohmic resistances in the stack materials and contact resistances at their interfaces which are non-negligible. Such deviation also depends on the in-stack positions of the terminals across which the individual cell voltages and the stack voltage are measured.

In order to gain more insight into the performance degradation by voltage increases of the WECs in a WE stack, a voltage breakdown analysis may optionally be performed on the measured polarisation curves for attributing voltage increases to individual WEC components (Flick *et al.*, 2015, Gerhardt *et al.*, 2021, Dizon *et al.*, 2022). This is accomplished by additive contributions of the various overvoltages to the OCV of the WEC given by equation (6.7.7a). Then, the voltage of the WEC is calculated as follows

$$U_{\text{WEC}} \text{ (V)} = U_{\text{OCV}} \text{ (V)} + U_{\text{act}} \text{ (V)} + I_{\text{dc}} \text{ (A)} \cdot R_{\text{lf}} \text{ (Ω)} + U_{\text{conc}} \text{ (V)}; \tag{6.7.6}$$

U_{act} is the activation polarisation voltage given by equation (6.7.7b), R_{lf} is the low-frequency resistance estimated as the slope of the polarisation curve ([31]) and U_{conc} is the concentration polarisation voltage given by equation (6.7.7c). Specifically, the voltage contributions are

- Open circuit voltage or open circuit potential (U_{OCP}) which is different to the reversible voltage due to

    - gas crossover leading to mixed electrode potentials,
    - locally different catalyst surface concentrations and
    - gas solubility at the water-ionomer-catalyst interface.

- Ohmic polarisation (**4.2.49**) represented by $I_{\text{dc}} \cdot R_{\text{lf}}$ where the low-frequency resistance or ohmic resistance of the WEC is due to

    - the electrodes including diffusion media,
    - the electrolyte, namely lye solution in AWE and AAEMWE and hydrated IEM in AEMWE and PEMWE, and
    - interfacial contact surfaces of the stack between WEC, biPs and current collectors.

- Activation polarisation (**4.2.4**) due to the kinetics of

    - the OER (3.1.2a), (3.1.3a) or (3.1.4a) at the anode and
    - the HER (3.1.2b), (3.1.3b) or (3.1.4b) at the cathode.

([31]) The low-frequency resistance can also be determined by EIS measurements (section 6.7.12), see equation (6.7.12).

- Concentration polarisation (**4.2.20**) due to mass transfer limitations in the electrodes of the stack including hindrance caused by gas bubble formation.

In the absence of gas crossover and other non-ideal conditions, the temperature-dependent open circuit voltage is calculated as follows (Bernt, 2019)

$$U_{\mathsf{OCV}}(T) \text{ (V)} = 1,2291 \text{ V} - 0,0008456 \text{ (V/K)} \left(T \text{ (K)} - 298,15 \text{ K}\right)$$

$$+ \frac{R_{\mathsf{g}} \text{ (J/(mol K))} \cdot T \text{ (K)}}{z \cdot F \text{ (C/mol)}} \log \left(\frac{p_{\mathsf{H_2}} \text{ (kPa)}}{p^0 \text{ (kPa)}} \cdot \left(\frac{p_{\mathsf{O_2}} \text{ (kPa)}}{p^0 \text{ (kPa)}} \right)^{0,5} \right); \tag{6.7.7a}$$

$p_{\mathsf{H_2}}$ and $p_{\mathsf{O_2}}$ are the partial pressure of hydrogen and partial pressure of oxygen, respectively. The activity of liquid water ($a_{\mathsf{H_2O}}$) is taken as unity. The exponent of 0,5 stems from the fact that half a mole of oxygen is generated by electrolysis from one mole of liquid water, see reaction (3.1.1). The temperature-dependent activation and concentration polarisation voltages are calculated as follows (Hernández-Gómez *et al.*, 2020)

$$U_{\mathsf{act}}(T) \text{ (V)} = \frac{R_{\mathsf{g}} \text{ (J/(mol K))} \cdot T \text{ (K)}}{z \cdot F \text{ (C/mol)}} \log \left(\left(\frac{I_{0,\mathsf{a}}(T) \text{ (A)}}{I_{\mathsf{a}} \text{ (A)}} \right)^{\alpha_{\mathsf{a}}} \cdot \left(\frac{I_{0,\mathsf{c}}(T) \text{ (A)}}{I_{\mathsf{c}} \text{ (A)}} \right)^{\alpha_{\mathsf{c}}} \right) \text{ and} \tag{6.7.7b}$$

$$U_{\mathsf{conc}}(T) \text{ (V)} = \frac{R_{\mathsf{g}} \text{ (J/(mol K))} \cdot T \text{ (K)}}{z \cdot F \text{ (C/mol)}} \log \left(\left(\frac{c_{\mathsf{O_2}} \text{ (mol)}}{c_{\mathsf{O_2}}^0 \text{ (mol)}} \right) \cdot \left(\frac{c_{\mathsf{H_2}} \text{ (mol)}}{c_{\mathsf{H_2}}^0 \text{ (mol)}} \right) \right); \tag{6.7.7c}$$

$I_{0,\mathsf{a}}$, I_{a}, $I_{0,\mathsf{c}}$, I_{c}, α_{a} and α_{c} are anodic exchange current, anodic current, cathodic exchange current, cathodic current, anodic charge transfer coefficient and cathodic charge transfer coefficient, respectively while $c_{\mathsf{O_2}}$ and $c_{\mathsf{H_2}}$ are the oxygen concentration and hydrogen concentration at the electrolyte-electrode interfaces, respectively and $c_{\mathsf{O_2}}^0$ and $c_{\mathsf{H_2}}^0$ are their respective equilibrium concentrations. Further information on voltage breakdown analysis is given elsewhere (Ma *et al.*, 2021, Falcão and Pinto, 2020, Gerhardt *et al.*, 2021).

6.7.12 EIS measurements

The electrical impedance (Z) of individual cells in a WE stack as a function of perturbation frequency (f) [32] shall be determined by applying the EU harmonised test procedure on EIS for WECs (Malkow *et al.*, 2018a) under the same test and operating conditions including the DC set point values as applied in the polarisation curve measurements (section 6.7.11). In case EIS measurements and polarisation curve measurements are conducted simultaneously, AC and DC contributions are contained in the current and voltage data. The test plan (section 6.6) shall specify the excitation type, magnitude, frequencies and the number of repetitions.

In Nyquist plots (**4.2.48**), the (negative) imaginary part of electrical impedance is plotted against the real part of electrical impedance, $(-)\mathfrak{Im}Z$ versus $\mathfrak{Re}Z$, Figure 6.1. The resulting graph displays one or more semi-arcs whereby the number of distinguishable semi-arcs coincides with the number of relaxation times or time constants (τ) due to polarisation processes such as charge build-up at and transfer across the WEC interfaces as well as species transport (convection, diffusion, migration, reaction, etc) within the WEC [33]. Often, semi-arcs overlap considerably so that not all time constants are identifiable. That is, not all polarisation processes may visually be detectable from Nyquist plots, see Figure 6.1.

In Bode plots (**4.2.14**), the modulus of electrical impedance [34] and its phase [35] are plotted against the frequency in logarithmic scale, $|Z|$, $\arg(Z)$ versus $\log f$, Figure 6.2. From a Bode plot, the values of the low-frequency resistance (R_{lf}) (see equation (6.7.12)) and the high-frequency resistance (R_{hf}) (see equation (6.7.9)) can often be read directly, which is not necessarily the case for a Nyquist plot, cf. Figure 6.2 and Figure 6.1.

[32] In EIS measurements, the output under potentiostatic conditions is electrical impedance, $Z=|Z|^2 Y^* =|Z| \, e^{\imath \arg(Z)}$; $|\cdot|$ denotes modulus or gain, $\arg(\cdot)$ denotes phase or argument, superscript $*$ denotes complex conjugation and $\imath$ is the imaginary unit with property, $(\pm\imath)^2 = -1$. Under galvanostatic conditions, the output is electrical admittance, $Y=|Y|^2 Z^* =|Y| \, e^{\imath \arg(Y)}$.

[33] The combination of any two distinct passive (lumped) circuit elements such as a capacitor having electrical admittance, $Y=\imath\omega C$, an inductor having electrical impedance, $Z=\imath\omega L$ and a resistor having electrical impedance, $Z=R$, arranged in parallel or, series makes up a characteristic time constant; $\omega=2\pi f$ is angular frequency. It is attributable to the dissipation of electric energy (E_{el}) by resistors accounting for the resistivity in bulk materials and resistance (R) of the various interfaces of a WEC or a WE stack due to electronic and ionic conduction as well as energy storage by capacitors accounting for capacitance (C, negative reactance) at electrically charged interfaces (*i.e.* electrolyte-electrode intersections) and inductors accounting for inductance (L, positive reactance) in conductors (*i.e.* wires, converters, etc). Non-ideal circuit elements include constant phase elements (CPEs) having electrical impedance, $Z=((\imath\omega)^\alpha Q_{\mathsf{C}})^{-1}$ or $Z=(\imath\omega)^\alpha Q_{\mathsf{L}}$ ($0<\alpha<1$ where α is a power exponent, Q_{C} is a non-ideal capacitance and Q_{L} is a non-ideal inductance) to account for frequency dispersion (Alexander *et al.*, 2016, Córdoba-Torres, 2017, Kartci *et al.*, 2020, Fitzek *et al.*, 2022) and distributed circuit elements (Warburg, Gerischer, etc) to account for species transport (Huang, 2018, Chowdhury and Kant, 2018, Boukamp, 2017). They too have individual (mean) time constants.

[34] Also, the real and imaginary part of electrical impedance may be displayed in Bode plots.

[35] Instead of phase or argument of electrical impedance, the tangent of loss angle of electrical impedance may be plotted against the logarithm of frequency (or angular frequency), $\tan(\mathfrak{Im}Z/\mathfrak{Re}Z)$ versus $\log f$ (or $\log \omega$).

Figure 6.1: Graphical representation of the real and imaginary parts of the electrical impedance of a water electrolysis cell in a Nyquist plot.
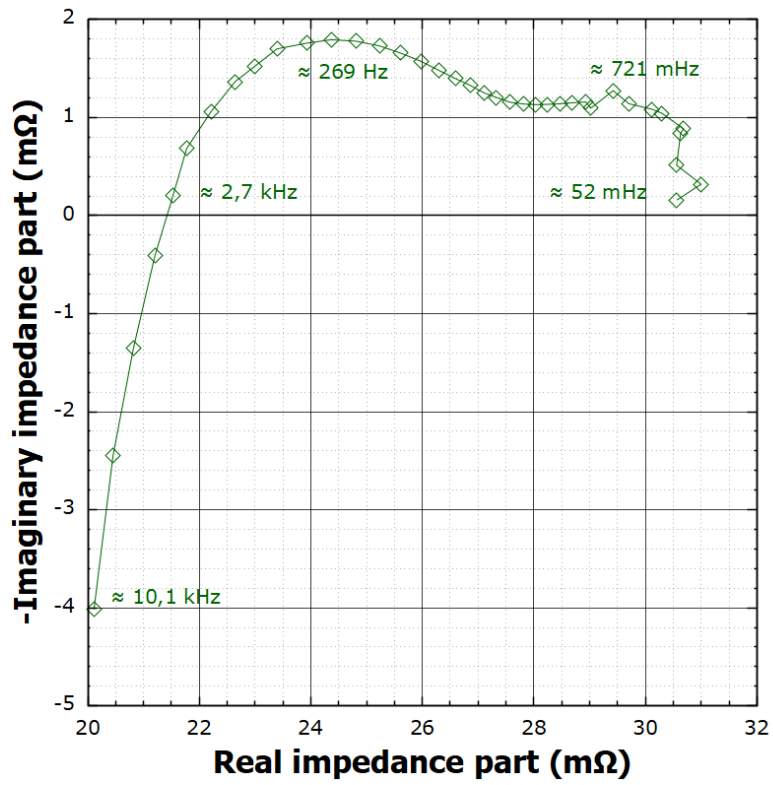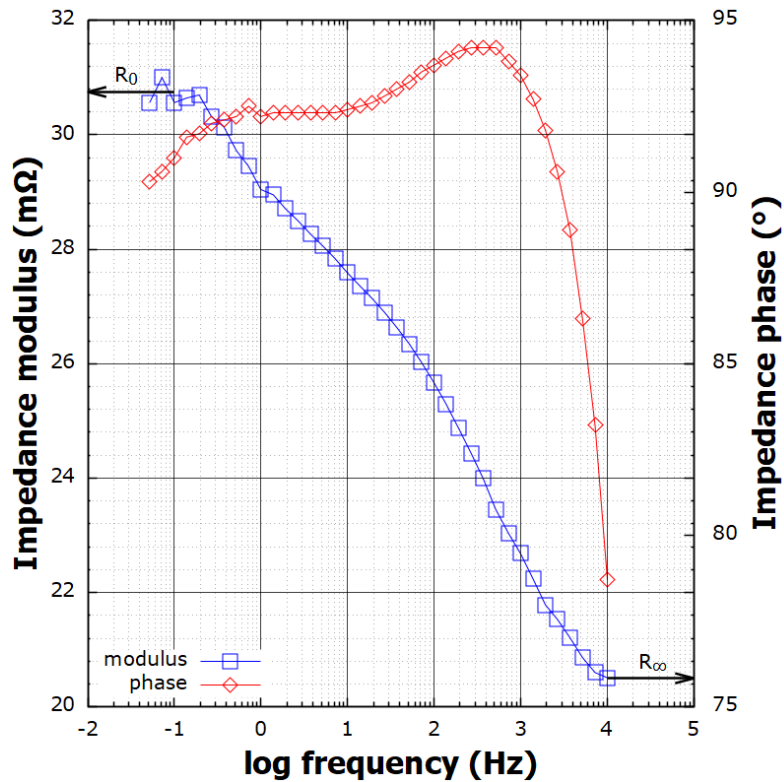

Source: JRC, 2023.

Figure 6.2: Graphical representation of the electrical impedance modulus and phase of a water electrolysis cell in a Bode plot.

Source: JRC, 2023.

35

In principle, the ohmic resistance is the infinite-frequency resistance (R_∞) that is the electrical impedance at high frequencies ($f \to \infty$) with vanishing reactance, $\mathfrak{Im}Z\,[f \to \infty] = 0$,

$$\lim_{f \to \infty} \mathfrak{Re}Z\,[f]\,(\Omega) \;=\; R_\infty\,(\Omega). \tag{6.7.8}$$

Practically, the ohmic resistance is the electrical impedance measured at the highest of the probed frequencies (f_max) where $\mathfrak{Im}Z\,[f \to f_\mathsf{max}] \to 0$,

$$\lim_{f \to f_\mathsf{max}} \mathfrak{Re}Z\,[f]\,(\Omega) \;\approx\; R_\mathsf{hf}\,(\Omega) \tag{6.7.9}$$

to basically represent the resistance of the electrolyte. Unfortunately, the reactance at f_max is often not negligible, $\mathfrak{Im}Z\,[f_\mathsf{max}] > 0$, see Figure 6.1. The polarisation resistance is the difference between the zero-frequency resistance (R_0) and the infinite-frequency resistance,

$$R_\mathsf{pol}\,(\Omega) \;=\; R_0\,(\Omega) \;-\; R_\infty\,(\Omega). \tag{6.7.10}$$

The zero-frequency resistance is the electrical impedance at low frequencies ($f \to 0$) with vanishing reactance, $\mathfrak{Im}Z\,[f \to 0] = 0$,

$$\lim_{f \to 0} \mathfrak{Re}Z\,[f]\,(\Omega) \;=\; R_0\,(\Omega). \tag{6.7.11}$$

Practically, the zero-frequency resistance is the electrical impedance measured at the lowest of the probed frequencies (f_min) where $\mathfrak{Im}Z\,[f \to f_\mathsf{min}] \to 0$,

$$\lim_{f \to f_\mathsf{min}} \mathfrak{Re}Z\,[f]\,(\Omega) \;\approx\; R_\mathsf{lf}\,(\Omega). \tag{6.7.12}$$

Consequently, the polarisation resistance is approximated to the difference between the low-frequency resistance and the high-frequency resistance,

$$R_\mathsf{pol}\,(\Omega) \;\approx\; R_\mathsf{lf}\,(\Omega) \;-\; R_\mathsf{hf}\,(\Omega). \tag{6.7.13}$$

The area-specific resistance is calculated as follows

$$R_\mathsf{ASR}\,(\mathsf{m}\Omega.\mathsf{cm}^2) \;=\; R_\mathsf{lf}\,(\Omega) \cdot A_\mathsf{act}\,(\mathsf{cm}^2) \cdot 1000\;\;\mathsf{m}\Omega/\Omega. \tag{6.7.14}$$

Also, the estimated value of the slope of the polarisation curve (section 6.7.11) may be used in place of R_lf to calculate R_ASR according to equation (6.7.14).

Guidance on EIS measurements (Siracusano *et al.*, 2018, Szekeres *et al.*, 2021) is provided by clause 10.7.2.2 of IEC 62282-7-2:2014 (IEC, 2014b) and clause 6.3.10 of IEC 62282-8-101:2020 (IEC, 2020c) while guidance on post processing of EIS data is provided by clause 7.6.3 of IEC 62282-8-101:2020 (IEC, 2020c). Note, useful software tools to perform such data post-processing are listed in term 403 on p. 66 (online version) of the recently published electrolysis terminology document (Malkow *et al.*, 2021).

Further, advanced EIS data analysis includes the method of distribution of uncorrelated relaxation times (DRT) (Boukamp, 2020) for detecting better resolved time constants (relaxation times) without explicit assumptions except for the applicability of the principle of superposition (**4.2.64**). Primarily, DRT analysis provides for the total number and the values of relaxation times being the time constants of relaxation phenomena occurring in WECs due to heat and species transport (conduction, convection, diffusion, migration, reaction, etc). Significant changes in these parameters upon prolonged in-stack exposure of a WEC under normal operating conditions or stressing operating conditions may occur due to degradation. Further, the number of time constants in the equivalent electric circuit (EEC) model should necessarily match the number of relaxation times unambiguously identified by DRT analysis. Also, the polarisation resistance is the area under the graph of the DRT (Malkow, 2019). Depending on the EIS data, the value of the DRT function can be real or complex (Malkow, 2021) ([36]).

Advantageously, the determined values of the time constants and the polarisation resistance may serve as initial start values for subsequent complex non-linear least squares (CNLS) fitting of the measured EIS data to a suitable EEC model simulating the observed WEC electrical impedances (Boukamp, 2004, Macdonald and Potter, 1987, Boukamp, 1986). This type of data post-processing, also known as parameter identification, may eventually identify WEC parameters as values of sought microscopic quantities (diffusion coefficients, permeabilities, reaction rates, etc). A simplified EEC model of an electrolyser connected to a DC source is presented in Figure 6.3 (Chen *et al.*, 2022).

([36]) Unfortunately, software codes to determine complex-valued DRT are not available to-date. Also, a theory of DRT functions with correlated relaxation times representative of interdependent (hierarchical, interacting, coupled or cooperative), spatially distributed or delayed polarisation processes (resistive-capacitive or resistive-inductive) prevailing in electrochemical cells (**4.2.32**) including WECs is yet missing.

Figure 6.3: Simplified EEC model of an electrolyser connected to a DC source; $C_{dl,a}$, $C_{dl,c}$, $R_{ct,a}$ and $R_{ct,c}$ are the temperature-dependent anodic double layer capacitance, cathodic double layer capacitance, anodic charge transfer resistance and cathodic charge transfer resistance, respectively and R_Ω is the temperature-dependent ohmic resistance.
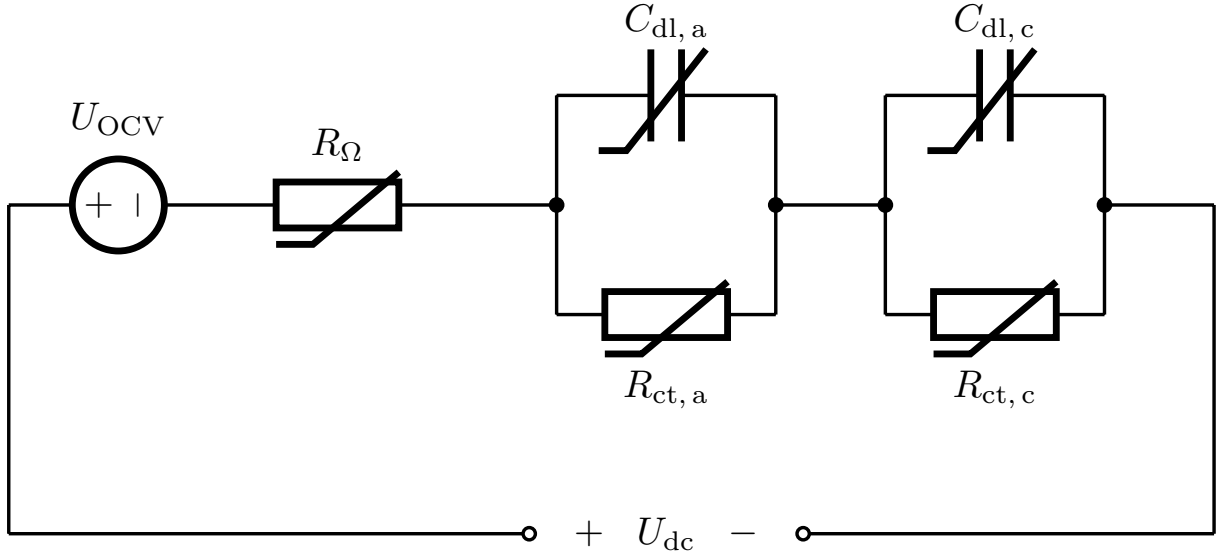
The anodic double layer capacitance, cathodic double layer capacitance, anodic charge transfer resistance and cathodic charge transfer resistance are calculated as follows

$$C_{dl,a}(T) \text{ (mF)} = \frac{\varepsilon(T) \text{ (F/m)} \cdot A_{act} \text{ (cm}^2)}{d_{dl} \text{ (nm)}} \cdot 10^5 \text{ cm}^2\text{/nm/m} \cdot 10^{-3} \text{ mF/F}, \tag{6.7.15a}$$

$$C_{dl,c}(T) \text{ (mF)} = \frac{\varepsilon(T) \text{ (F/m)} \cdot A_{act} \text{ (cm}^2)}{d_{dl} \text{ (nm)}} \cdot 10^5 \text{ cm}^2\text{/nm/m} \cdot 10^{-3} \text{ mF/F}, \tag{6.7.15b}$$

$$R_{ct,a}(T) \text{ (}\Omega\text{)} = \frac{R_g \text{ (J/(mol K))} \cdot T \text{ (K)}}{z \cdot F \text{ (C/mol)} \cdot I_{0,a}(T) \text{ (A)}} \text{ and} \tag{6.7.15c}$$

$$R_{ct,c}(T) \text{ (}\Omega\text{)} = \frac{R_g \text{ (J/(mol K))} \cdot T \text{ (K)}}{z \cdot F \text{ (C/mol)} \cdot I_{0,c}(T) \text{ (A)}}; \tag{6.7.15d}$$

ε is the absolute permittivity of the double layer having length d_{dl}.

6.7.13 Efficiency determination

The energy efficiency based on HHV under SATP conditions of hydrogen ($\eta^0_{HHV,e}$), the energy efficiency based on LHV under SATP conditions of hydrogen ($\eta^0_{LHV,e}$), the electrical efficiency based on HHV under SATP conditions of hydrogen ($\eta^0_{HHV,el}$) and the electrical efficiency based on LHV under SATP conditions of hydrogen ($\eta^0_{LHV,el}$) of a WE stack shall be determined applying the recently published energy performance testing procedure (Malkow and Pilenga, 2023a) under the same test and operating conditions as applied in the polarisation curve measurements. These four efficiencies are defined as

$$\eta^0_{HHV,e} \text{ (\%)} = \frac{q_{n,H_2} \text{ (mol/h)} \cdot HHV_{H_2} \text{ (kWh/mol)}}{P_{el,dc} \text{ (kW)} + P_{th} \text{ (kW)} + P_{compr} \text{ (kW)}} \cdot 100 \text{ \%}, \tag{6.7.16a}$$

$$\eta^0_{LHV,e} \text{ (\%)} = \frac{q_{n,H_2} \text{ (mol/h)} \cdot LHV_{H_2} \text{ (kWh/mol)}}{P_{el,dc} \text{ (kW)} + P_{th} \text{ (kW)} + P_{compr} \text{ (kW)}} \cdot 100 \text{ \%}, \tag{6.7.16b}$$

$$\eta^0_{HHV,el} \text{ (\%)} = \frac{q_{n,H_2} \text{ (mol/h)} \cdot HHV_{H_2} \text{ (kWh/mol)}}{P_{el,dc} \text{ (kW)}} \cdot 100 \text{ \% and} \tag{6.7.16c}$$

$$\eta^0_{LHV,el} \text{ (\%)} = \frac{q_{n,H_2} \text{ (mol/h)} \cdot LHV_{H_2} \text{ (kWh/mol)}}{P_{el,dc} \text{ (kW)}} \cdot 100 \text{ \%}; \tag{6.7.16d}$$

HHV_{H_2} = 79,4 kWh/mol and LHV_{H_2} = 67,2 kWh/mol are respectively the higher heating value and the lower heating value of hydrogen under SATP conditions (Tsotridis and Pilenga, 2018).

6.8 Operation profiles

6.8.1 General

Operation profiles, whether profiles of the input electric power, input direct current or input DC voltage versus time (t), are intended to simulate, under given test conditions (section 6.3), stack operation for use in the application concerned. Apart from simulated operation profiles (Alia *et al.*, 2019, Allidières *et al.*, 2019, Aßmann *et al.*, 2020, Tsotridis and Pilenga, 2021, Malkow and Pilenga, 2023b, Reissner *et al.*, 2020), this includes real-world operation profiles (duty cycles) derived from RES-based power profiles typical for the intermittent supply of electricity to a WE system by various RES types, namely PV power (**4.2.59**) and wind power (**4.2.80**).

Herein, we use open data of the Belgian electricity grid with a 15 minutes time resolution (Elia Transmission Belgium SA, 2023) by normalising the measured electric power (P_{el}) by the monitored peak electric power to derive operation profiles for PV electric power (Figure 6.4 and Figure 6.5) and wind turbine (WT) electric power (Figure 6.6 and Figure 6.7).

For testing, the derived profiles are expressed in terms of input electric power or translated into input current using a typical value of rated voltage or translated into input voltage using the rated current. The time interval of a profile (duty cycle) is usually a fixed period comprising the time required to carry out a given number of consecutive profiles of the same type or a sequence of profiles of different types. Thus, individual profiles (duty cycles) may constitute building blocks of a test sequence specified in the test plan (section 6.6).

6.8.2 Graphical representation

Figure 6.4 shows graphical representations of daily operation profiles (normalised set point versus duration) derived from PV electric power for two randomly selected summer and winter weeks in Brussels. Figure 6.5 shows the graphical representation of an operation profile for one randomly selected year of PV electric power.

Figure 6.6 shows the graphical representation of daily operation profiles derived from onshore WT electric power in Flanders and offshore WT electric power in Belgium for the same two summer and winter weeks as selected in Figure 6.4. These profiles may likewise be used as building blocks for a sequence of operation profiles to test a WE stack supplied by WT electric power. Figure 6.7 shows the graphical representation of an operation profile for one year of onshore and offshore WT electric power, which includes the four weekly operation profiles presented in Figure 6.6.

Figure 6.4: Daily operation profiles derived from weekly PV electric power for WE stack testing. The four weeks are random selections. They are part of the year selected in Figure 6.5.
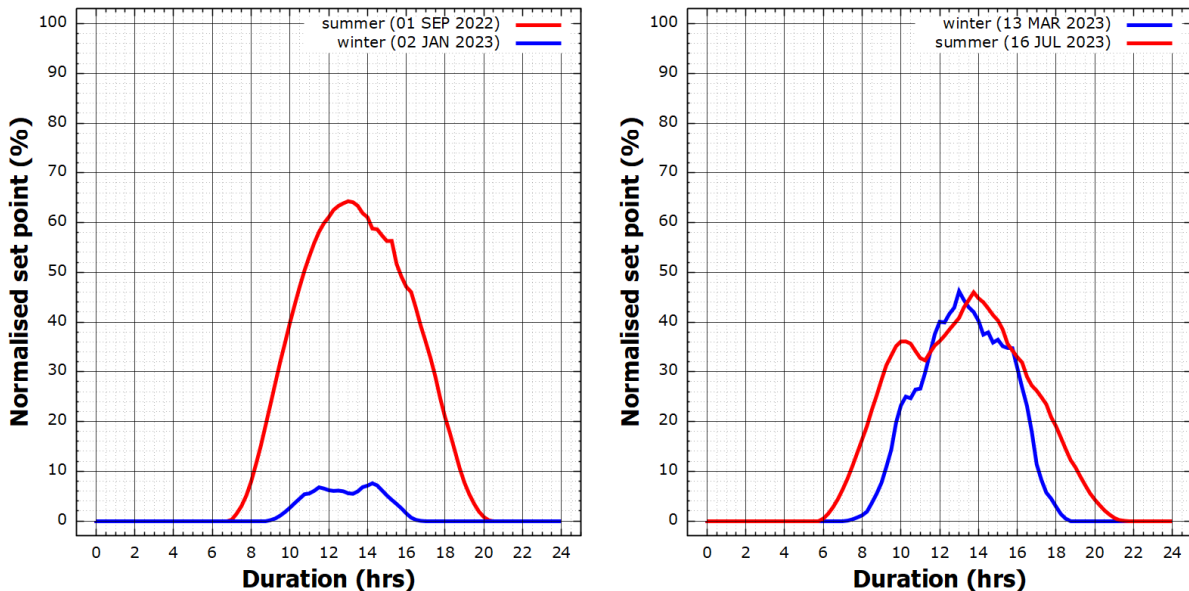
Continue to next page

38
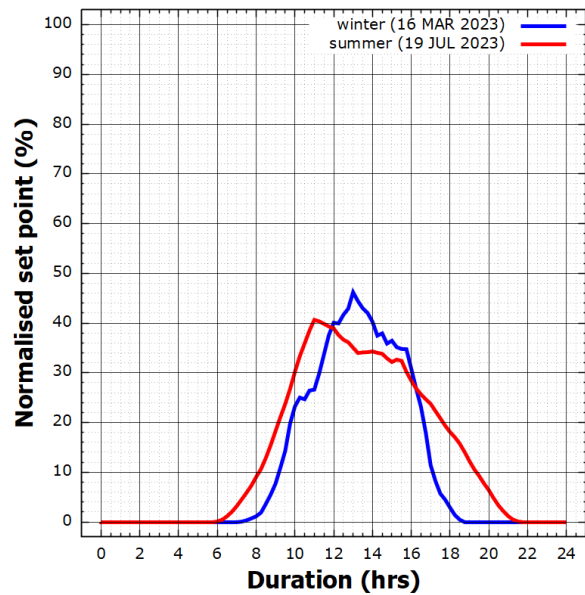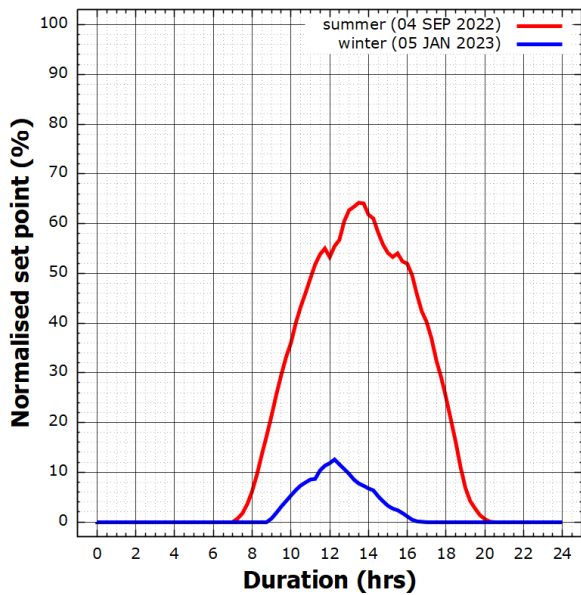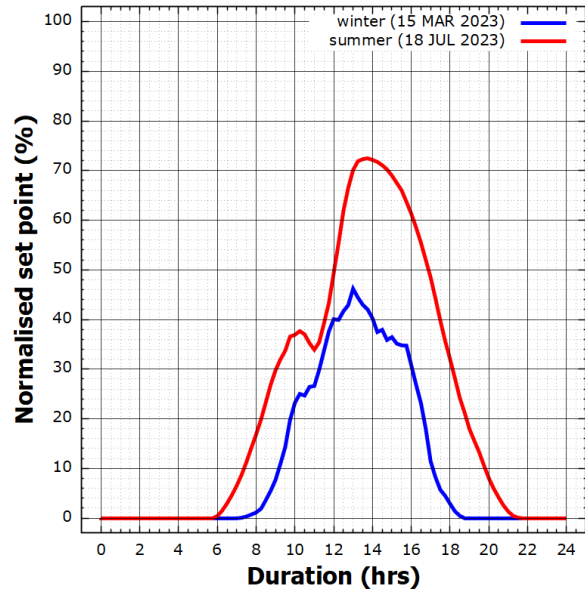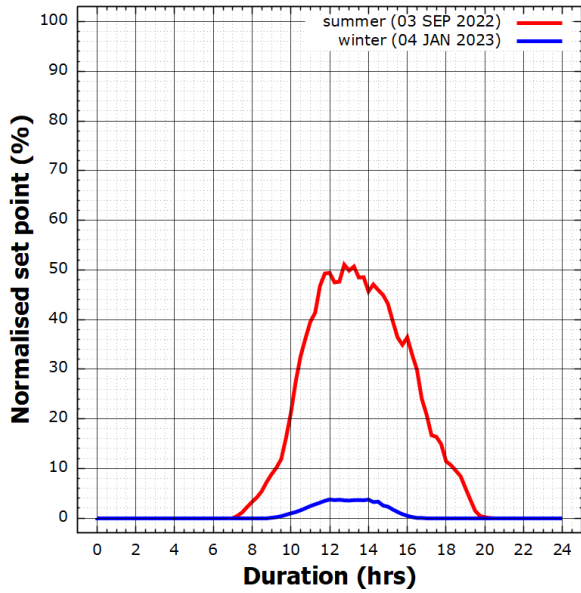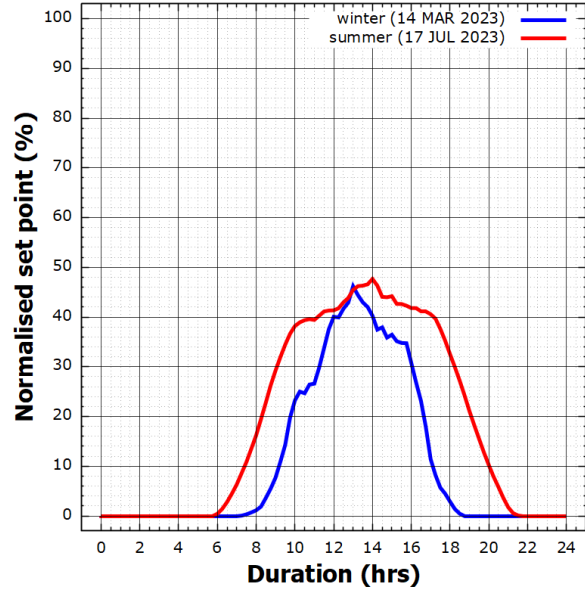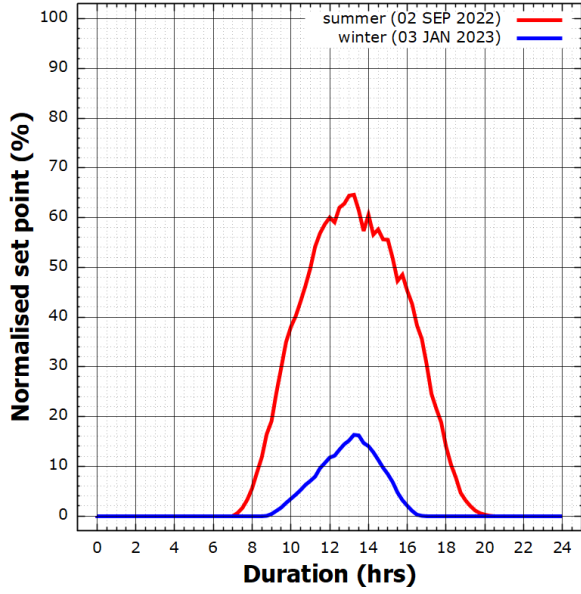
Figure 6.4 – continued from previous page

Figure 6.4 – continued from previous page

Source: JRC, 2023 (Malkow, 2023a).
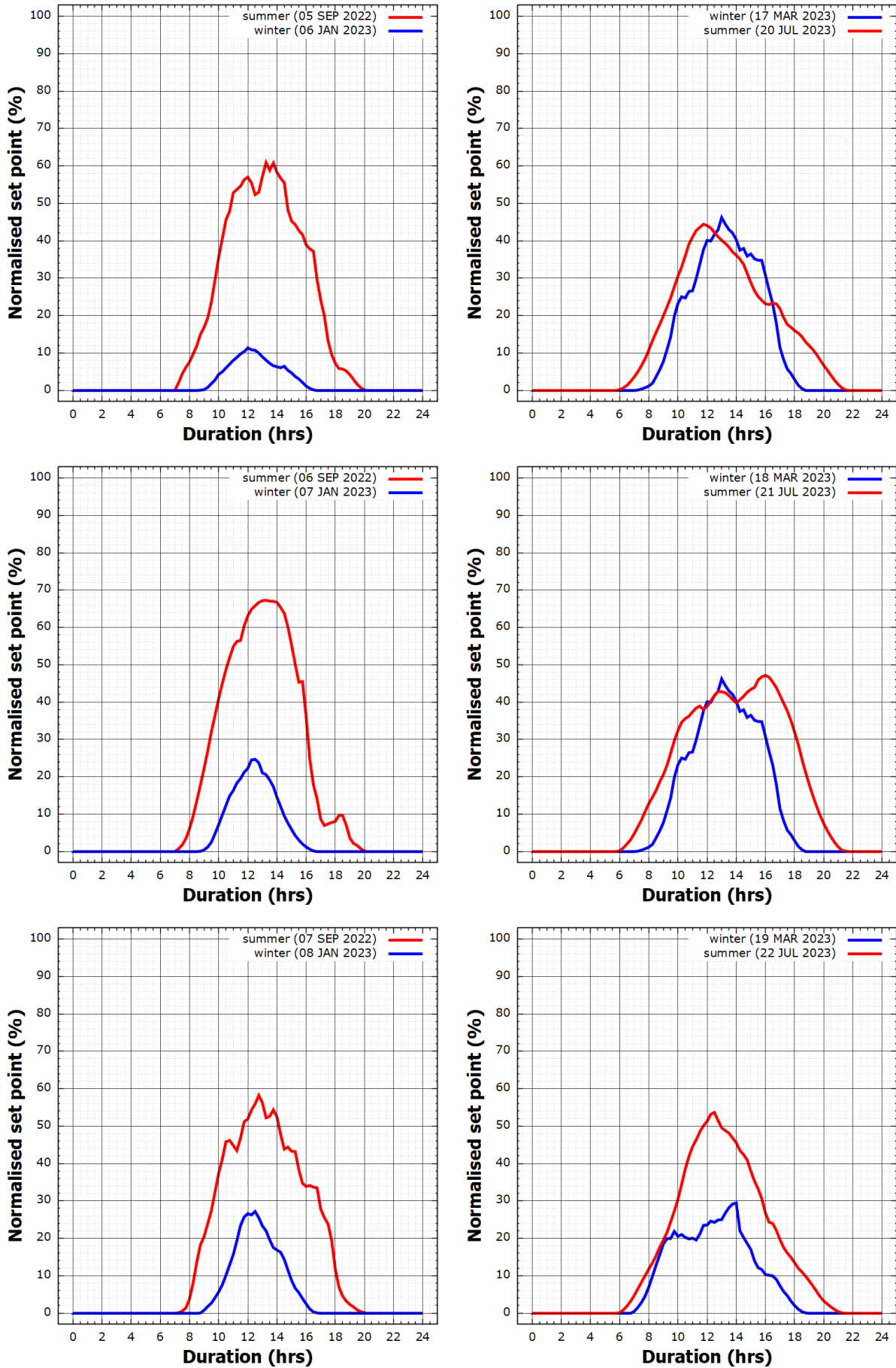
40

Figure 6.5: Operation profile derived from one year PV electric power for long-term WE stack testing. The year with its start and end dates is a random selection.
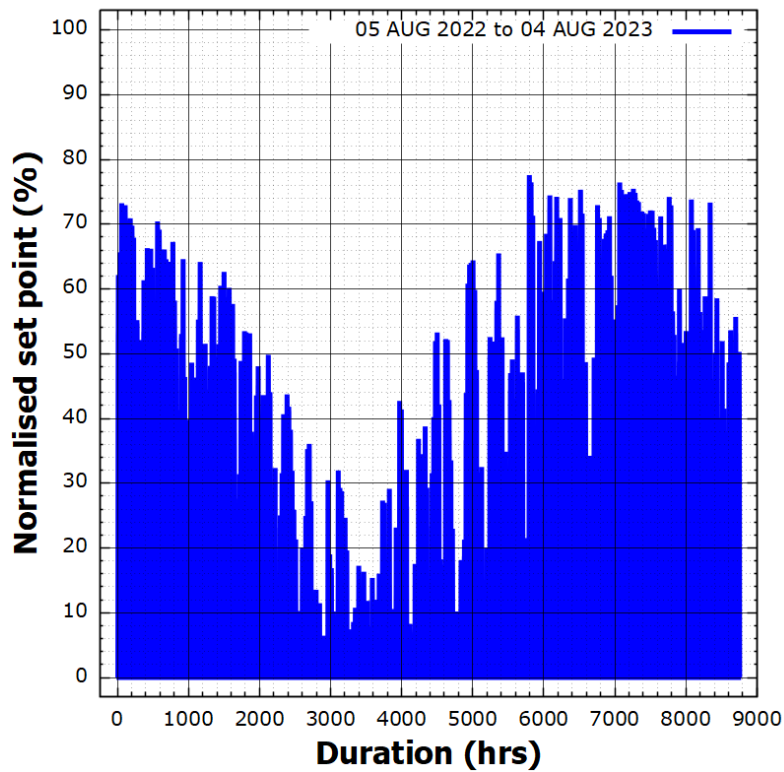
Source: JRC, 2023 (Malkow, 2023a).

Figure 6.6: Daily operation profiles derived from weekly onshore and offshore WT electric power for WE stack testing. The same four summer and winter weeks as in Figure 6.4 were used.
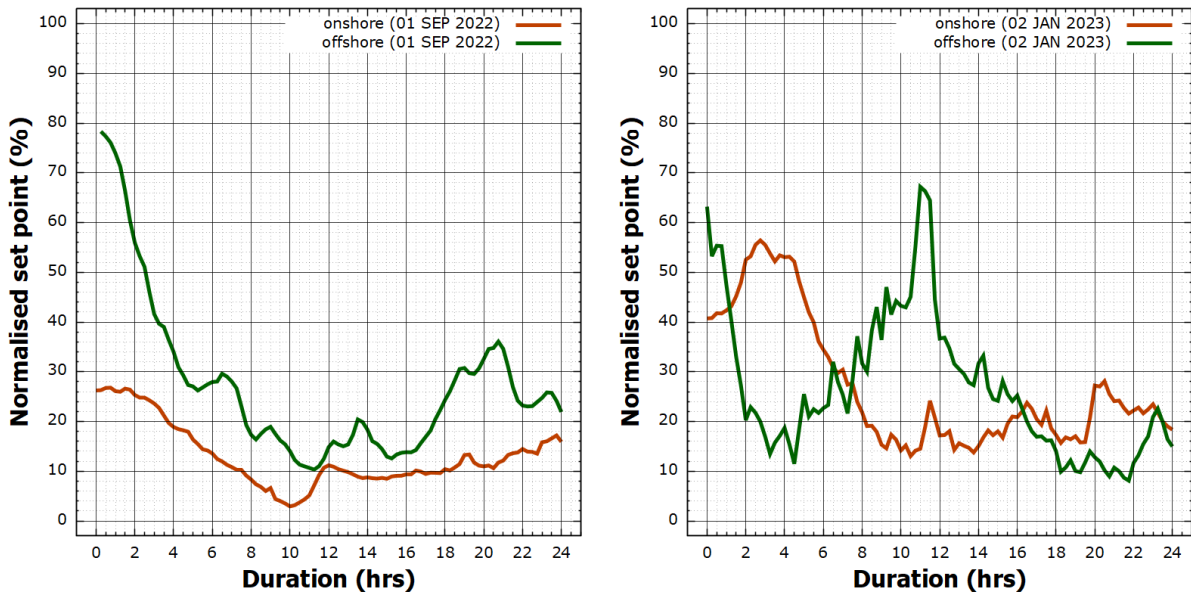
Continue to next page
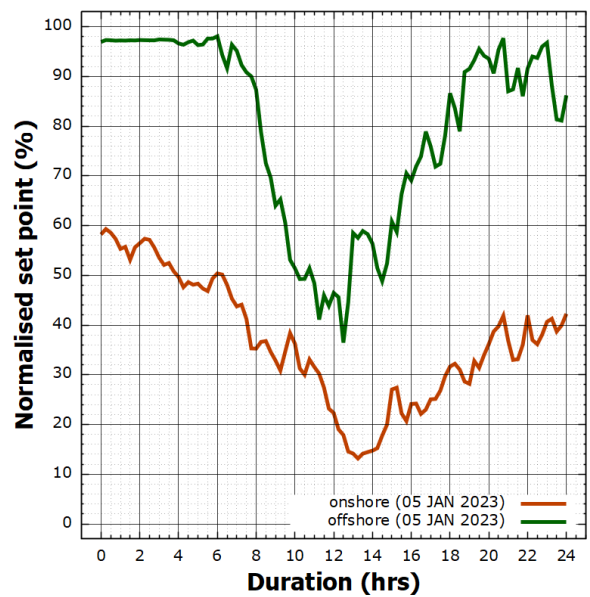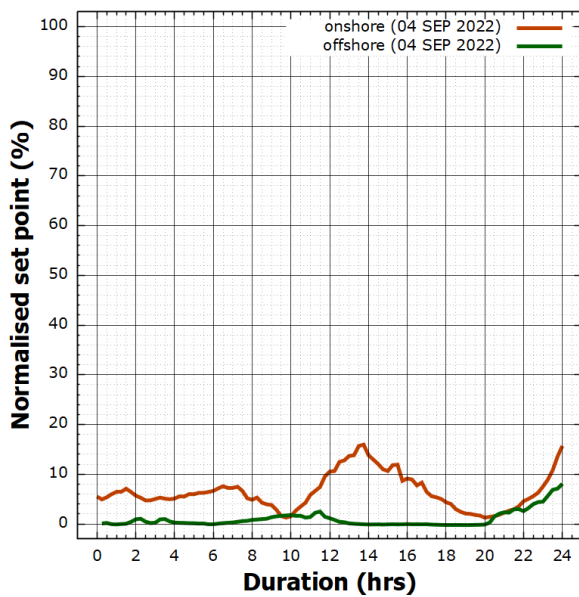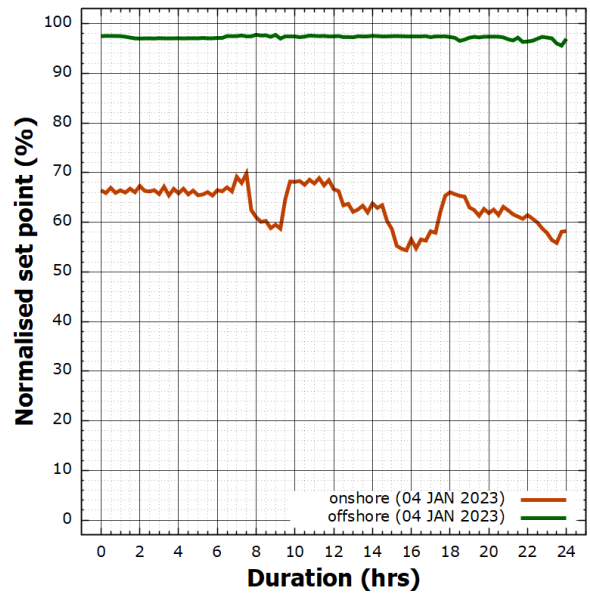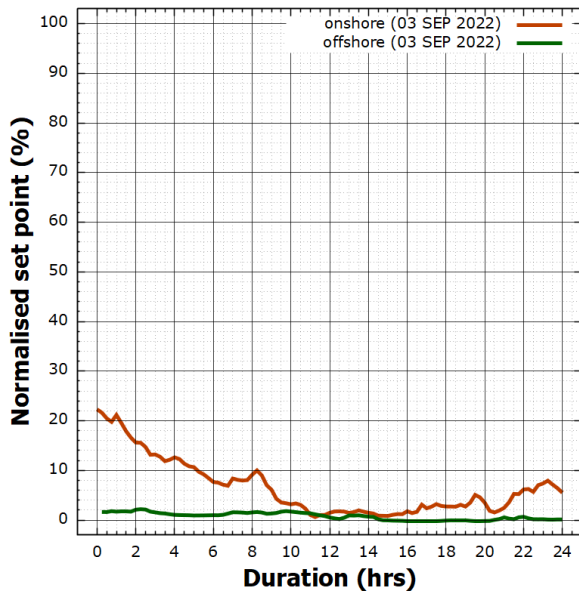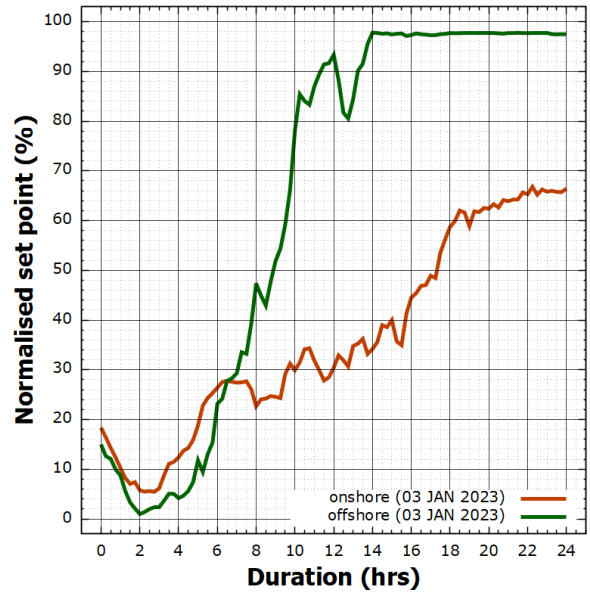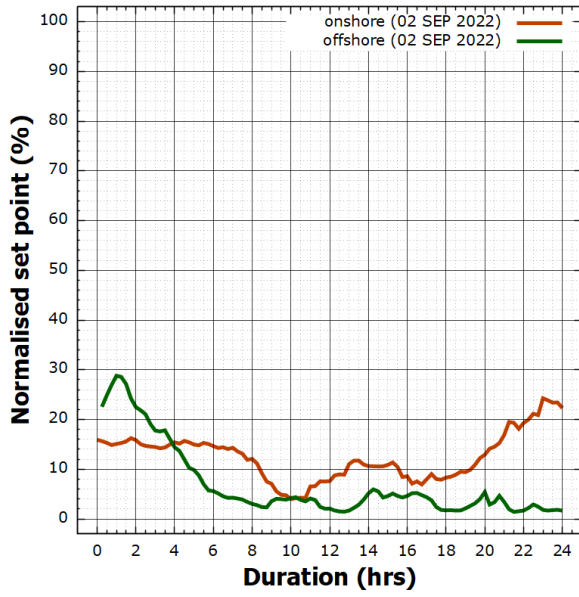
41
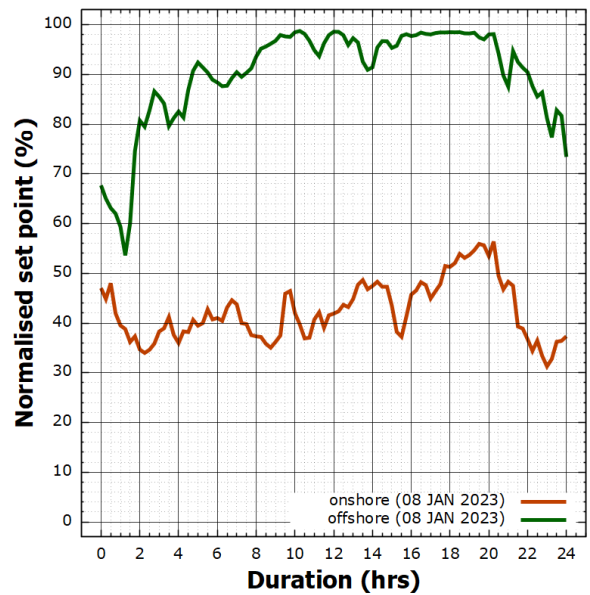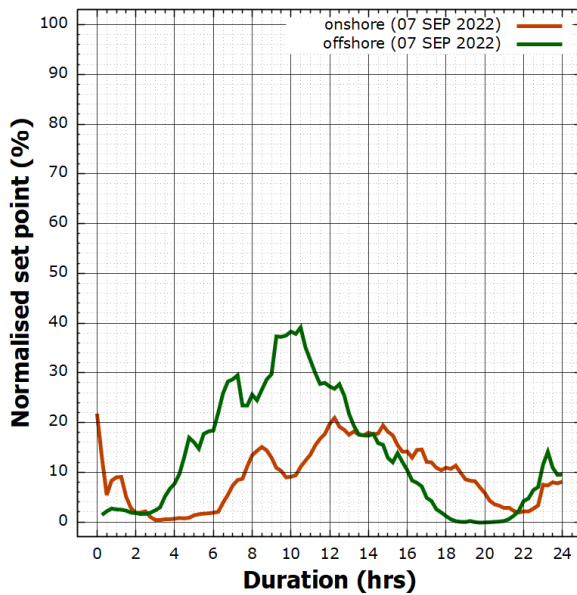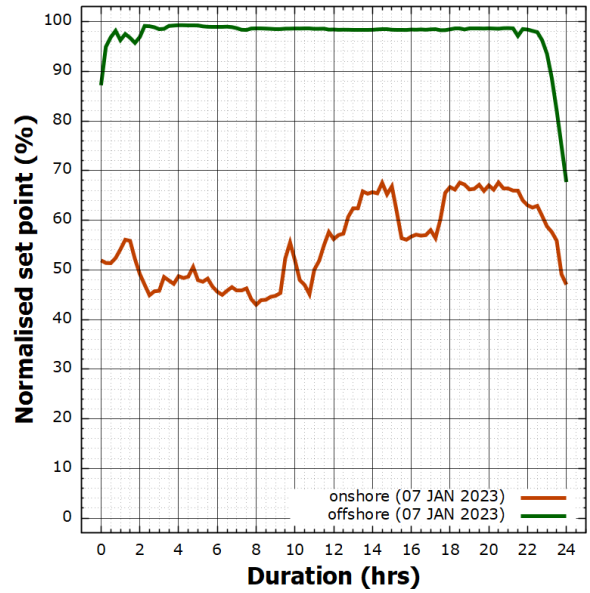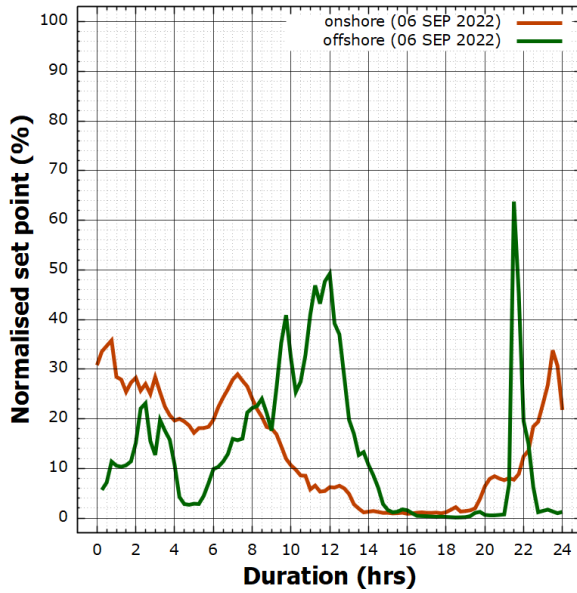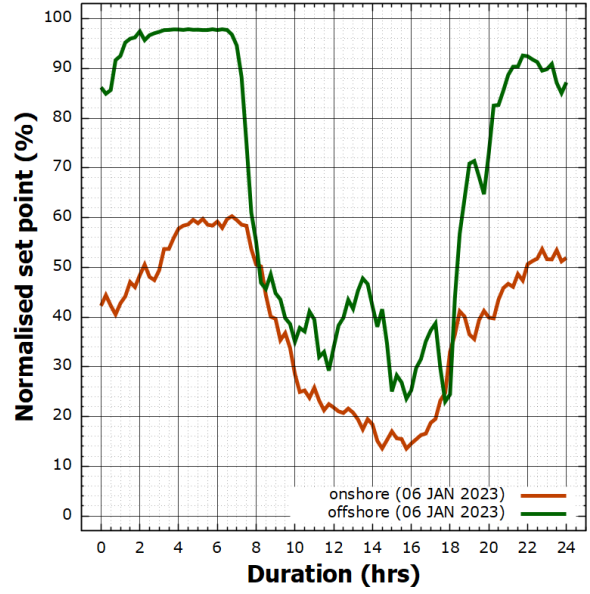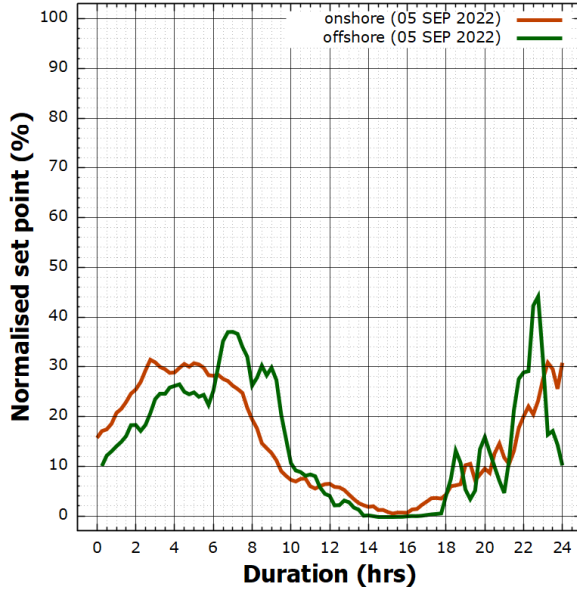
Figure 6.6 – continued from previous page
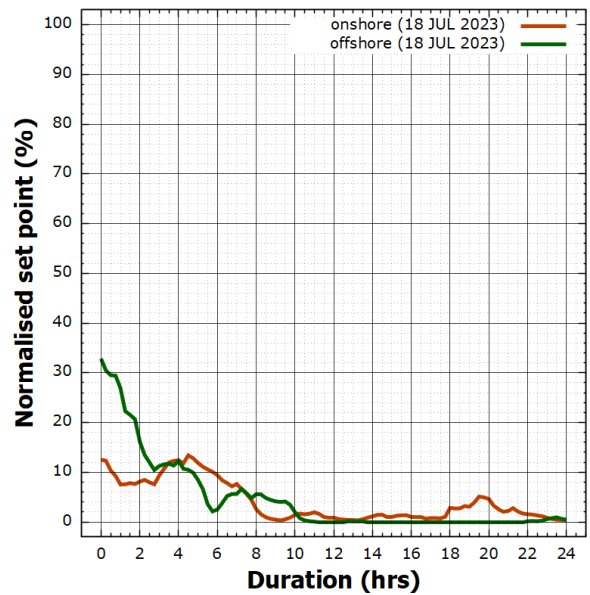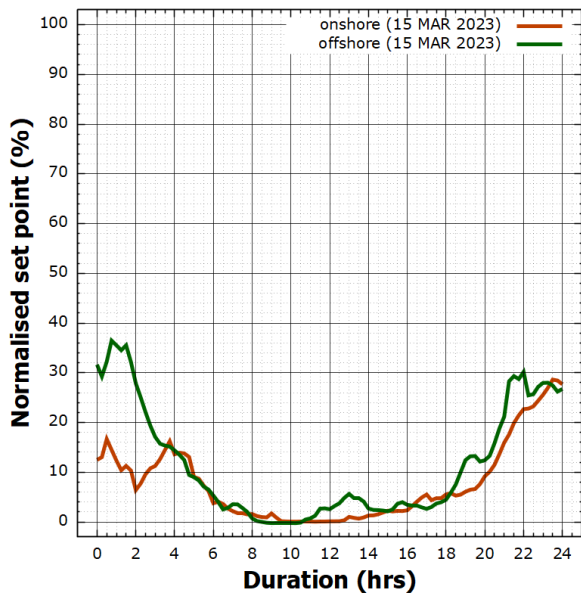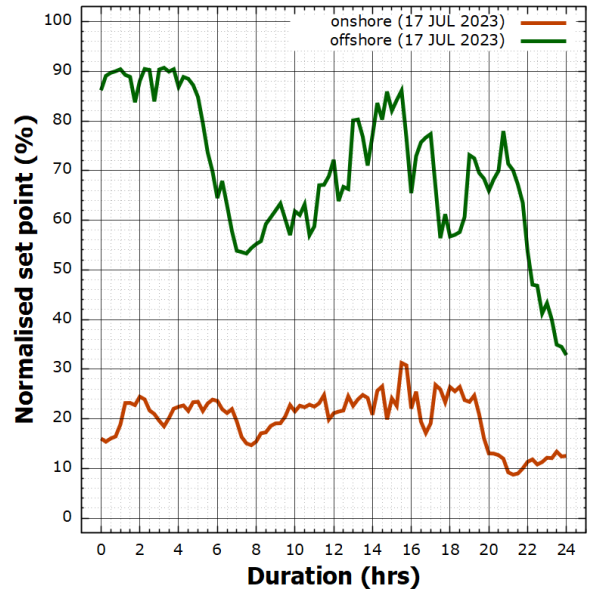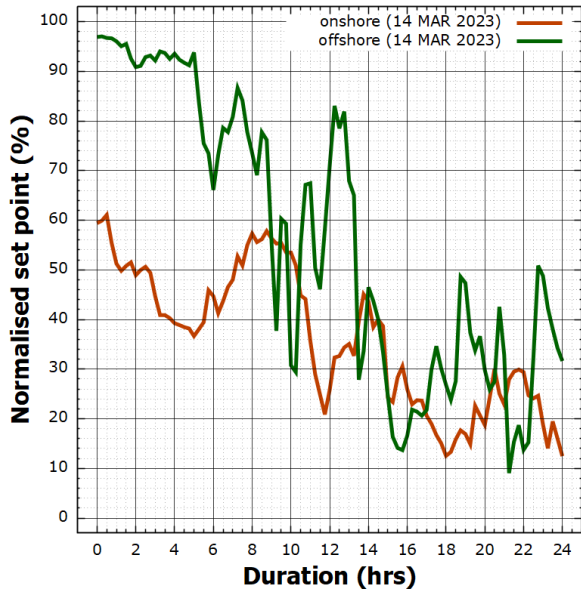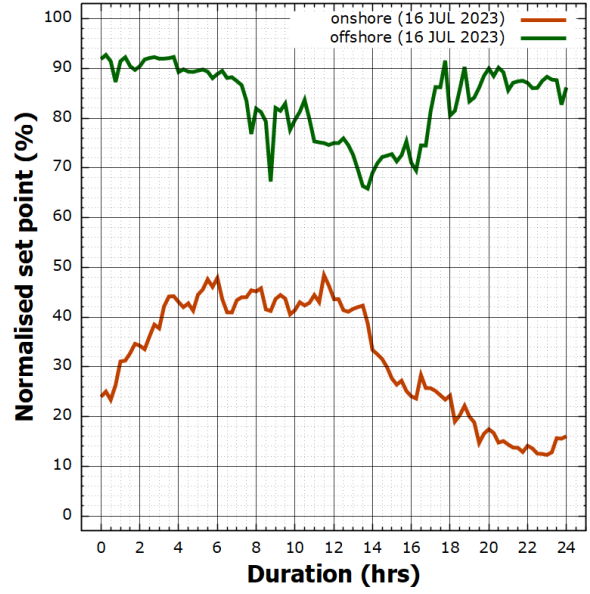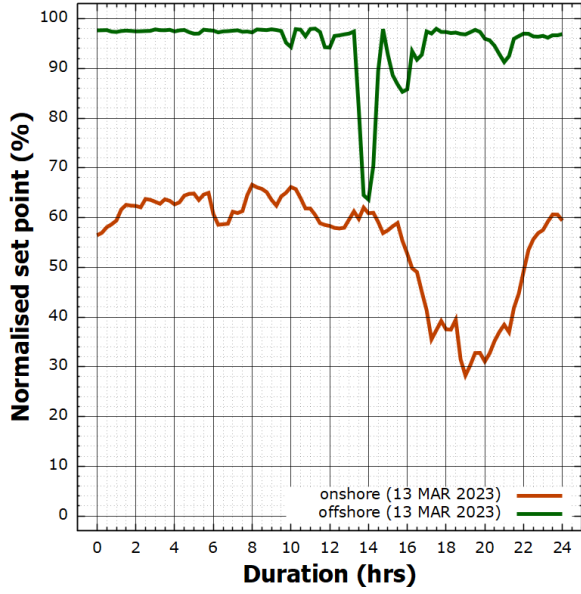
Figure 6.6 – continued from previous page

Figure 6.6 – continued from previous page
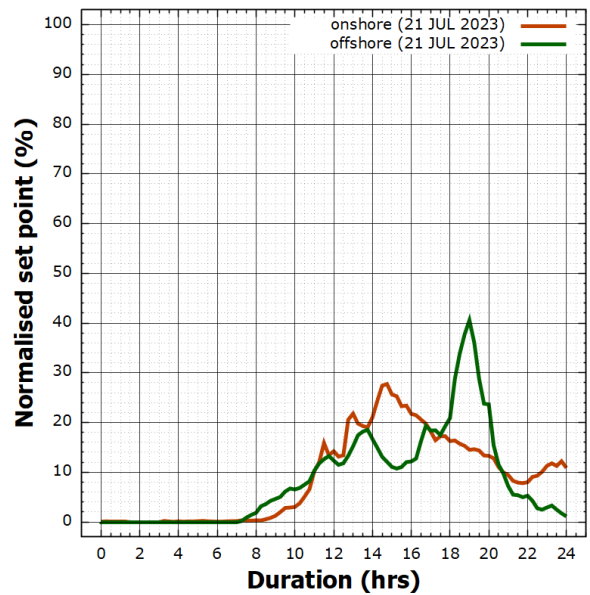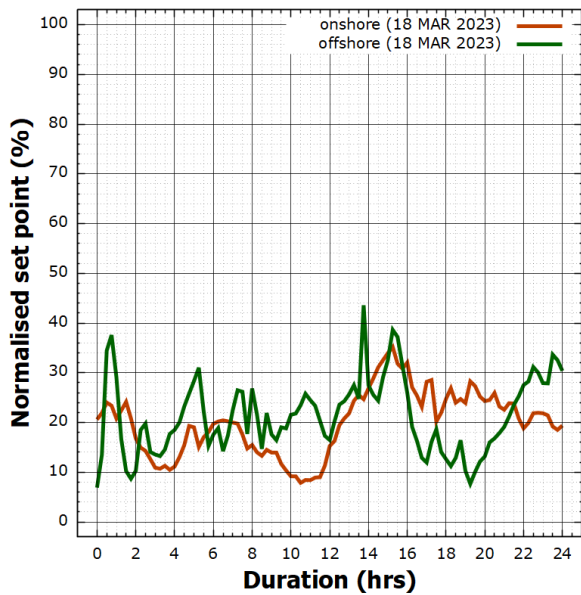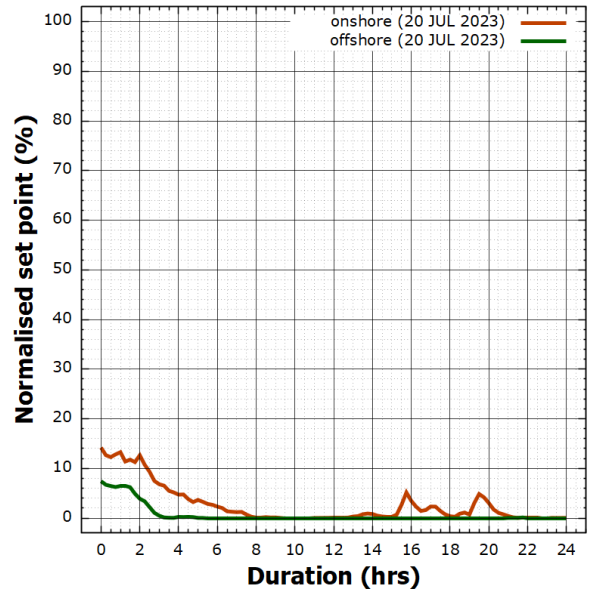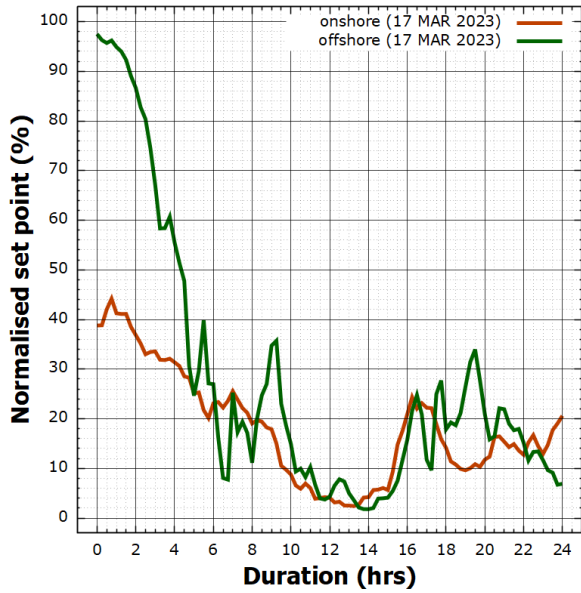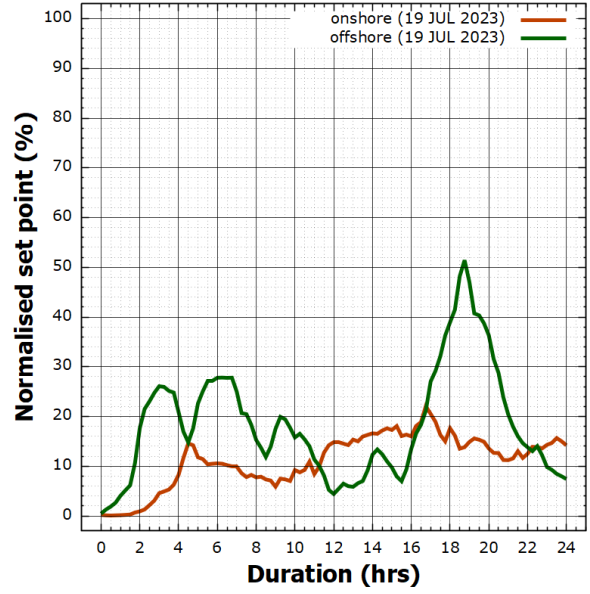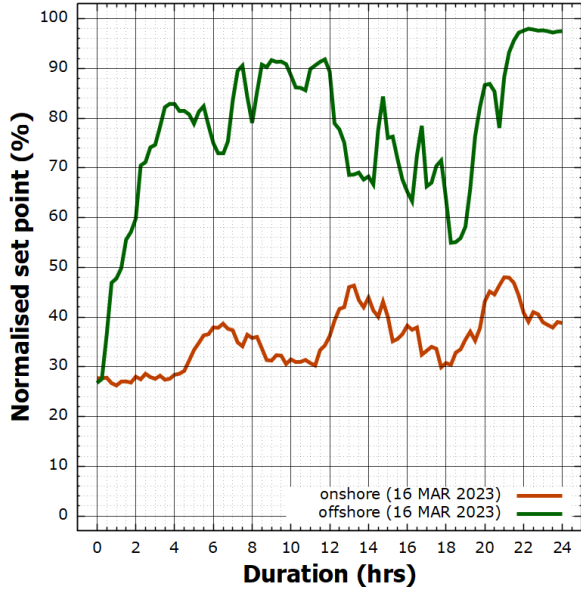
Figure 6.6 – continued from previous page

Figure 6.6 – continued from previous page
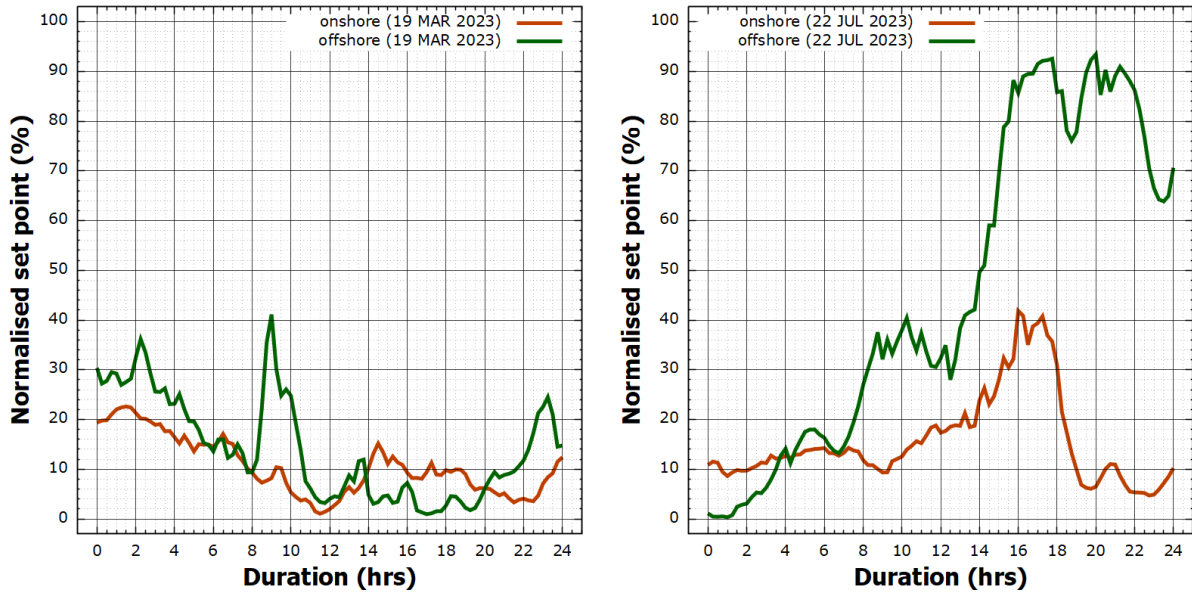
Figure 6.7: Operation profile derived from one year onshore and offshore WT electric power for long-term WE stack testing. The start and end dates are the same as in Figure 6.5.
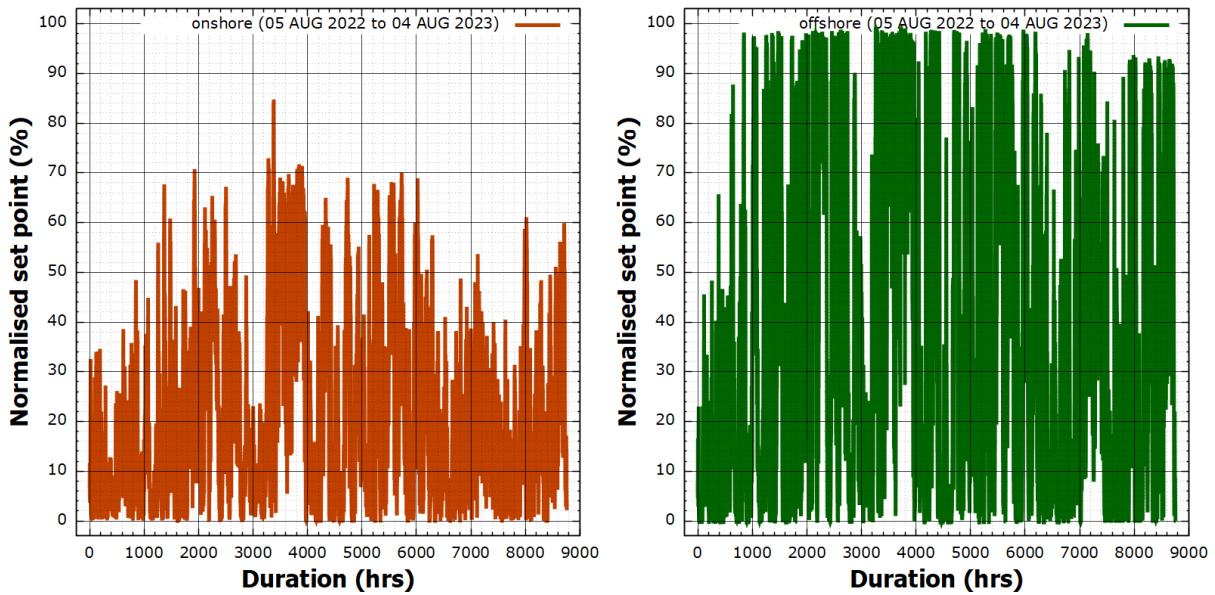
In Figure 6.4 to Figure 6.7, the normalised set point is either the ratio of the specified input

- electric power to its nominal (rated) value ($P_{\text{el, nom}}$) specified by the manufacturer, namely

$$\text{Normalised electric power set point (\%)} = \frac{P_{\text{el, in}}\ (\text{kW})}{P_{\text{el, nom}}\ (\text{kW})} \cdot 100\ \%,$$

- current to its nominal (rated) value (I_{nom}) specified by the manufacturer, namely

$$\text{Normalised current set point (\%)} = \frac{I_{\text{in}}\ (\text{A})}{I_{\text{nom}}\ (\text{A})} \cdot 100\ \%\ \text{ or}$$

- voltage to its nominal (rated) value (U_{nom}) specified by the manufacturer, namely

$$\text{Normalised voltage set point (\%)} = \frac{U_{\text{in}}\ (\text{kV})}{U_{\text{nom}}\ (\text{kV})} \cdot 100\ \%.$$

46

The operation profiles displayed in Figure 6.4 to Figure 6.5 should only be applied where the specification of the WE stack by the manufacturer allow operation at zero input electric power or zero input current. If not, the profiles should be adapted accordingly, for example, by adding a positive offset.

In an AST campaign, the daily operation profiles displayed in Figure 6.4 and Figure 6.6 may be combined and used together with appropriate compression factors as building blocks for one or other sequence of operation profiles forming simulated duty cycles to test WE stacks supplied by fluctuating RES-derived electricity stemming from variable PV electric power and/or WT electric power.

Similarly, the yearly operation profiles displayed in Figure 6.5 and Figure 6.7 may also be combined using appropriate compression factors for accelerated stress testing of WE stacks. Without any compressed duration, these profiles could also serve in accelerated lifetime testing of WE stacks.

6.9 Durability tests

6.9.1 General

Durability tests (**4.2.28**) on WE stacks evaluate the ability of the stack to maintain its performance characteristics under specified test conditions for a given time interval ([37]) either at constant "steady-state" operation (section 6.9.2) or variable operation (section 6.9.3). Combinations of both modes of operation typical for a stack in a given application are possible. Preferably, the original duration of each interval comprises one thousand or more hours of stack operation.

In addition to performance tests at BoT and EoT, performance tests (section 6.7) may, as an option, be conducted intermittently at intervals (k=1,2,...) to determine one or more KPIs. Importantly, BoT should not be BoL for a stack. The stack should operate for a sufficient long period recommended by the manufacturer with a minimum of 1000 hours of operation in order to overcome the phase of possible initial high degradation, which is common after operating the stack for the first time.

The inability of a stack to maintain its performance characteristics during durability testing in accordance with a specified stop criterion is considered a stack failure.

6.9.2 Constant stack operation

Durability testing of a WE stack under constant current or constant voltage should be conducted in accordance with clause 7.3 of IEC 62282-8-102:2019 (IEC, 2019b).

Constant stack operation is performed by two similar methods namely

Method A) Constant current method by setting the current to its specified value according to the test plan (section 6.6) and maintain it until the stack voltage is stabilised within ± 5 mV for every cell in the stack upon which the test is carried out for its specified duration (section 6.6) while recording the current, stack voltage and stack operating temperature as minimum.

Method B) Constant voltage method by setting the stack voltage to its specified value according to the test plan (section 6.6) and maintain it until the current has stabilised within ± 2 % upon which the test is carried out for its specified duration (section 6.6) while recording the current, stack voltage and stack operating temperature as minimum.

6.9.3 Variable stack operation

Durability testing of a WE stack under variable power, current or voltage using operation profiles (section 6.8) should be conducted in accordance with clause 7.4 of IEC 62282-8-102:2019 (IEC, 2019b).

The test is carried out by setting the specified test conditions (section 6.3) including stressing operating conditions (section 6.5) to the stack and maintain these conditions either for a specified duration or until a specified voltage is obtained according to the test plan (section 6.6) while applying the operation profiles to the stack. As minimum, the current, stack voltage and stack operating temperature shall be recorded throughout the test.

6.10 Determination of KPIs

For a given stack current density (J_{stack}), stack operating temperature (T_{stack}) and pressure of hydrogen (p_{H_2}), the durability of a WE stack at an elapsed time interval t_k is assessed from the difference (deviation) of the

---

([37]) The interval may comprise a specified duration or the time required to complete a given number or sequence of operation profiles (duty cycles).

stack voltage at that instant, $U(t_k)$ and the stack voltage at t_0, $U(t_0)$, by calculating the total rate of change of voltage ($\Delta_{\text{tot}}^k U$), whether positive (degradation) or negative (improvement), as follows ([38])

$$\Delta_{\text{tot}}^k U \ (\mu\text{V/h}) \ = \ \frac{U(t_k) \ (\text{kV}) \ - \ U(t_0) \ (\text{kV})}{t_k \ (\text{h}) \ - \ t_0 \ (\text{h})} \cdot f_{\text{compr}} \cdot 10^9 \ \mu\text{V/kV};\tag{6.10.1}$$

t_k is the time elapsed from BoT at t_0 until the time at the end of interval k whether for constant stack operation (section 6.9.2) or variable stack operation (section 6.9.3). At both instants, t_0 and t_k, the stack voltages shall be determined from polarisation curve measurements (section 6.7.11) conducted under galvanostatic conditions. The stack current density is usually the one occurring at the thermal-neutral voltage of the stack when operated under given conditions of temperature and pressure of hydrogen at BoT. But it may, according to the test plan, be the stack current density occurring at a stack voltage different from the thermal-neutral voltage ([39]).

The relative rate of change of voltage ($\Delta_{\text{rel}}^k U$) corresponding to a minimum of one thousand hours of stack operation times the compression factor ([40]), whether positive (degradation) or negative (improvement), is calculated as follows (McPhail *et al.*, 2022)

$$\Delta_{\text{rel}}^k U \ (\%) \ = \ \left(\frac{U(t_k) \ (\text{kV})}{U(t_0) \ (\text{kV})} \ - \ 1 \right) \cdot \frac{1000 \ (\text{h}) \cdot f_{\text{compr}}}{t_k \ (\text{h})} \cdot 100 \ \%.\tag{6.10.2}$$

Multiplying the total rate of change of voltage by the direct current at which the stack voltages, $U(t_k)$ and $U(t_0)$, were determined in polarisation curve measurements, the total rate of change of power ($\Delta_{\text{tot}}^k P$) is calculated, whether positive (degradation) or negative (improvement), as follows

$$\Delta_{\text{tot}}^k P \ (\text{mW/h}) \ = \ \frac{P(t_k) \ (\text{kW}) \ - \ P(t_0) \ (\text{kW})}{t_k \ (\text{h}) \ - \ t_0 \ (\text{h})} \cdot f_{\text{compr}} \cdot 10^6 \ \text{mV/kV}\tag{6.10.3}$$

where the power at t_k and t_0, $P(t_k)$ and $P(t_0)$, are calculated as follows

$$P(t_k) \ (\text{kW}) = \ U(t_k) \ (\text{kV}) \cdot I_{\text{dc}}(t_k) \ (\text{A}) \ \text{and}\tag{6.10.4a}$$

$$P(t_0) \ (\text{kW}) = \ U(t_0) \ (\text{kV}) \cdot I_{\text{dc}}(t_0) \ (\text{A});\tag{6.10.4b}$$

$I_{\text{dc}}(t_k)$ and $I_{\text{dc}}(t_0)$ is the direct current at t_k and t_0, respectively. In principle, the current applied during the polarisation curve measurements at t_k and t_0 should be the same but measured current values may eventually deviate slightly from this assumption. Accordingly, the relative rate of change of power ($\Delta_{\text{rel}}^k P$) is calculated, whether positive (degradation) or negative (improvement), as follows

$$\Delta_{\text{rel}}^k P \ (\%) \ = \ \left(\frac{P(t_k) \ (\text{kW})}{P(t_0) \ (\text{kW})} \ - \ 1 \right) \cdot \frac{1000 \ (\text{h}) \cdot f_{\text{compr}}}{t_k \ (\text{h})} \cdot 100 \ \%.\tag{6.10.5}$$

Note, the total rate of change of power and the relative rate of change of power are useful KPIs when comparing performance degradation of WE stacks determined under potentiostatic conditions as oppose to the recommended galvanostatic conditions.

Importantly, equation (6.10.1) and equation (6.10.2) determine the performance degradation of a WE stack only in terms of absolute and relative voltage deviation, respectively. They do not encompass accompanying changes in the hydrogen output rate, see equation (6.7.1), due to leakage and gas crossover, if any.

Then, the performance degradation of a WE stack should also be assessed from the difference in the stack voltage at t_k normalised by the volumetric flow rate of hydrogen, see equation (6.7.2), at that instant ($q_{\text{V,H}_2}(t_k)$) and the stack voltage at t_0 normalised by the volumetric flow rate of hydrogen at the latter instant ($q_{\text{V,H}_2}(t_k)$) being the total change of voltage per unit of hydrogen volumetric flow rate ($\Delta_{q_{\text{V,H}_2}}^k U$) as well as the difference in the stack voltage at t_k normalised by the mass flow rate of hydrogen, see equation (6.7.4), at that instant ($q_{\text{m,H}_2}(t_k)$) and the stack voltage at t_0 normalised by the mass flow rate of hydrogen at the latter instant ($q_{\text{m,H}_2}(t_0)$) being the total change of voltage per unit of hydrogen mass flow rate ($\Delta_{q_{\text{m,H}_2}}^k U$) calculated, whether positive (degradation) or negative (improvement), as follows (Suermann *et al.*, 2019)

$$\Delta_{q_{\text{V,H}_2}}^k U \ (\mu\text{V/m}_{\text{H}_2}^3/\text{h}) \ = \ \left(\frac{U(t_k) \ (\text{kV})}{q_{\text{V,H}_2}(t_k) \ (\text{m}^3/\text{h})} \ - \ \frac{U(t_0) \ (\text{kV})}{q_{\text{V,H}_2}(t_0) \ (\text{m}^3/\text{h})} \right) \cdot f_{\text{compr}} \cdot 10^9 \ \mu\text{V/kV} \ \text{and}\tag{6.10.6a}$$

([38]) The SRIA 2024 and 2030 targets are 0,11 % and 0,10 % of performance degradation per one thousand hours of AWE operation. These values are 0,9 % and 0,5 % for AEMEL and 0,15 % and 0,12 % for PEMEL (see footnote 25 and Table 6.1).

([39]) In case the total rate of change of voltage is determined for more than one value of stack current density, stack operating temperature or pressure of hydrogen, appropriate indices should be added to $\Delta_{\text{tot}}^k U$ and similarly to $\Delta_{\text{rel}}^k U$ given by equation (6.10.2), $\Delta_{\text{tot}}^k P$ given by equation (6.10.3) and $\Delta_{\text{rel}}^k P$ given by equation (6.10.5),$\Delta_{q_{\text{V,H}_2}}^k U$ and $\Delta_{q_{\text{V,H}_2}}^k U$ given by equation (6.10.6) as well as $\Delta_{q_{\text{V,H}_2}}^k E$ and $\Delta_{q_{\text{V,H}_2}}^k E$ given by equation (6.10.7).

([40]) The compression factor is unity for accelerated lifetime testing.

$$\Delta^k_{q_{m,H_2}} U \ (\mu V/kg_{H_2}/h) \ = \ \left(\frac{U(t_k) \ (kV)}{q_{m,H_2}(t_k) \ (kg/h)} - \frac{U(t_0) \ (kV)}{q_{m,H_2}(t_0) \ (kg/h)} \right) \cdot f_{compr} \cdot 10^9 \ \mu V/kV. \qquad (6.10.6b)$$

As for the stack voltages used in equation (6.10.1), both type of hydrogen flow rates (section 6.7.8) are determined as average values simultaneously with their corresponding stack voltages during polarisation curve measurements. Then, the total change of energy per unit of volume of hydrogen ($\Delta^k_{q_{V,H_2}} E$) and the total change of energy per unit of mass of hydrogen ($\Delta^k_{q_{m,H_2}} E$) are calculated, whether positive (degradation) or negative (improvement), as follows

$$\Delta^k_{q_{V,H_2}} E \ (mWh/m^3_{H_2}) \ = \ \left(\frac{P(t_k) \ (kW)}{q_{V,H_2}(t_k) \ (m^3/h)} - \frac{P(t_0) \ (kW)}{q_{V,H_2}(t_0) \ (m^3/h)} \right) \cdot f_{compr} \cdot 10^6 \ mW/kW \ \ and \quad (6.10.7a)$$

$$\Delta^k_{q_{m,H_2}} E \ (mWh/kg_{H_2}) \ = \ \left(\frac{P(t_k) \ (kW)}{q_{m,H_2}(t_k) \ (kg/h)} - \frac{P(t_0) \ (kW)}{q_{m,H_2}(t_0) \ (kg/h)} \right) \cdot f_{compr} \cdot 10^6 \ mW/kW. \qquad (6.10.7b)$$

The uniformity of the performance degradation of a WE stack in terms of cell voltages may be assessed by the total rate of change of mean absolute error average cell voltage ($\Delta^k_{tot} MAE_{\overline{U_{cell}}}$), the relative rate of change of mean absolute error average cell voltage ($\Delta^k_{rel} MAE_{\overline{U_{cell}}}$), the total rate of change of standard deviation of average cell voltage ($\Delta^k_{tot} SD_{\overline{U_{cell}}}$) and the relative rate of change of standard deviation of average cell voltage ($\Delta^k_{rel} SD_{\overline{U_{cell}}}$) calculated as follows ([41])

$$\Delta^k_{tot} MAE_{\overline{U_{cell}}} \ (\mu V/h) \ = \ \frac{MAE_{\overline{U_{cell}}}(t_k) \ (mV) \ - \ MAE_{\overline{U_{cell}}}(t_0) \ (mV)}{t_k \ (h) \ - \ t_0 \ (h)} \cdot f_{compr} \cdot 10^3 \ \mu V/mV, \qquad (6.10.8a)$$

$$\Delta^k_{rel} MAE_{\overline{U_{cell}}} \ (\%) \ = \ \left(\frac{\overline{U_{cell}}(t_0) \ (V) \cdot MAE_{\overline{U_{cell}}}(t_k) \ (mV)}{\overline{U_{cell}}(t_k) \ (V) \cdot MAE_{\overline{U_{cell}}}(t_0) \ (mV)} - 1 \right) \cdot \frac{1000 \ (h) \cdot f_{compr}}{t_k \ (h)} \cdot 100 \ \%, \quad (6.10.8b)$$

$$\Delta^k_{tot} SD_{\overline{U_{cell}}} \ (\mu V/h) \ = \ \frac{SD_{\overline{U_{cell}}}(t_k) \ (mV) \ - \ SD_{\overline{U_{cell}}}(t_0) \ (mV)}{t_k \ (h) \ - \ t_0 \ (h)} \cdot f_{compr} \cdot 10^3 \ \mu V/mV \ \ and \qquad (6.10.8c)$$

$$\Delta^k_{rel} SD_{\overline{U_{cell}}} \ (\%) \ = \ \left(\frac{\overline{U_{cell}}(t_0) \ (V) \cdot SD_{\overline{U_{cell}}}(t_k) \ (mV)}{\overline{U_{cell}}(t_k) \ (V) \cdot SD_{\overline{U_{cell}}}(t_0) \ (mV)} - 1 \right) \cdot \frac{1000 \ (h) \cdot f_{compr}}{t_k \ (h)} \cdot 100 \ \%; \quad (6.10.8d)$$

$MAE_{\overline{U_{cell}}}(t_k)$, $SD_{\overline{U_{cell}}}(t_k)$ and $\overline{U_{cell}}(t_k)$ are respectively the mean absolute error of average cell voltage, standard deviation of average cell voltage and average cell voltage at t_k while $MAE_{\overline{U_{cell}}}(t_0)$, $SD_{\overline{U_{cell}}}(t_0)$ and $\overline{U_{cell}}(t_0)$ are the same quantities but at t_0. They are calculated from the cell voltages determined during polarisation curve measurements.

Further, the performance degradation of a WE stack for a given stack current density, stack operating temperature and pressure of hydrogen may be assessed by the total rate of change of area-specific resistance ($\Delta^k_{tot} R_{ASR}$) and the total rate of change of ohmic resistance ($\Delta^k_{tot} R_{\Omega}$), whether positive (degradation) or negative (improvement), calculated as follows ([42])

$$\Delta^k_{tot} R_{ASR} \ (m\Omega.cm^2/h) \ = \ \frac{R_{ASR}(t_k) \ (m\Omega.cm^2) \ - \ R_{ASR}(t_0) \ (m\Omega.cm^2)}{t_k \ (h) \ - \ t_0 \ (h)} \cdot f_{compr} \ \ and \qquad (6.10.9a)$$

$$\Delta^k_{tot} R_{\Omega} \ (m\Omega/h) \ = \ \frac{R_{\Omega}(t_k) \ (m\Omega) \ - \ R_{\Omega}(t_0) \ (m\Omega)}{t_k \ (h) \ - \ t_0 \ (h)} \cdot f_{compr}; \qquad (6.10.9b)$$

$R_{ASR}(t_k)$ and $R_{ASR}(t_0)$ are the area-specific resistances at respectively t_k and t_0 while $R_{\Omega}(t_k)$ and $R_{\Omega}(t_0)$ are the ohmic resistances at these two instants. They are determined from EIS measurements (section 6.7.12) conducted under galvanostatic conditions. The relative rate of change of area-specific resistance ($\Delta^k_{rel} R_{ASR}$) and the relative rate of change of ohmic resistance ($\Delta^k_{rel} R_{\Omega}$) corresponding to a minimum of one thousand hours of stack operation times the compression factor, whether positive (degradation) or negative (improvement), are calculated as follows

$$\Delta^k_{rel} R_{ASR} \ (\%) \ = \ \left(\frac{R_{ASR}(t_k) \ (m\Omega.cm^2)}{R_{ASR}(t_0) \ (m\Omega.cm^2)} - 1 \right) \cdot \frac{1000 \ (h) \cdot f_{compr}}{t_k \ (h)} \cdot 100 \ \% \ \ and \qquad (6.10.10a)$$

([41]) In case the total rate of change of mean absolute error average cell voltage, the relative rate of change of mean absolute error average cell voltage, the total rate of change of standard deviation of average cell voltage and the relative rate of change of standard deviation of average cell voltage are determined for more than one value of stack current density, stack operating temperature or pressure of hydrogen, appropriate indices should be added to $\Delta^k_{tot} MAE_{\overline{U_{cell}}}$, $\Delta^k_{rel} MAE_{\overline{U_{cell}}}$, $\Delta^k_{tot} SD_{\overline{U_{cell}}}$ and $\Delta^k_{rel} SD_{\overline{U_{cell}}}$ given by equation (6.10.8).

([42]) In case the total rate of change of area-specific resistance and the total rate of change of ohmic resistance are determined for more than one value of stack current density, stack operating temperature or pressure of hydrogen, appropriate indices should be added to $\Delta^k_{tot} R_{ASR}$ and $\Delta^k_{tot} R_{\Omega}$ given by equation (6.10.9) and similarly to $\Delta^k_{rel} R_{ASR}$ and $\Delta^k_{rel} R_{\Omega}$ given by equation (6.10.10).

$$\Delta_{\text{rel}}^{\,k} R_\Omega \ (\%) \ = \ \left(\frac{R_\Omega(t_k) \ (\text{m}\Omega)}{R_\Omega(t_0) \ (\text{m}\Omega)} \ - \ 1 \right) \cdot \frac{1000 \ (\text{h}) \cdot f_{\text{compr}}}{t_k \ (\text{h})} \cdot 100 \ \%. \tag{6.10.10b}$$

For a given input current (input voltage or input electric power) and stack operating temperature, the durability of a WE stack at an elapsed time interval t_k is assessed from the difference of the energy efficiency based on HHV under SATP conditions of hydrogen ($\eta_{\text{HHV,e}}^0$), the energy efficiency based on LHV under SATP conditions of hydrogen ($\eta_{\text{LHV,e}}^0$), the electrical efficiency based on HHV under SATP conditions of hydrogen ($\eta_{\text{HHV,e}}^0$) and the electrical efficiency based on LHV under SATP conditions of hydrogen ($\eta_{\text{LHV,e}}^0$) at t_k and t_0 by calculating the total rate of change of energy efficiency based on HHV under SATP conditions of hydrogen ($\Delta_{\text{tot}}^{\,k} \eta_{\text{HHV,e}}^0$), the total rate of change of energy efficiency based on LHV under SATP conditions of hydrogen ($\Delta_{\text{tot}}^{\,k} \eta_{\text{LHV,e}}^0$), the total rate of change of electrical efficiency based on HHV under SATP conditions of hydrogen ($\Delta_{\text{tot}}^{\,k} \eta_{\text{HHV,el}}^0$) and the total rate of change of electrical efficiency based on LHV under SATP conditions of hydrogen ($\Delta_{\text{tot}}^{\,k} \eta_{\text{LHV,el}}^0$), whether positive (degradation) or negative (improvement), as follows [43]

$$\Delta_{\text{tot}}^{\,k} \eta_{\text{HHV,e}}^0 \ (\%/\text{h}) \ = \ \frac{\eta_{\text{HHV,e}}^0(t_k) \ (\%) \ - \ \eta_{\text{HHV,e}}^0(t_0) \ (\%)}{t_k \ (\text{h}) \ - \ t_0 \ (\text{h})} \cdot f_{\text{compr}}, \tag{6.10.11a}$$

$$\Delta_{\text{tot}}^{\,k} \eta_{\text{LHV,e}}^0 \ (\%/\text{h}) \ = \ \frac{\eta_{\text{LHV,e}}^0(t_k) \ (\%) \ - \ \eta_{\text{LHV,e}}^0(t_0) \ (\%)}{t_k \ (\text{h}) \ - \ t_0 \ (\text{h})} \cdot f_{\text{compr}}, \tag{6.10.11b}$$

$$\Delta_{\text{tot}}^{\,k} \eta_{\text{HHV,el}}^0 \ (\%/\text{h}) \ = \ \frac{\eta_{\text{HHV,el}}^0(t_k) \ (\%) \ - \ \eta_{\text{HHV,el}}^0(t_0) \ (\%)}{t_k \ (\text{h}) \ - \ t_0 \ (\text{h})} \cdot f_{\text{compr}} \ \text{and} \tag{6.10.11c}$$

$$\Delta_{\text{tot}}^{\,k} \eta_{\text{LHV,el}}^0 \ (\%/\text{h}) \ = \ \frac{\eta_{\text{LHV,el}}^0(t_k) \ (\%) \ - \ \eta_{\text{LHV,el}}^0(t_0) \ (\%)}{t_k \ (\text{h}) \ - \ t_0 \ (\text{h})} \cdot f_{\text{compr}}; \tag{6.10.11d}$$

$\eta_{\text{HHV,e}}^0(t_k)$, $\eta_{\text{LHV,e}}^0(t_k)$, $\eta_{\text{HHV,el}}^0(t_k)$ and $\eta_{\text{LHV,el}}^0(t_k)$ are respectively the energy efficiency based on HHV under SATP conditions of hydrogen, the energy efficiency based on LHV under SATP conditions of hydrogen, the electrical efficiency based on HHV under SATP conditions of hydrogen and the electrical efficiency based on LHV under SATP conditions of hydrogen at t_k while $\eta_{\text{HHV,e}}^0(t_0)$, $\eta_{\text{LHV,e}}^0(t_0)$, $\eta_{\text{HHV,el}}^0(t_0)$ and $\eta_{\text{LHV,el}}^0(t_0)$ are these efficiencies at t_0. At both instants, t_k and t_0, these energy efficiencies are determined in accordance with section 6.7.13 during polarisation curve measurements. The relative rate of change of energy efficiency based on HHV under SATP conditions of hydrogen ($\Delta_{\text{rel}}^{\,k} \eta_{\text{HHV,e}}^0$), the relative rate of change of energy efficiency based on LHV under SATP conditions of hydrogen ($\Delta_{\text{rel}}^{\,k} \eta_{\text{LHV,e}}^0$), the relative rate of change of electrical efficiency based on HHV under SATP conditions of hydrogen ($\Delta_{\text{rel}}^{\,k} \eta_{\text{HHV,el}}^0$) and the relative rate of change of electrical efficiency based on LHV under SATP conditions of hydrogen ($\Delta_{\text{rel}}^{\,k} \eta_{\text{LHV,el}}^0$) corresponding to a minimum of one thousand hours of stack operation times the compression factor are calculated, whether positive (degradation) or negative (improvement), as follows

$$\Delta_{\text{rel}}^{\,k} \eta_{\text{HHV,e}}^0 \ (\%) \ = \ \left(\frac{\eta_{\text{HHV,e}}^0(t_k) \ (\%)}{\eta_{\text{HHV,e}}^0(t_0) \ (\%)} \ - \ 1 \right) \cdot \frac{1000 \ (\text{h}) \cdot f_{\text{compr}}}{t_k \ (\text{h})} \cdot 100 \ (\%), \tag{6.10.12a}$$

$$\Delta_{\text{rel}}^{\,k} \eta_{\text{LHV,e}}^0 \ (\%) \ = \ \left(\frac{\eta_{\text{LHV,e}}^0(t_k) \ (\%)}{\eta_{\text{LHV,e}}^0(t_0) \ (\%)} \ - \ 1 \right) \cdot \frac{1000 \ (\text{h}) \cdot f_{\text{compr}}}{t_k \ (\text{h})} \cdot 100 \ (\%), \tag{6.10.12b}$$

$$\Delta_{\text{rel}}^{\,k} \eta_{\text{HHV,el}}^0 \ (\%) \ = \ \left(\frac{\eta_{\text{HHV,el}}^0(t_k) \ (\%)}{\eta_{\text{HHV,el}}^0(t_0) \ (\%)} \ - \ 1 \right) \cdot \frac{1000 \ (\text{h}) \cdot f_{\text{compr}}}{t_k \ (\text{h})} \cdot 100 \ (\%) \ \text{and} \tag{6.10.12c}$$

$$\Delta_{\text{rel}}^{\,k} \eta_{\text{LHV,el}}^0 \ (\%) \ = \ \left(\frac{\eta_{\text{LHV,el}}^0(t_k) \ (\%)}{\eta_{\text{LHV,el}}^0(t_0) \ (\%)} \ - \ 1 \right) \cdot \frac{1000 \ (\text{h}) \cdot f_{\text{compr}}}{t_k \ (\text{h})} \cdot 100 \ (\%). \tag{6.10.12d}$$

The input direct current (input DC voltage or input electric power) and the stack operating temperature are their rated values given by the stack manufacturer unless otherwise specified in the test plan.

---

[43] In case the total rate of change of energy efficiency based on HHV under SATP conditions of hydrogen, the total rate of change of energy efficiency based on LHV under SATP conditions of hydrogen, the total rate of change of electrical efficiency based on HHV under SATP conditions of hydrogen and the total rate of change of electrical efficiency based on LHV under SATP conditions of hydrogen are determined for more than one value of input current (input voltage, input electric power) or stack current density, appropriate indices should be added to $\Delta_{\text{tot}}^{\,k} \eta_{\text{HHV,e}}^0$, $\Delta_{\text{tot}}^{\,k} \eta_{\text{LHV,e}}^0$, $\Delta_{\text{tot}}^{\,k} \eta_{\text{HHV,el}}^0$ and $\Delta_{\text{tot}}^{\,k} \eta_{\text{LHV,el}}^0$ given by equation (6.10.11) and similarly to $\Delta_{\text{rel}}^{\,k} \eta_{\text{HHV,e}}^0$, $\Delta_{\text{rel}}^{\,k} \eta_{\text{LHV,e}}^0$, $\Delta_{\text{rel}}^{\,k} \eta_{\text{HHV,el}}^0$ and $\Delta_{\text{rel}}^{\,k} \eta_{\text{LHV,el}}^0$ given by equation (6.10.12).

7 Presentation of test results

Table 7.1 lists the TOPs as results of performance tests (section 6.7) and durability test (section 6.9).

Table 7.1: Test output parameter as test results

TOP (unit)	Description	Test method
Performance tests		
$P_{\mathrm{el,in}}$ (kW)	input electric power	section 6.7.1
I_{in} (A)	input current	section 6.7.2
U_{in} (kV)	input voltage	section 6.7.3
P_{th} (kW)	thermal power	section 6.7.4
P_{compr} (kW)	power of compression	section 6.7.5
t_{resp} (s)	response time	section 6.7.6
E_{ramp} (kJ/s)	ramp energy	section 6.7.6
$\mathrm{pH}_{\mathrm{lye}}$	pH value of lye solution [1]	section 6.7.7
$\sigma_{\mathrm{el,lye}}$ (mS)	electrical conductivity of lye solution [1]	section 6.7.7
pH_{w}	pH value of liquid water [2]	section 6.7.7
$\sigma_{\mathrm{el,w}}$ (mS)	electrical conductivity of liquid water [2]	section 6.7.7
$q_{\mathrm{n,H_2}}$ (mol/h)	molar flow rate of hydrogen	section 6.7.8
$x_{\mathrm{n,H_2}}$ (mol/mol)	molar concentration of hydrogen	section 6.7.8
$q_{\mathrm{V,H_2}}$ (mol/h)	volumetric flow rate of hydrogen	section 6.7.8
$q_{\mathrm{m,H_2}}$ (mol/h)	mass flow rate of hydrogen	section 6.7.8
$q_{\mathrm{n,O_2}}$ (mol/h)	molar flow rate of oxygen	section 6.7.9
$x_{\mathrm{n,O_2}}$ (mol/mol)	molar concentration of oxygen	section 6.7.9
c_{F} (μg/l)	fluoride concentration [3]	section 6.7.10
c_{PFAS} (ng/l)	PFAS concentration [3]	section 6.7.10
c_{PAH} (ng/l)	PAH concentration [2]	section 6.7.10
c_{Ca} (μg/l)	calcium concentration	section 6.7.10
c_{Cl} (μg/l)	chloride concentration	section 6.7.10
c_{Cu} (μg/l)	copper concentration	section 6.7.10
c_{Fe} (μg/l)	iron concentration	section 6.7.10
c_{K} (μg/l)	potassium concentration	section 6.7.10
c_{Mg} (μg/l)	magnesium concentration	section 6.7.10
c_{Na} (μg/l)	sodium concentration	section 6.7.10
c_{Ni} (μg/l)	nickel concentration	section 6.7.10
I_{stack} (A)	stack current	section 6.7.11
J_{stack} (A/cm^2)	stack current density	section 6.7.11
U_{stack} (kV)	stack voltage	section 6.7.11
$U_{\mathrm{cell,n}}$ (V)	voltage of cell n	section 6.7.11
$\overline{U}_{\mathrm{cell}}$ (V)	average cell voltage	section 6.7.11
$\mathrm{MAE}_{\overline{U}_{\mathrm{cell}}}$ (mV)	mean absolute error of average cell voltage	section 6.7.11
$\mathrm{SD}_{\overline{U}_{\mathrm{cell}}}$ (mV)	standard deviation of average cell voltage	section 6.7.11
R_{Ω} (Ω)	ohmic resistance	section 6.7.12
R_{ASR} (mΩ.cm^2)	area-specific resistance [4]	section 6.7.12
$\eta_{\mathrm{HHV,e}}^{0}$ (%)	energy efficiency based on HHV under SATP conditions	section 6.7.13
$\eta_{\mathrm{LHV,e}}^{0}$ (%)	energy efficiency based on LHV under SATP conditions	section 6.7.13
$\eta_{\mathrm{HHV,el}}^{0}$ (%)	electrical efficiency based on HHV under SATP conditions	section 6.7.13
$\eta_{\mathrm{LHV,el}}^{0}$ (%)	electrical efficiency based on LHV under SATP conditions	section 6.7.13
Durability tests		
$\Delta_{\mathrm{tot}}^{k} U$ (μV/h)	total rate of change of voltage	section 6.10
$\Delta_{\mathrm{rel}}^{k} U$ (μV/h)	relative rate of change of voltage	section 6.10
$\Delta_{\mathrm{tot}}^{k} P$ (mW/h)	total rate of change of power	section 6.10
$\Delta_{\mathrm{rel}}^{k} P$ (%)	relative rate of change of power	section 6.10
$\Delta_{q_{\mathrm{V,H_2}}}^{k} U$ (μV/m$^3_{\mathrm{H_2}}$/h)	total change of voltage per unit of hydrogen volumetric flow rate	section 6.10
$\Delta_{q_{\mathrm{m,H_2}}}^{k} U$ (μV/kg$_{\mathrm{H_2}}$/h)	total change of voltage per unit of hydrogen mass flow rate	section 6.10
$\Delta_{q_{\mathrm{V,H_2}}}^{k} E$ (mWh/m$^3_{\mathrm{H_2}}$)	total change of energy per unit of volume of hydrogen	section 6.10
$\Delta_{q_{\mathrm{m,H_2}}}^{k} E$ (mWh/kg$_{\mathrm{H_2}}$)	total change of energy per unit of mass of hydrogen	section 6.10

Continue to next page

Table 7.1 – continued from previous page

$\Delta^{k}_{\mathrm{tot}}\,\mathrm{MAE}\,\overline{U_{\mathrm{cell}}}\,(\mu\mathrm{V/h})$	total rate of change of mean absolute error average cell voltage	section 6.10
$\Delta^{k}_{\mathrm{rel}}\,\mathrm{MAE}\,\overline{U_{\mathrm{cell}}}\,(\%)$	relative rate of change of mean absolute error average cell voltage	section 6.10
$\Delta^{k}_{\mathrm{tot}}\,\mathrm{SD}\,\overline{U_{\mathrm{cell}}}\,(\mu\mathrm{V/h})$	total rate of change of standard deviation of average cell voltage	section 6.10
$\Delta^{k}_{\mathrm{rel}}\,\mathrm{SD}\,\overline{U_{\mathrm{cell}}}\,(\%)$	relative rate of change of standard deviation of average cell voltage	section 6.10
$\Delta^{k}_{\mathrm{tot}}\,R_{\mathrm{ASR}}\,(\mathrm{m}\Omega.\mathrm{cm}^2/\mathrm{h})$	total rate of change of area-specific resistance	section 6.10
$\Delta^{k}_{\mathrm{tot}}\,R_{\Omega}\,(\mathrm{m}\Omega/\mathrm{h})$	total rate of change of ohmic resistance	section 6.10
$\Delta^{k}_{\mathrm{rel}}\,R_{\mathrm{ASR}}\,(\%)$	relative rate of change of area-specific resistance	section 6.10
$\Delta^{k}_{\mathrm{rel}}\,R_{\Omega}\,(\%)$	relative rate of change of ohmic resistance	section 6.10
$\Delta^{k}_{\mathrm{tot}}\,\eta^{0}_{\mathrm{HHV,e}}\,(\%/\mathrm{h})$	total rate of change of energy efficiency based on HHV under SATP conditions of hydrogen	section 6.10
$\Delta^{k}_{\mathrm{rel}}\,\eta^{0}_{\mathrm{HHV,e}}\,(\%)$	relative rate of change of energy efficiency based on HHV under SATP conditions of hydrogen	section 6.10
$\Delta^{k}_{\mathrm{tot}}\,\eta^{0}_{\mathrm{LHV,e}}\,(\%/\mathrm{h})$	total rate of change of energy efficiency based on LHV under SATP conditions of hydrogen	section 6.10
$\Delta^{k}_{\mathrm{rel}}\,\eta^{0}_{\mathrm{LHV,e}}\,(\%)$	relative rate of change of energy efficiency based on LHV under SATP conditions of hydrogen	section 6.10
$\Delta^{k}_{\mathrm{tot}}\,\eta^{0}_{\mathrm{HHV,el}}\,(\%/\mathrm{h})$	total rate of change of electrical efficiency based on HHV under SATP conditions of hydrogen	section 6.10
$\Delta^{k}_{\mathrm{rel}}\,\eta^{0}_{\mathrm{HHV,el}}\,(\%)$	relative rate of change of electrical efficiency based on HHV under SATP conditions of hydrogen	section 6.10
$\Delta^{k}_{\mathrm{tot}}\,\eta^{0}_{\mathrm{LHV,el}}\,(\%/\mathrm{h})$	total rate of change of electrical efficiency based on LHV under SATP conditions of hydrogen	section 6.10
$\Delta^{k}_{\mathrm{rel}}\,\eta^{0}_{\mathrm{LHV,el}}\,(\%)$	relative rate of change of electrical efficiency based on LHV under SATP conditions of hydrogen	section 6.10

Note: According to the test plan (section 6.6), TOPs may be obtained as functions of TIPs or other TOPs as well as time (test duration), number of operation profiles or sequence(s) of such profiles. By adding appropriate indices to the concerned TOP, TOPs of same type are distinguished.
[1] measured for AWE and AAEMWE stacks
[2] measured for AEMWE and PEMWE stacks
[3] measured for PEMWE stacks
[4] The method of R_{lf} estimation whether polarisation curve measurements or EIS measurements shall be stated.
Source: JRC, 2023

The test results should, as appropriate, be reported along with their standard uncertainties (u) or combined standard uncertainties (u_{c}) in accordance with the GUM (JCGM, 2008, JCGM, 2009, JCGM, 2020).

In addition to tabulated test results, TOPs of durability tests should be presented graphically, for example, to show their evolution with time or the number and sequence(s) of operation profiles. Their standard uncertainties or combined standard uncertainties should constitute error bars for a specified level of confidence (JCGM, 2008).

8 Conclusions with final remarks

This report proposes testing protocols for accelerated stress testing of low-temperature WE stacks to determine their performance degradation when used in WE systems generating bulk amounts of clean hydrogen in P-to-H_2 applications for H_2-to-P, hydrogen-to-mobility (H_2-to-M) and H_2-to-I processes using fluctuating electricity from RES such as PV and WT electric power. They rely on test methods of ISO and IEC standards and testing procedures developed as part of the EU water electrolysis harmonisation activities.

These protocols allow for an adequate comparison of WEL technologies in stacks, whether of AEC type in AWE, AEMEC type in AEMWE and AAEMWE, or PEMEC type in PEMWE. They also allow to compare the performance degradation of different stacks of the same type but different in design, configuration and WEC materials used. Intended for use by the research community and industry alike, these protocols provide built-in flexibility. In fact, performance tests may selectively be performed, and in addition to the exemplified RES-based operation profiles, application-oriented duty cycles may be employed in durability tests.

Also, the user is free to substitute one or another test method in a particular campaign when deemed more appropriate for the intended use of the WE stack in the application concerned. All tests shall be conducted safely (Annex A) and with due care, the recording of all relevant test parameters, whether TIPs or TOPs, shall be followed as required, and the reported test results (Annex B) shall be stated along with their uncertainties.

The application of various stress parameters and their combination to WE stacks during an AST campaign, the use of a structured DoE approach may not necessarily guarantee the induction of degradation phenomena previously identified in stacks tested under similar operating conditions and dynamic operation modes. However, given the wealth of test data gathered from WE stacks subjected to accelerated stress testing, advanced statistical analysis (IEC, 2010, IEC, 2011, IEC, 2017b) and physics-based modelling could potentially unveil performance degradation patterns in WE stacks and establish correlations with the applied stressing operating conditions.

This could be achieved through the effective utilisation of machine learning (ML) (**4.2.47**) algorithms (Mohamed *et al.*, 2022, Sayed-Ahmed *et al.*, 2024) and other artificial intelligence (AI) (**4.2.11**) techniques (Chavez-Ramirez *et al.*, 2011, Jha *et al.*, 2017, Bahr *et al.*, 2020) on the acquired test results which should always be made open access. A data-driven approach holds promise for developing transfer functions that express the relationship between WE stack performance degradation, applied stress parameters, and the reduction of test duration. This aligns with the ultimate goal of accelerated stress testing, which is to minimise R&D costs and expedite the maturation of WE stacks for cost-effective, long-term operation to generate clean hydrogen in bulk amounts using electricity from RESs.

References

Carrara, S., Bobba, S., Blagoeva, D., Dias, P. A., Cavalli, A., Georgitzikis, K., Grohol, M., Itul, A., Kuzov, T., Latunussa, C., Lyons, L., Malano, G., Maury, T., Arce, A. P., Somers, J., Telsnig, T., Veeh, C., Wittmer, D., Black, C., Pennington, D. and Christou, M., 'Supply chain analysis and material demand forecast in strategic technologies and sectors in the EU: a foresight study', JRC Science for Policy report EUR 31437 EN, European Commission, 2023. doi: 10.2760/386650.

Cartaxo, M., Fernandes, J., Gomes, M., Pinho, H., Nunes, V. and Coelho, P., 'Hydrogen production via wastewater electrolysis – an integrated approach review', In 'Innovations in Smart Cities Applications', , edited by M. B. Ahmed, A. A. Boudhir, . R. Karaș, V. Jain, and S. MellouliVol. 5. Springer International Publishing, Cham, pp. 671–680. doi:10.1007/978-3-030-94191-8_54. URL `http://hdl.handle.net/10400.26/39663`.

Chavez-Ramirez, A. U., Munoz-Guerrero, R., Sanchez-Huerta, V., Ramirez-Arredondo, J. M., Ornelas, R., Arriaga, L. G., Siracusano, S., Brunaccini, G., Napoli, G., Antonucci, V. and Aricó, A. S., 'Dynamic model of a pem electrolyzer based on artificial neural networks', *Journal of New Materials for Electrochemical Systems*, Vol. 14, No 2, 2011, pp. 113–119. doi:10.14447/jnmes.v14i2.119.

Clapp, M., Zalitis, C. M. and Ryan, M., 'Perspectives on current and future iridium demand and iridium oxide catalysts for PEM water electrolysis', *Catalysis Letters*, Vol. 420, 2023, p. 114140. doi:10.1016/j.cattod.2023.114140.

Elia Transmission Belgium SA, 'Grid data Open data'. online, 05 August 2023. URL `https://opendata.elia.be`.

CNR, 'Enhanced performance and cost-effective materials for long-term operation of PEM water electrolysers coupled to renewable power sources', Project information, CORDIS, 2012. URL `https://cordis.europa.eu/project/id/300081`.

CNR, 'High Performance PEM Electrolyzer for Cost-effective Grid Balancing Applications', Project information, CORDIS, 2016. doi:10.3030/700008. URL `https://cordis.europa.eu/project/id/700008`.

CNR, 'Anion Exchange Membrane Electrolysis for Renewable Hydrogen Production on a Wide-Scale', Project information, CORDIS, 2020. doi:10.3030/875024. URL `https://cordis.europa.eu/project/id/875024`.

DLR, 'Novel modular stack design for high pressure PEM water electrolyzer technology with wide operation range and reduced cost', Project information, CORDIS, 2018. doi:10.3030/779478. URL `https://cordis.europa.eu/project/id/779478`.

DLR, 'Cost-effective PROton Exchange MEmbrane WaTer Electrolyser for Efficient and Sustainable Power-to-H2 Technology', Project information, CORDIS, 2020a. doi:10.3030/862253. URL `https://cordis.europa.eu/project/id/862253`.

DLR, 'Next Generation Alkaline Membrane Water Electrolysers with Improved Components and Materials', Project information, CORDIS, 2020b. doi:10.3030/875118. URL `https://cordis.europa.eu/project/id/875118`.

JCGM, 'Evaluation of measurement data – Guide to the expression of uncertainty in measurement', GUM: Guide to the Expression of Uncertainty in Measurement JCGM 100:2008, Joint Committee for Guides in Metrology, 2008. URL `https://www.bipm.org/utils/common/documents/jcgm/JCGM_100_2008_E.pdf`.

JCGM, 'Evaluation of measurement data – An introduction to the Guide to the expression of uncertainty in measurement and related documents', GUM: Guide to the Expression of Uncertainty in Measurement JCGM 104:2009, Joint Committee for Guides in Metrology, 2009. URL `https://www.bipm.org/documents/20126/2071204/JCGM_104_2009.pdf`.

JCGM, 'Guide to the expression of uncertainty in measurement – Part 6: Developing and using measurement models', GUM: Guide to the Expression of Uncertainty in Measurement JCGM GUM-6:2020, Joint Committee for Guides in Metrology, 2020. URL `https://www.bipm.org/documents/20126/2071204/JCGM_GUM_6_2020.pdf/d4e77d99-3870-0908-ff37-c1b6a230a337?version=1.8&t=1659083073972&download=true`.

Bahr, M., Gusak, A., Stypka, S. and Oberschachtsiek, B., 'Artificial neural networks for aging simulation of electrolysis stacks', *Chemie-Ingenieur-Technik*, Vol. 92, 10 2020, pp. 1610–1617. doi:10.1002/cite.202000089.

Fitzek, K., de Haart, U., Fang, Q. and Lehnert, W., 'High-frequency features in the distribution of relaxation times related to frequency dispersion effects in SOFCs', *Journal of the Electrochemical Society*, Vol. 169, No 1, 2022, p. 014501. doi:10.1149/1945-7111/ac4372.

Du, N., Roy, C., Peach, R., Turnbull, M., Thiele, S. and Bock, C., 'Anion-exchange membrane water electrolyzers', *Chemical Reviews*, Vol. 122, No 13, 2022, pp. 11830–11895. doi:10.1021/acs.chemrev.1c00854.

Kartci, A., Herencsár, N., Tenreiro Machado, J. and Brančík, L., 'History and progress of fractional-order element passive emulators: A review', *Radioengineering Proceedings of Czech and Slovak Technical Universities*, Vol. 29, No 2, 2020, pp. 296–304. doi:10.13164/re.2020.0296.

EC, 'COMMUNICATION FROM THE COMMISSION TO THE EUROPEAN PARLIAMENT, THE COUNCIL, THE EUROPEAN ECONOMIC AND SOCIAL COMMITTEE AND THE COMMITTEE OF THE REGIONS Chemicals Strategy for Sustainability Towards a Toxic-Free Environment', Communication COM/2020/667 final, European Commission, Brussels (BE), 14 October 2020a. URL https://eur-lex.europa.eu/legal-content/EN/TXT/?uri=COM:2020:667:FIN.

EC, 'Poly- and perfluoroalkyl substances (PFAS)', Commission staff working document SWD(2020) 249 final, European Commission, Brussels (BE), 14 October 2020b. URL https://eur-lex.europa.eu/legal-content/EN/TXT/PDF/?uri=CELEX:52020SC0249.

Suermann, M., Bensmann, B. and Hanke-Rauschenbach, R., 'Degradation of proton exchange membrane (PEM) water electrolysis cells: Looking beyond the cell voltage increase', *Journal of the Electrochemical Society*, Vol. 166, No 10, 2019, p. F645. doi:10.1149/2.1451910jes.

Lettenmeier, P., Wang, R., Abouatallah, R., Helmly, S., Morawietz, T., Hiesgen, R., Kolb, S., Burggraf, F., Kallo, J., Gago, A. S. and Friedrich, K. A., 'Durable membrane electrode assemblies for proton exchange membrane electrolyzer systems operating at high current densities', *Electrochimica Acta*, Vol. 210, 2016, pp. 502–511. doi:10.1016/j.electacta.2016.04.164.

Dizon, A., Schuler, T., Weber, A. Z., Danilovic, N. and Bender, G., 'Advanced voltage break down analysis by statistical open-source tool case study based on polymer electrolyte water electrolysis', *ECS Meeting Abstracts*, Vol. MA2022-02, No 39, 2022, p. 1400. doi:10.1149/MA2022-02391400mtgabs.

Macdonald, J. R. and Potter, L. D., 'A flexible procedure for analyzing impedance spectroscopy results: Description and illustrations', *Solid State Ionics*, Vol. 24, No 1, 1987, pp. 61–79. doi:10.1016/0167-2738(87)90068-3.

Mohamed, A., Ibrahem, H. and Kim, K., 'Machine learning-based simulation for proton exchange membrane electrolyzer cell', *Energy Reports*, Vol. 8, 2022, pp. 13425–13437. doi:10.1016/j.egyr.2022.09.135.

Tomić, A. Z., Pivac, I. and Barbir, F., 'A review of testing procedures for proton exchange membrane electrolyzer degradation', *Journal of Power Sources*, Vol. 557, 2023, p. 232569. doi:10.1016/j.jpowsour.2022.232569.

Ehlers, J. C., Feidenhans'l, A. A., Therkildsen, K. T. and Larrazábal, G. O., 'Affordable green hydrogen from alkaline water electrolysis: Key research needs from an industrial perspective', *ACS Energy Letters*, Vol. 8, No 3, 2023, pp. 1502–1509. doi:10.1021/acsenergylett.2c02897.

Malkow, K. T., 'A theory of distribution functions of relaxation times for the deconvolution of immittance data', *Journal of Electroanalytical Chemistry*, Vol. 838, No 4, 2019, pp. 221–231. URL https://www.sciencedirect.com/science/article/pii/S1572665719300670.

Gerhardt, M. R., Pant, L. M., Bui, J. C., Crothers, A. R., Ehlinger, V. M., Fornaciari, J. C., Liu, J. and Weber, A. Z., 'Method—practices and pitfalls in voltage breakdown analysis of electrochemical energy-conversion systems', *Journal of the Electrochemical Society*, Vol. 168, No 7, 2021, p. 074503. doi:10.1149/1945-7111/abf061.

Shih, A. J., de Oliveira Monteiro, M. C., Dattila, F., Pavesi, D., Philips, M., Marques da Silva, A. H., Vos, R. E., Ojha, K., Park, S., van der Heijden, O., Marcandalli, G., Goyal, A., Villalba, M., Chen, X., Gunasooriya, G. T. K. K., McCrum, I., Mom, R., López, N. and Koper, M. T. M., 'Water electrolysis', *Nature Reviews Methods Primers*, Vol. 2, 2022, p. 84. doi:10.1038/s43586-022-00164-0.

McPhail, S. J., Frangini, S., Laurencin, J., Effori, E., Abaza, A., Padinjarethil, A. K., Hagen, A., Léon, A., Brisse, A., Vladikova, D., Burdin, B., Bianchi, F. R., Bosio, B., Piccardo, P., Spotorno, R., Uchida, H., Polverino, P., Adinolfi, E. A., Postiglione, F., Lee, J.-H., Moussaoui, H. and Van herle, J., 'Addressing planar solid oxide cell degradation mechanisms: A critical review of selected components', *Electrochemical Science Advances*, Vol. 2, No 5, 2022, p. e2100024. doi:10.1002/elsa.202100024.

Kumar, S. S. and Lim, H., 'Recent advances in hydrogen production through proton exchange membrane water electrolysis – a review', *Sustainable Energy Fuels*, Vol. 7, No 15, 2023, pp. 3560–3583. doi:10.1039/D3SE00336A.

Huang, J., 'Diffusion impedance of electroactive materials, electrolytic solutions and porous electrodes: Warburg impedance and beyond', *Electrochimica Acta*, Vol. 281, 2018, pp. 170–188. doi:10.1016/j.electacta.2018.05.136.

Becker, H., Murawski, J., Shinde, D. V., Stephens, I. E. L., Hinds, G. and Smith, G., 'Impact of impurities on water electrolysis: a review', *Sustainable Energy Fuels*, Vol. 7, 2023, pp. 1565–1603. doi:10.1039/D2SE01517J.

Allidières, L., Brisse, A., Millet, P., Valentin, S. and Zeller, M., 'On the ability of pem water electrolysers to provide power grid services', *International Journal of Hydrogen Energy*, Vol. 44, No 20, 2019, pp. 9690–9700. doi:10.1016/j.ijhydene.2018.11.186.

Kumar, S. S. and Lim, H., 'An overview of water electrolysis technologies for green hydrogen production', *Energy Reports*, Vol. 8, 2022, pp. 13793–13813. doi:10.1016/j.egyr.2022.10.127.

Reissner, R., Goudis, D., Bourasseau, C., Lacroix, V., Lavaille, G., You, S., Greenhalgh, D. A., Green, B., Abadia, L., Imboden, C., Marcuello, P. and Bornstein, M., 'Qualifying tests of electrolysers for grid services – finalized testing protocol', QualyGridS Deliverable D7.9, Deutsches Zentrum für Luft- und Raumfahrt e. V., Commissariat à l'énergie atomique et aux énergies alternatives, Danmarks Tekniske Universitet, ITM Power plc, Fundación para el Desarrollo de las Tecnologías del Hidrógeno en Aragón, Hochschule Luzern, Sunfire GmbH, Nel ASA, 30 Sepetmber 2020. doi:10.5281/zenodo.3937273. URL `https://zenodo.org/record/3937273`.

EP and Council, 'Approximation of the laws of the Member States concerning equipment and protective systems intended for use in potentially explosive atmospheres', Directive 94/9/EC, Publications Office of the European Union, Brussels (BE), 23 March 1994. URL `http://data.europa.eu/eli/dir/1994/9/oj`. OJ L 100 of 19.4.1994.

EP and Council, 'General Product Safety', Directive 2001/95/EC, Publications Office of the European Union, Brussels (BE), 3 December 2001. URL `http://data.europa.eu/eli/dir/2001/95/oj`. OJ L 11 of 15.1.2002.

EP and Council, 'Machinery, and amending Directive 95/16/EC', Directive 2006/42/EC, Publications Office of the European Union, Brussels (BE), 17 May 2006. URL `http://data.europa.eu/eli/dir/2006/42/oj`. OJ L 157 of 9.6.2006.

EP and Council, 'Harmonisation of the laws of the Member States relating to electromagnetic compatibility', Directive 2014/30/EU, Publications Office of the European Union, Brussels (BE), 26 February 2014a. URL `http://data.europa.eu/eli/dir/2014/30/oj`. OJ L 96 of 29.3.2014.

EP and Council, 'Harmonisation of the laws of the Member States relating to equipment and protective systems intended for use in potentially explosive atmospheres', Directive 2014/34/EU, Publications Office of the European Union, Brussels (BE), 26 February 2014b. URL `http://data.europa.eu/eli/dir/2014/34/oj`. OJ L 96 of 29.3.2014.

EP and Council, 'Harmonisation of the laws of the Member States relating to the making available on the market of electrical equipment designed for use within certain voltage limits', Directive 2014/35/EU, Publications Office of the European Union, Brussels (BE), 26 February 2014c. URL `http://data.europa.eu/eli/dir/2014/35/oj`. OJ L 96 of 29.3.2014.

EP and Council, 'Harmonisation of the laws of the Member States relating to the making available on the market of pressure equipment', Directive 2014/68/EU, Publications Office of the European Union, Brussels (BE), 15 May 2014d. URL `http://data.europa.eu/eli/dir/2014/68/oj`. OJ L 189 of 27.6.2014.

IEC, 'Possible safety and health hazards in the use of alkaline secondary cells and batteries – Guide to equipment manufacturers and users', Technical Report IEC TR 61438:1996, International Electrotechnical Commission, Geneva (CH), 1996. URL `https://webstore.iec.ch/publication/5455`.

IEC, 'Guide for the statistical analysis of ageing test data – Part 2: Validation of procedures for statistical analysis of censored normally distributed data', Technical Report IEC TR 60493-2:2010, International Electrotechnical Commission, Geneva (CH), 2010. URL `https://webstore.iec.ch/publication/2260`.

IEC, 'Guide for the statistical analysis of ageing test data – Part 1: Methods based on mean values of normally distributed test results', International Standard IEC 60493-1:2011, International Electrotechnical Commission, Geneva (CH), 2011. URL `https://webstore.iec.ch/publication/2259`.

IEC, 'Explosive atmospheres – Part 17: Electrical installations inspection and maintenance', International Standard IEC 60079-17:2013, International Electrotechnical Commission, Geneva (CH), 2013. URL `https://webstore.iec.ch/publication/631`.

IEC, 'Explosive atmospheres – Part 14: Electrical installations design, selection and erection', International Standard IEC 60079-14:2013, International Electrotechnical Commission, Geneva (CH), 2014a. URL `https://webstore.iec.ch/publication/628`.

IEC, 'Fuel cell technologies – Part 7-2: Test methods – Single cell and stack performance tests for solid oxide fuel cells (SOFC)', International Standard IEC 62282-7-2:2014, International Electrotechnical Commission, Geneva (CH), 2014b. URL `https://webstore.iec.ch/publication/6766`.

IEC, 'Safety requirements for electrical equipment for measurement, control, and laboratory use – Part 1: General requirements', International Standard IEC 61010-1:2010+AMD1:2016 CSV, International Electrotechnical Commission, Geneva (CH), 2016. URL `https://webstore.iec.ch/publication/59769`.

IEC, 'Explosive atmospheres – Part 0: Equipment – General requirements', International Standard IEC 60079-0:2017, International Electrotechnical Commission, Geneva (CH), 2017a. URL `https://webstore.iec.ch/publication/32878`.

IEC, 'Guidelines for the statistical analysis of ageing test data – Part 3: Minimum specimen numbers at different test conditions with given experimental data', Technical Report IEC TR 60493-3:2017, International Electrotechnical Commission, Geneva (CH), 2017b. URL `https://webstore.iec.ch/publication/27934`.

IEC, 'Safety of machinery – Electrical equipment of machines – Part 11: Requirements for equipment for voltages above 1 000 V AC or 1 500 V DC and not exceeding 36 kV', International Standard IEC 60204-11:2018 RLV, International Electrotechnical Commission, Geneva (CH), 2018. URL `https://webstore.iec.ch/publication/63667`.

IEC, 'Fuel cell technologies – Part 3-100: Stationary fuel cell power systems – Safety', International Standard IEC 62282-3-100:2019, International Electrotechnical Commission, Geneva (CH), 2019a. URL `https://webstore.iec.ch/publication/59780`.

IEC, 'Fuel cell technologies – Part 8-102: Energy storage systems using fuel cell modules in reverse mode – Test procedures for the performance of single cells and stacks with proton exchange membrane, including reversible operation', International Standard IEC 62282-8-102:2019, International Electrotechnical Commission, Geneva (CH), 2019b. URL `https://webstore.iec.ch/publication/30534`.

IEC, 'Explosive atmospheres – Part 10-1: Classification of areas – Explosive gas atmospheres', International Standard IEC 60079-10-1:2020, International Electrotechnical Commission, Geneva (CH), 2020a. URL `https://webstore.iec.ch/publication/63327`.

IEC, 'Fuel cell technologies – Part 2-100: Fuel cell modules – Safety', International Standard IEC 62282-2-100:2020, International Electrotechnical Commission, Geneva (CH), 2020b. URL `https://webstore.iec.ch/publication/59780`.

IEC, 'Fuel cell technologies – Part 8-101: Energy storage systems using fuel cell modules in reverse mode – Test procedures for the performance of solid oxide single cells and stacks, including reversible operation', International Standard IEC 62282-8-101:2020, International Electrotechnical Commission, Geneva (CH), 2020c. URL `https://webstore.iec.ch/publication/33278`.

IEC, 'Fuel cell technologies – Part 8-201: Energy storage systems using fuel cell modules in reverse mode – Test procedures for the performance of power-to-power systems', International Standard IEC 62282-8-201:2020, International Electrotechnical Commission, Geneva (CH), 2020d. URL `https://webstore.iec.ch/publication/31519`.

IEC, 'Safety of machinery – Electrical equipment of machines – Part 1: General requirements', International Standard IEC 60204-1:2016+AMD1:2021 CSV, International Electrotechnical Commission, Geneva (CH), 2021a. URL `https://webstore.iec.ch/publication/71256`.

IEC, 'Safety of machinery – Electrical equipment of machines – Part 1: General requirements', International Standard IEC 60204-1:2016+AMD1:2021 CSV, International Electrotechnical Commission, Geneva (CH), 2021b. URL `https://webstore.iec.ch/publication/71256`.

IEC, 'Amendment 1 – Fuel cell technologies – Part 3-201: Stationary fuel cell power systems – Performance test methods for small fuel cell power systems', International Standard IEC 62282-3-201:2017+AMD1:2022 CSV, International Electrotechnical Commission, Geneva (CH), 2022. URL `https://webstore.iec.ch/publication/65282`.

ISO, 'Water quality – Determination of calcium content – EDTA titrimetric method', International standard ISO 6058:1984, International Organization for Standardization, Geneva (CH), 1984a. URL `https://www.iso.org/standard/12257.html`.

ISO, 'Water quality – Determination of the sum of calcium and magnesium – EDTA titrimetric method', International standard ISO 6059:1984, International Organization for Standardization, Geneva (CH), 1984b. URL `https://www.iso.org/standard/12258.html`.

ISO, 'Water quality – Determination of electrical conductivity', International Standard ISO 7888:1985, International Organization for Standardization, Geneva (CH), 1985. URL `https://www.iso.org/standard/14838.html`.

ISO, 'Water quality – Determination of calcium and magnesium – Atomic absorption spectrometric method', International standard ISO 7980:1986, International Organization for Standardization, Geneva (CH), 1986a. URL `https://www.iso.org/standard/14972.html`.

ISO, 'Water quality – Determination of cobalt, nickel, copper, zinc, cadmium and lead – Flame atomic absorption spectrometric methods', International standard ISO 8288:1986, International Organization for Standardization, Geneva (CH), 1986b. URL `https://www.iso.org/standard/15408.html`.

ISO, 'Water for analytical laboratory use – Specification and test methods', International standard ISO 3696:1987, International Organization for Standardization, Geneva (CH), 1987. URL `https://www.iso.org/standard/9169.html`.

ISO, 'Water quality – Determination of iron – Spectrometric method using 1,10-phenanthroline', International standard ISO 6332:1988, International Organization for Standardization, Geneva (CH), 1988. URL `https://www.iso.org/standard/12630.html`.

ISO, 'Water quality – Determination of chloride – Silver nitrate titration with chromate indicator (Mohr's method)', International standard ISO 9297:1989, International Organization for Standardization, Geneva (CH), 1989. URL `https://www.iso.org/standard/16952.html`.

ISO, 'Water quality – Determination of fluoride – Part 1: Electrochemical probe method for potable and lightly polluted water', International standard ISO 10359-1:1992, International Organization for Standardization, Geneva (CH), 1992. URL `https://www.iso.org/standard/18416.html`.

ISO, 'Water quality – Determination of sodium and potassium – Part 1: Determination of sodium by atomic absorption spectrometry', International standard ISO 9964-1:1993, International Organization for Standardization, Geneva (CH), 1993a. URL `https://www.iso.org/standard/17869.html`.

ISO, 'Water quality – Determination of sodium and potassium – Part 2: Determination of potassium by atomic absorption spectrometry', International standard ISO 9964-2:1993, International Organization for Standardization, Geneva (CH), 1993b. URL `https://www.iso.org/standard/17870.html`.

ISO, 'Water quality – Determination of sodium and potassium – Part 3: Determination of sodium and potassium by flame emission spectrometry', International standard ISO 9964-3:1993, International Organization for Standardization, Geneva (CH), 1993c. URL `https://www.iso.org/standard/17871.html`.

ISO, 'Water quality – Determination of fluoride – Part 2: Determination of inorganically bound total fluoride after digestion and distillation', International standard ISO 10359-2:1994, International Organization for Standardization, Geneva (CH), 1994. URL `https://www.iso.org/standard/18417.html`.

ISO, 'Water quality — Determination of dissolved anions by liquid chromatography of ions — Part 4: Determination of chlorate, chloride and chlorite in water with low contamination', International Standard ISO 10304-4:1997, International Organization for Standardization, Geneva (CH), 1997. URL `https://www.iso.org/standard/22573.html`.

ISO, 'Water quality – Determination of dissolved Li+, Na+, NH4+, K+, Mn2+, Ca2+, Mg2+, Sr2+ and Ba2+ using ion chromatography – Method for water and waste water', International standard ISO 14911:1998, International Organization for Standardization, Geneva (CH), 1998. URL `https://www.iso.org/standard/25591.html`.

ISO, 'Liquid hydrogen – Land vehicle fuelling system interface', International Standard ISO 13984:1999, International Organization for Standardization, Geneva (CH), 1999. URL `https://www.iso.org/standard/23570.html`.

ISO, 'Water quality — Determination of chloride by flow analysis (CFA and FIA) and photometric or potentiometric detection', International standard ISO 15682:2000, International Organization for Standardization, Geneva (CH), 2000. URL `https://www.iso.org/standard/27984.html`.

ISO, 'Water quality — Determination of 15 Polycyclic aromatic hydrocarbons (PAH) in water by HPLC with fluorescence detection after liquid-liquid extraction', International standard ISO 17993:2002, International Organization for Standardization, Geneva (CH), 2002. URL `https://www.iso.org/standard/31666.html`.

ISO, 'Water quality – Determination of polycyclic aromatic hydrocarbons (PAH) – Part 1: Determination of six PAH by high-performance thin-layer liquid chromatography with fluorescence detection after liquid–liquid extraction', International standard ISO 7981-1:2005, International Organization for Standardization, Geneva (CH), 2005a. URL `https://www.iso.org/standard/33883.html`.

ISO, 'Water quality – Determination of polycyclic aromatic hydrocarbons (PAH) – Part 2: Determination of six PAH by high-performance liquid chromatography with fluorescence detection after liquid–liquid extraction', International standard ISO 7981-2:2005, International Organization for Standardization, Geneva (CH), 2005b. URL `https://www.iso.org/standard/33884.html`.

ISO, 'Water quality – Determination of dissolved anions by liquid chromatography of ions – Part 1: Determination of bromide, chloride, fluoride, nitrate, nitrite, phosphate and sulfate', International standard ISO 10304-1:2007, International Organization for Standardization, Geneva (CH), 2007. URL `https://www.iso.org/standard/46004.html`.

ISO, 'Water quality – Determination of pH', International Standard ISO 10523:2008, International Organization for Standardization, Geneva (CH), 2008. URL `https://www.iso.org/standard/51994.html`.

ISO, 'Earth-moving machinery and mobile road construction machinery – Worksite data exchange – Part 1: System architecture', International Standard ISO 15143-1:2010, International Organization for Standardization, Geneva (CH), 2010a. URL `https://www.iso.org/standard/37406.html`.

ISO, 'Hydrogen generators using fuel processing technologies – Part 2: Test method for performance', International Standard ISO 16110-2:2010, International Organization for Standardization, Geneva (CH), 2010b. URL `https://www.iso.org/standard/41046.html`.

ISO, 'Quantitative methods in process improvement – Six Sigma – Part 2: Tools and techniques', Technical Report ISO 13053-2:2011, International Organization for Standardization, Geneva (CH), 2011a. URL `https://www.iso.org/standard/52902.html`.

ISO, 'Water quality – Determination of 16 polycyclic aromatic hydrocarbons (PAH) in water – Method using gas chromatography with mass spectrometric detection (GC–MS)', International standard ISO 28540:2011, International Organization for Standardization, Geneva (CH), 2011b. URL `https://www.iso.org/standard/44752.html`.

ISO, 'Water quality – Determination of selected parameters by discrete analysis systems – Part 1: Ammonium, nitrate, nitrite, chloride, orthophosphate, sulfate and silicate with photometric detection', International standard ISO 15923-1:2013, International Organization for Standardization, Geneva (CH), 2013. URL `https://www.iso.org/standard/55559.html`.

ISO, 'Automation systems and integration Key performance indicators (KPIs) for manufacturing operations management Part 1: Overview, concepts and terminology', International Standard ISO 22400-1:2014, International Organization for Standardization, Geneva (CH), 2014. URL `https://www.iso.org/standard/56847.html`.

ISO, 'Basic considerations for the safety of hydrogen systems', Technical Report ISO/TR 15916:2015, International Organization for Standardization, Geneva (CH), 2015. URL `https://www.iso.org/standard/69212.html`.

ISO, 'Information technology – Data centres – Key performance indicators – Part 3: Renewable energy factor (REF)', International Standard ISO/IEC 30134-3:2016, International Organization for Standardization, International Electrotechnical Commission, Geneva (CH), 2016a. URL `https://www.iso.org/standard/66127.html`.

ISO, 'Water quality – Determination of fluoride using flow analysis (FIA and CFA) — Part 1: Method using flow injection analysis (FIA) and spectrometric detection after off-line distillation', Technical Specification ISO/TS 17951-1:2016, International Organization for Standardization, Geneva (CH), 2016b. URL `https://www.iso.org/standard/71104.html`.

ISO, 'Energy performance of buildings – Overarching EPB assessment – Part 1: General framework and procedures', International Standard ISO 52000-1:2017, International Organization for Standardization, Geneva (CH), 2017a. URL `https://www.iso.org/standard/65601.html`.

ISO, 'Water quality – Determination of selected parameters by discrete analysis systems – Part 2: Chromium(VI), fluoride, total alkalinity, total hardness, calcium, magnesium, iron, iron(II), manganese and aluminium with photometric detection', Technical Specification ISO/TS 15923-2:2017, International Organization for Standardization, Geneva (CH), 2017b. URL `https://www.iso.org/standard/66484.html`.

ISO, 'Occupational health and safety management systems – Requirements with guidance for use', International Standard ISO 45001:2018, International Organization for Standardization, Geneva (CH), 2018. URL `https://www.iso.org/standard/63787.html`.

ISO, 'Hydrogen generators using water electrolysis – Industrial, commercial, and residential applications', International Standard ISO 22734:2019, International Organization for Standardization, Geneva (CH), 2019a. URL `https://www.iso.org/standard/69212.html`.

ISO, 'Solvents for paints and varnishes – Demineralized water for industrial applications – Specification and test methods', International standard ISO 23321:2019, International Organization for Standardization, Geneva (CH), 2019b. URL `https://www.iso.org/standard/75230.html`.

ISO, 'Water quality – Determination of Perfluoroalkyl and polyfluoroalkyl substances (PFAS) in water – Method using solid phase extraction and Liquid chromatography-tandem Mass spectrometry (LC-MS/MS)', International standard ISO 21675:2019, International Organization for Standardization, Geneva (CH), 2019c. URL `https://www.iso.org/standard/71338.html`.

ISO, 'Corrosion of metals and alloys – Vocabulary', International Standard ISO 8044:2020, International Organization for Standardization, Geneva (CH), 2020a. URL `https://www.iso.org/standard/71134.html`.

ISO, 'Environmental management – Vocabulary', International Standard ISO 14050:2020, International Organization for Standardization, Geneva (CH), 2020b. URL `https://www.iso.org/standard/75300.html`.

ISO, 'Environmental management systems – Guidelines for incorporating material circulation in design and development', International Standard ISO 14009:2020, International Organization for Standardization, Geneva (CH), 2020c. URL `https://www.iso.org/standard/43244.html`.

ISO, 'Gaseous hydrogen – Fuelling stations – Part 1: General requirements', International Standard ISO 19880-1:2020, International Organization for Standardization, Geneva (CH), 2020d. URL `https://www.iso.org/standard/71940.html`.

ISO, 'Information technology – Home Electronic System (HES) application model – Part 3-8: GridWise transactive energy framework', Technical Report ISO/IEC TR 15067-3-8:2020, International Organization for Standardization, International Electrotechnical Commission, Geneva (CH), 2020e. URL `https://www.iso.org/standard/81781.html`.

ISO, 'Guidelines for performance evaluation of treatment technologies for water reuse systems – Part 6: Ion exchange and electrodialysis', International Standard ISO 20468-6:2021, International Organization for Standardization, Geneva (CH), 2021a. URL `https://www.iso.org/standard/74908.html`.

ISO, 'Safety of machinery – Relationship with ISO 12100 – Part 5: Implications of artificial intelligence machine learning', Technical Report ISO/TR 22100-5:2021, International Organization for Standardization, Geneva (CH), 2021b. URL `https://www.iso.org/standard/80778.html`.

ISO, 'Buildings and civil engineering works – Vocabulary – Part 3: Sustainability terms', International Standarda ISO 6707-3:2022, International Organization for Standardization, Geneva (CH), 2022a. URL `https://www.iso.org/standard/80456.html`.

ISO, 'Electronic fee collection — Pre-study on the use of vehicle licence plate information and automatic number plate recognition (ANPR) technologies', Technical Report ISO/TR 6026:2022, International Organization for Standardization, Geneva (CH), 2022b. URL `https://www.iso.org/standard/81956.html`.

ISO, 'Water quality – Determination of dissolved anions by liquid chromatography of ions – Part 4: Determination of chlorate, chloride and chlorite in water with low contamination', International standard ISO 10304-4:2022, International Organization for Standardization, Geneva (CH), 2022c. URL `https://www.iso.org/standard/81538.html`.

ISO and IEC, 'Energy efficiency and renewable energy sources – Common international terminology – Part 1: Energy efficiency', International Standard ISO/IEC 13273-1:2015, International Organization for Standardization, International Electrotechnical Commission, Geneva (CH), 2015a. URL `https://www.iso.org/standard/62606.html`.

ISO and IEC, 'Energy efficiency and renewable energy sources – Common international terminology – Part 2: Renewable energy sources', International Standard ISO/IEC 13273-2:2015, International Organization for Standardization, International Electrotechnical Commission, Geneva (CH), 2015b. URL `https://www.iso.org/standard/62607.html`.

ISO and IEC, 'Information technology – Security techniques – Information security controls for the energy utility industry', International Standard ISO/IEC 27019:2017, International Organization for Standardization, International Electrotechnical Commission, Geneva (CH), 2017. URL `https://www.iso.org/standard/68091.html`.

ISO and IEC, 'Principles and rules for the structure and drafting of ISO and IEC documents', ISO/IEC Directives, Part 2, Ninth edition, International Organization for Standardization, International Electrotechnical Commission, Geneva (CH), 2021. URL `https://www.iso.org/sites/directives/current/part2/index.xhtml`.

ISO, IEC and IEEE, 'Systems and software engineering – Requirements for testers and reviewers of information for users', International Standard ISO/IEC/IEEE 26513:2017, International Organization for Standardization, International Electrotechnical Commission, Institute of Electrical and Electronics Engineers, Geneva (CH), 2017. URL `https://www.iso.org/standard/67417.html`.

Kibsgaard, J. and Chorkendorff, I., 'Considerations for the scaling-up of water splitting catalysts', *Nature Energy*, Vol. 4, 2019, pp. 430–433. doi:10.1038/s41560-019-0407-1.

Chen, C., Tse, Y.-L. S., Lindberg, G. E., Knight, C. and Voth, G. A., 'Hydroxide solvation and transport in anion exchange membranes', *Journal American Chemical Society*, Vol. 138, No 3, 2016, pp. 991–1000. doi:10.1021/jacs.5b11951.

Dong, D., Zhang, W., van Duin, A. C. T. and Bedrov, D., 'Grotthuss versus vehicular transport of hydroxide in anion-exchange membranes: Insight from combined reactive and nonreactive molecular simulations', *Journal of Physical Chemistry Letters*, Vol. 9, No 4, 2018, pp. 825–829. doi:10.1021/acs.jpclett.8b00004.

Carmo, M., Fritz, D. L., Mergel, J. and Stolten, D., 'A comprehensive review on PEM water electrolysis', *International Journal of Hydrogen Energy*, Vol. 38, No 12, 2013, pp. 4901–4934. ISSN 0360-3199. doi:10.1016/j.ijhydene.2013.01.151.

Chen, M., Chou, S.-F., Blaabjerg, F. and Davari, P., 'Overview of power electronic converter topologies enabling large-scale hydrogen production via water electrolysis', *Applied Sciences*, Vol. 12, No 4, 2022, p. 1906. doi:10.3390/app12041906.

Alia, S. M., Stariha, S. and Borup, R. L., 'Electrolyzer durability at low catalyst loading and with dynamic operation', *Journal of the Electrochemical Society*, Vol. 116, No 15, 2019, pp. F1164–F1172. doi:10.1149/2.0231915jes.

Ma, Z., Witteman, L., Wrubel, J. A. and Bender, G., 'A comprehensive modeling method for proton exchange membrane electrolyzer development', *International Journal of Hydrogen Energy*, Vol. 46, No 34, 2021, pp. 17627–17643. doi:10.1016/j.ijhydene.2021.02.170.

Hernández-Gómez, Á., Ramirez, V. and Guilbert, D., 'Investigation of pem electrolyzer modeling: Electrical domain, efficiency, and specific energy consumption', *International Journal of Hydrogen Energy*, Vol. 45, No 29, 2020, pp. 14625–14639. doi:10.1016/j.ijhydene.2020.03.195.

Haleem, A. A., Nagasawa, K., Kuroda, Y., Nishiki, Y., Zaenal, A. and Mitsushima, S., 'A new accelerated durability test protocol for water oxidation electrocatalysts of renewable energy powered alkaline water electrolyzers', *Electrochemistry*, Vol. 89, No 2, 2021, pp. 186–191. doi:10.5796/electrochemistry.20-00156.

Mennemann, C., Haag, S., Borgardt, E., Rost, U., Neumann, J. and Roth, J., 'Definition of test plan of electrolyser only and coupled system', PROMETH2 Deliverable D5.2, AIR LIQUIDE Forschung und Entwicklung GmbH, iGas Energy GmbH, ProPuls GmbH, Westfälische Hochschule, 29 September 2021. URL `https://promet-h2.eu/wp-content/uploads/definition-of-test-plan-of-electrolyser-only-and-coupled-system.pdf`.

Alexander, C. L., Tribollet, B. and Orazem, M. E., 'Influence of micrometric-scale electrode heterogeneity on electrochemical impedance spectroscopy', *Electrochimica Acta*, Vol. 201, 2016, pp. 374–379. doi:10.1016/j.electacta.2016.02.133.

Falcão, D. S. and Pinto, A. M. F. R., 'A review on PEM electrolyzer modelling: Guidelines for beginners', *Journal of Cleaner Production*, Vol. 261, 2020, p. 121184. doi:10.1016/j.jclepro.2020.121184.

Ausfelder, F., Beilmann, C., Bertau, M., Bräuninger, S., Heinzel, A., Hoer, R., Koch, W., Mahlendorf, F., Metzelthin, A., Peuckert, M., Plass, L., Räuchle, K., Reuter, M., Schaub, G., Schiebahn, S., Schwab, E., Schüth, F., Stolten, D., Teßmer, G., Wagemann, K. and Ziegahn, K.-F., 'Energy storage as part of a secure energy supply', *ChemBioEng Reviews*, Vol. 4, No 3, 2017, pp. 144–210. doi:10.1002/cben.201700004.

Fouda-Onana, F., 'AEM WE testing protocols', NEWELY Deliverable D5.1, Commissariat à l'énergie atomique et aux énergies alternatives, 01 July 2020. URL `https://cordis.europa.eu/project/id/875118/results`.

Tsotridis, G. and Pilenga, A., 'EU harmonised terminology for low temperature water electrolysis for energy storage applications', JRC112082, EUR 29300 EN, KJ-NA-29300-EN-N. Publications Office of the European Union, Luxembourg (L), 2018. ISBN 978-92-79-90387-8. doi:10.2760/138987. URL `http://publications.jrc.ec.europa.eu/repository/handle/JRC112082`.

Tsotridis, G. and Pilenga, A., 'EU harmonised protocols for testing of low temperature water electrolysers', JRC122565, EUR 30752 EN, KJ-NA-30752-EN-N. Publications Office of the European Union, Luxembourg (L), 2021. ISBN 978-92-76-39266-8. doi:10.2760/58880. URL `https://publications.jrc.ec.europa.eu/repository/handle/JRC122565`.

Sdanghi, G., Maranzana, G., Celzard, A. and Fierro, V., 'Towards non-mechanical hybrid hydrogen compression for decentralized hydrogen facilities', *energies*, Vol. 13, 2020, p. 3145. doi:10.3390/en13123145.

Sayed-Ahmed, H., Árpad Istvan Toldy and Santasalo-Aarnio, A., 'Dynamic operation of proton exchange membrane electrolyzers – critical review', *Renewable and Sustainable Energy Review*, Vol. 189, 2024, p. 113883. doi:10.1016/j.rser.2023.113883.

Brauns, J. and Turek, T., 'Alkaline water electrolysis powered by renewable energy: A review', *processes*, Vol. 8, 2020, p. 248. doi:10.3390/pr8020248.

Chatenet, M., Pollet, B. G., Dekel, D. R., Dionigi, F., Deseure, J., Millet, P., Braatz, R. D., Bazant, M. Z., Eikerling, M., Staffell, I., Balcombe, P., Shao-Horn, Y. and Schäfer, H., 'Water electrolysis: from textbook knowledge to the latest scientific strategies and industrial developments', *Chemical Society Reviews*, Vol. 51, 2022, pp. 4583–4762. doi:10.1039/D0CS01079K.

Bernt, M. P., *Analysis of Voltage Losses and Degradation Phenomena in PEM Water Electrolyzers*. Dissertation, Technische Universität München, 2019. URL `https://d-nb.info/1185637885/34`.

Tahan, M.-R., 'Recent advances in hydrogen compressors for use in large-scale renewable energy integration', *International Journal of Hydrogen Energy*, Vol. 47, No 83, 2022, pp. 35275–35292. doi:10.1016/j.ijhydene.2022.08.128.

Chowdhury, N. R. and Kant, R., 'Theory of generalized Gerischer impedance for quasi-reversible charge transfer at rough and finite fractal electrodes', *Electrochimica Acta*, Vol. 281, 2018, pp. 445–458. doi:10.1016/j.electacta.2018.05.140.

Kiemel, S., Smolinka, T., Lehner, F., Full, J., Sauer, A. and Miehe, R., 'Critical materials for water electrolysers at the example of the energy transition in Germany', *International Journal of Energy Research*, Vol. 45, 2 2021, p. 9914–9935. doi:10.1002/er.6487.

Jha, S. K., Bilalovic, J., Jha, A., Patel, N. and Zhang, H., 'Renewable energy: Present research and future scope of artificial intelligence', *Renewable and Sustainable Energy Review*, Vol. 77, 2017, pp. 297–317. ISSN 1364-0321. doi:10.1016/j.rser.2017.04.018.

Durmuş, G. N. B., Özgür Çolpan, C. and Devrim, Y., 'A review on the development of the electrochemical hydrogen compressors', *Journal of Power Sources*, Vol. 494, 2021, p. 229743. doi:10.1016/j.jpowsour.2021.229743.

Córdoba-Torres, P., 'Relationship between constant-phase element (CPE) parameters and physical properties of films with a distributed resistivity', *Electrochimica Acta*, Vol. 225, No 592-604, 2017. doi:10.1016/j.electacta.2016.12.087.

Aßmann, P., Gago, A. S., Gazdzicki, P., Friedrich, K. A. and Wark, M., 'Toward developing accelerated stress tests for proton exchange membrane electrolyzers', *Current Opinion in Electrochemistry*, Vol. 21, 2020, pp. 225–233. doi:10.1016/j.coelec.2020.02.024.

Flick, S., Dhanushkodi, S. R. and Mérida, W., 'Transport phenomena in polymer electrolyte membrane fuel cells via voltage loss breakdown', *Journal of Power Sources*, Vol. 280, 2015, pp. 97–106. doi:10.1016/j.jpowsour.2015.01.099.

Stiber, S., Garcia Sanchez, D., Meital, S., Siracusano, S. and Gago, A., '1st document of available testing protocols for electrolysers: additional needs and needs for PROMET', PROMETH2 Deliverable D3.2, Deutsches Zentrum für Luft- und Raumfahrt e. V., Consiglio Nazionale delle Ricerche, Forschungszentrum Jülich GmbH, 30 November 2020. URL `https://cordis.europa.eu/project/id/862253/results`.

Lickert, T., Fischer, S., Young, J. L., Klose, S., Franzetti, I., Hahn, D., Kang, Z., Shviro, M., Scheepers, F., Carmo, M., Smolinka, T., Bender, G. and Metz, S., 'Advances in benchmarking and round robin testing for PEM water electrolysis: Reference protocol and hardware', *Applied Energy*, Vol. 352, 2023, p. 121898. doi:10.1016/j.apenergy.2023.121898.

Malkow, K. T., Pilenga, A. and Blagoeva, D., 'EU harmonised terminology for hydrogen generated by electrolysis', EUR 30324 EN, KJ-NA-30324-EN-N. Publications Office of the European Union, Luxembourg (L), 2021. ISBN 978-92-76-21042-9. doi:10.2760/732809. URL https://publications.jrc.ec.europa.eu/repository/handle/JRC120120.

Malkow, T. and Pilenga, A., 'EU harmonised testing procedure: Determination of water electrolyser energy performance', JRC Validated Methods, Reference Methods and Measurements Report KJ-07-22-323-EN-N, Publications Office of the European Union, Luxembourg (L), 2023a. doi:10.2760/922894. URL https://publications.jrc.ec.europa.eu/repository/handle/JRC128292.

Malkow, T. and Pilenga, A., 'EU harmonised testing protocols for high-temperature steam electrolysis', JRC Validated Methods, Reference Methods and Measurements Report KJ-03-22-290-EN-N, Publications Office of the European Union, Luxembourg (L), 2023b. doi:10.2760/7940. URL https://publications.jrc.ec.europa.eu/repository/handle/JRC129387.

Malkow, T., Pilenga, A. and Tsotridis, G., 'EU harmonised test procedure: electrochemical impedance spectroscopy for water electrolysis cells', JRC Validated Methods, Reference Methods and Measurements Report KJ-NA-29267-EN-N, European Commission, Luxembourg (Luxembourg), 2018a. doi:10.2760/8984. URL https://publications.jrc.ec.europa.eu/repository/handle/JRC107053.

Malkow, T., Pilenga, A., Tsotridis, G. and De Marco, G., 'EU harmonised polarisation curve test method for low-temperature water electrolysis', JRC Validated Methods, Reference Methods and Measurements Report KJ-NA-29182-EN-N, European Commission, Luxembourg (Luxembourg), 2018b. doi:10.2760/179509. URL https://publications.jrc.ec.europa.eu/repository/handle/JRC104045.

Boukamp, B. A., 'A nonlinear least squares fit procedure for analysis of immittance data of electrochemical systems', *Solid State Ionics*, Vol. 20, No 1, 1986, pp. 31–44. doi:10.1016/0167-2738(86)90031-7.

Boukamp, B. A., 'Electrochemical impedance spectroscopy in solid state ionics: recent advances', *Solid State Ionics*, Vol. 169, No 1, 2004, pp. 65–73. doi:10.1016/j.ssi.2003.07.002. Proceedings of the Annual Meeting of International Society of Electrochemistry.

Boukamp, B. A., 'Derivation of a distribution function of relaxation times for the (fractal) finite length Warburg', *Electrochimica Acta*, Vol. 252, 2017, pp. 154–163. doi:10.1016/j.electacta.2017.08.154.

Boukamp, B. A., 'Distribution (function) of relaxation times, successor to complex nonlinear least squares analysis of electrochemical impedance spectroscopy?', *Journal of Physics: Energy*, Vol. 2, No 4, 2020, p. 042001. doi:10.1088/2515-7655/aba9e0. URL https://dx.doi.org/10.1088/2515-7655/aba9e0.

Miller, H. A., Bouzek, K., Hnat, J., Loos, S., Bernäcker, C. I., Weißgärber, T., Röntzsch, L. and Meier-Haack, J., 'Green hydrogen from anion exchange membrane water electrolysis: a review of recent developments in critical materials and operating conditions', *Sustainable Energy Fuels*, Vol. 4, 2020, pp. 2114–2133. doi:10.1039/C9SE01240K.

Aricò, A. S., Carbone, A., Zignani, S., Monforte, G., Minutoli, M., Girolamo, M., Patti, A., Bottari, M., Jones, D., Cavaliere, S., Dupont, M., Rozière, J., Tal-Gutelmacher, E., Amel, A., Jones, S., Wright, J., van Dijk, N., Grahl-Madsen, L., Odgaard, M., Schutyser, W. and Knauf, S., 'Harmonised test protocols for assessing AEM electrolysis components, cells and stacks in a wide range of operating temperature and pressure', ANIONE Deliverable D2.1, Consiglio Nazionale delle Ricerche, Centre national de la recherche scientifique, Pocelltech, PV3 Technologies Ltd, IRD Fuel Cells A/S, Hydrogenics Europe NV, 24 June July 2020. URL https://anione.eu/wp-content/uploads/2020/07/D2.1-%E2%80%93-Harmonised-test-protocols.pdf.

Aricò, A. S., Briguglio, N., Siracusano, S., Baglio, V., Lister, R., Greenhalgh, D., Yeomans, K., Yu, H., van Dijk, N., Bonelli, R., Subinas, J., Dupont, M., Bourgogne, D., Merlo, L., Moukheiber, E., Tsotridis, G., Malkow, T. and Pilenga, A., 'Protocols for Stack and System Characterisation', ELECTROHYPEM Deliverable D2.2, Consiglio Nazionale delle Ricerche, ITM Power plc, TRE SpA TOZZI Renewable Energy, Centre national de la recherche scientifique, Solvay Speciality Polymers Italy SpA, Joint Research Centre, 09 August 2013. URL https://www.electrohypem.eu/data/D2-2_PROTOCOLS-FOR-STACK-AND-SYSTEM-CHARACTERISATION.pdf.

Aricò, A. S., Siracusano, S., Briguglio, N., Baglio, V., Van Dijk, N., Yildirim, H., Greenhalgh, D., Merlo, L., Tonella, S., Grahl-Madsen, L., Kielmann, G. and Steinigeweg, S., 'Protocols for characterisation of system components and electrolysis system assessment', HPEM2GAS Deliverable D2.1, Consiglio Nazionale delle Ricerche – Istituto di Tecnologie Avanzate per l'Energia "Nicola Giordano", ITM Power (Trading) Limited, Solvay speciality Polymers Italy SpA, IRD Fuel Cells A/S, Stadtwerke Emden GmbH, Hochschule Emden/Leer, 30 September 2016. URL `https://cordis.europa.eu/project/id/700008/results`.

Aricò, A. S., Siracusano, S., Briguglio, N., Trocino, S., Baglio, V., Greenhalgh, D., Hody, S., Oldani, C., Tonella, S., Infantino, M. and Grahl-Madsen, L., 'Harmonised test protocols for assessing system components, stack and balance of plant in a wide range of operating temperature and pressures', NEPTUNE Deliverable D2.1, Consiglio Nazionale delle Ricerche, ITM Power plc, Engie, Solvay Speciality Polymers Italy SpA, EWII Fuel Cells A/S, 12 July 2018. URL `https://cordis.europa.eu/project/id/779540/results`.

Siracusano, S., Trocino, S., Briguglio, N., Baglio, V. and Aricò, A. S., 'Electrochemical impedance spectroscopy as a diagnostic tool in polymer electrolyte membrane electrolysis', *materials*, Vol. 11, No 8, 2018, p. 1368. doi:10.3390/ma11081368.

ITM Power plc, 'Next Generation PEM Electrolyser under New Extremes', Project information, CORDIS, 2018. doi:10.3030/779540. URL `https://cordis.europa.eu/project/id/779540`.

Khan, M. A., Al-Attas, T., Roy, S., Rahman, M. M., Ghaffour, N., Thangadurai, V., Larter, S., Hu, J., Ajayan, P. M. and Kibria, M. G., 'Seawater electrolysis for hydrogen production: a solution looking for a problem?', *Energy & Environmental Science*, Vol. 14, 2021, pp. 4831–4839. doi:10.1039/D1EE00870F.

Malkow, K. T., 'One year time series of relative electric photovoltaic power dataset'. September 2023a. doi:10.5281/zenodo.8316473. URL `https://doi.org/10.5281/zenodo.8316473`.

Malkow, K. T., 'One year time series of relative electric (onshore and offshore) wind turbine power datasets'. September 2023b. doi:10.5281/zenodo.8316692. URL `https://doi.org/10.5281/zenodo.8316692`.

Malkow, T., 'Complex valued DRT explained – DRT estimation by deconvolution of EIS data'. 2021. doi:10.5281/zenodo.5718121. URL `https://doi.org/10.5281/zenodo.5718121`.

Marciuš, D., Kovač, A. and Firak, M., 'Electrochemical hydrogen compressor: Recent progress and challenges', *International Journal of Hydrogen Energy*, Vol. 47, No 57, 2022, pp. 24179–24193. doi:10.1016/j.ijhydene.2022.04.134.

Mayerhöfer, B., McLaughlin, D., Böhm, T., Hegelheimer, M., Seeberger, D. and Thiele, S., 'Bipolar membrane electrode assemblies for water electrolysis', *ACS Applied Energy Materials*, Vol. 3, No 10, 2020, pp. 9635–9644. doi:10.1021/acsaem.0c01127.

Parache, F., Schneider, H., Turpin, C., Richet, N., Debellemanière, O., Éric Bru, Thieu, A. T., Bertail, C. and Marot, C., 'Impact of power converter current ripple on the degradation of pem electrolyzer performances', *membranes*, Vol. 12, No 2, 2022, p. 109. doi:10.3390/membranes12020109.

Santoro, C., Lavacchi, A., Mustarelli, P., Di Noto, V., Elbaz, L., Dekel, D. R. and Jaouen, F., 'What is next in anion-exchange membrane water electrolyzers? bottlenecks, benefits, and future', *Chemistry-Sustainability-Energy-Materials*, Vol. 15, No 8, 2022, p. e202200027. doi:10.1002/cssc.202200027.

Schmucker, M., Gully, T. A., AlexeiSchmidt, Schmidt, B., Bromberger, K., Disch, J., Butschke, B., Burgenmeister, B., Sonnenberg, K., Riedel, S. and Krossing, I., 'Investigations toward a non-aqueous hybrid redox-flow battery with a manganese-based anolyte and catholyte', *Advanced Energy Materials*, Vol. 11, No 24, 2021, p. 2101261. doi:10.1002/aenm.202101261.

Strataki, E., 'Compliance test protocols and analytics', PRETZEL Deliverable D2.2, Centre for Research & Technology, Hellas, 31 August 2018. URL `https://cordis.europa.eu/project/id/779478/results`.

Szekeres, K. J., Vesztergom, S., Ujvári, M. and Láng, G. G., 'Methods for the determination of valid impedance spectra in non-stationary electrochemical systems: Concepts and techniques of practical importance', *ChemElectroChem*, Vol. 8, No 7, 2021, pp. 1233–1250. doi:10.1002/celc.202100093.

VERBUND Energy4Business GmbH, 'Hydrogen meeting FUTURE needs of low carbon manufacturing value chains', Project information, CORDIS, 2017. doi:10.3030/735503. URL `https://cordis.europa.eu/project/id/735503`.

List of Abbreviations and Acronyms

A/S Aktieselskab

AAEMEC alkaline anion exchange polymer membrane electrolysis cell

AAEMWE alkaline anion exchange polymer membrane water electrolyser

AAS atomic absorption spectrometry

AC alternating current

AC/DC AC-to-DC

AEC alkaline water electrolysis cell

AEL alkaline water electrolysis

AEM anion exchange polymer membrane

AEMEC anion exchange polymer membrane water electrolysis cell

AEMEL anion exchange membrane water electrolysis

AEMWE anion exchange polymer membrane water electrolyser

AG Aktiengesellschaft

AI artificial intelligence

ALT accelerated lifetime testing

AMD amendment

ANIONE Anion Exchange Membrane Electrolysis for Renewable Hydrogen Production on a Wide-Scale

ANPR automatic number plate recognition

ARMINES Association pour la Recherche et le Développement des Méthodes et Processus Industriels

AS Aktsiaselts

ASA Allmennaksjeselskap

ASR area-specific resistance

AST accelerated stress testing

ATEX Appareils destinés à être utilisés en atmosphères explosibles

AWE alkaline water electrolyser

AWI approved working item

biP bipolar plate

BoL beginning-of-life

BoP balance of plant

BoT beginning-of-test

BPMEL bipolar polymer membrane water electrolysis

BPMWE bipolar polymer membrane water electrolyser

BPMWEC bipolar polymer membrane water electrolysis cell

BV besloten vennootschap

BVBA Besloten Vennootschap met Beperkte Aansprakelijkheid

CAPEX capital expenditure

CC BY 4.0 Creative Commons Attribution 4.0 International

CEA Commissariat à l'énergie atomique et aux énergies alternatives

CERTH Centre for Research & Technology, Hellas

CFA continuous flow analysis

CGH$_2$ compressed gaseous hydrogen

CH Switzerland

CL catalyst layer

Clean H$_2$ JU Clean Hydrogen Joint Undertaking

CNLS complex non-linear least squares

CNR Consiglio Nazionale delle Ricerche

CNRS Centre national de la recherche scientifique

CORDIS Community Research and Development Information Service

CPE constant phase element

CRM critical raw materials

CSIC Consejo Superior de Investigaciones Científicas

CSV consolidated version

DAQ data acquisition

DC direct current

DC/DC DC-to-DC

DER distributed energy resources

DLR Deutsches Zentrum für Luft- und Raumfahrt e. V.

DoE design of experiment

doi digital object identifier

DRT distribution of uncorrelated relaxation times

EC European Commission

ECN Stichting Energieonderzoek Centrum Nederland

EDTA ethylenediaminetetraacetic acid

EEA European Economic Area

EEC equivalent electric circuit

EESS electrical energy storage system

EIS electrochemical impedance spectroscopy

ELECTROHYPEM Enhanced performance and cost-effective materials for long-term operation of PEM water electrolysers coupled to renewable power sources

EMC electromagnetic compatibility

EN English

ENSMP École nationale supérieure des mines de Paris

EoT end-of-test

ES energy storage

EU European Union

EUR European Union Report

ΕΠΕ Εταιρεία Περιορισμένης Ευθύνης

FBK Fondazione Bruno Kessler

FC fuel cell

FCH2JU Fuel Cells and Hydrogen second Joint Undertaking

FES flame emission spectrometry

FHa Fundación para el Desarrollo de las Tecnologías del Hidrógeno en Aragón

FIA flow injection analysis

FZJ Forschungszentrum Jülich GmbH

GC gas chromatography

GDL gas diffusion layer

GLP good laboratory practice

GmbH Gesellschaft mit beschränkter Haftung

GUM Guide to the expression of uncertainty in measurement

H2FUTURE Hydrogen meeting FUTURE needs of low carbon manufacturing value chains

H_2-to-I hydrogen-to-industry

H_2-to-M hydrogen-to-mobility

H_2-to-P hydrogen-to-power

HER hydrogen evolution reaction

HES Home Electronic System

HHV higher heating value

HPEM2GAS High Performance PEM Electrolyzer for Cost-effective Grid Balancing Applications

HPLC high-performance liquid chromatography

HPTLC high-performance thin-layer liquid chromatography

HRFB hybrid redox flow battery

IC ion chromatography

ICT Institut für Chemische Technologie

IEC International Electrotechnical Commission

IEEE Institute of Electrical and Electronics Engineers

IEM ion exchange membrane

IEV International Electrotechnical Vocabulary

ISBN international standard book number

ISO International Organization for Standardization

ISSN international standard serial number

JCGM Joint Committee for Guides in Metrology

JRC Joint Research Centre

KG Kommanditgesellschaft

KIST Korea Institute of Science and Technology

KPI key performance indicator

L Luxembourg

LC liquid chromatography

LH_2 liquid hydrogen

LHV lower heating value

LT low-temperature

LTWE low-temperature water electrolyser

2314 **LTWEL** low-temperature water electrolysis
2315 **LV** low-voltage
2316 **LVD** Low-Voltage Directive
2317 **ML** machine learning
2318 **MPL** micro-porous layer
2319 **MS** mass spectrometry
2320 **MV** medium-voltage
2321 **NC** national committee
2322 **NEPTUNE** Next Generation PEM Electrolyser under New Extremes
2323 **NEWELY** Next Generation Alkaline Membrane Water Electrolysers with Improved Components and Materials
2324 **NV** naamloze vennootschap
2325 **OCP** open circuit potential
2326 **OCV** open circuit voltage
2327 **OER** oxygen evolution reaction
2328 **OHS** occupational health and safety
2329 **OJ** Official Journal
2330 **P-to-C** power-to-chemical
2331 **P-to-F** power-to-fuel
2332 **P-to-G** power-to-gas
2333 **P-to-H$_2$** power-to-hydrogen
2334 **P-to-L** power-to-liquid
2335 **P-to-M** power-to-mobility
2336 **P-to-X** power-to-X
2337 **PAH** polycyclic aromatic hydrocarbons
2338 **PDF** portable document format
2339 **PED** Pressure Equipment Directive
2340 **PEM** proton exchange polymer membrane
2341 **PEMEC** proton exchange polymer membrane water electrolysis cell
2342 **PEMEL** proton exchange membrane water electrolysis
2343 **PEMWE** proton exchange polymer membrane water electrolyser
2344 **PFAS** perfluoroalkyl and polyfluoroalkyl substances
2345 **PFC** per- and polyfluorinated compounds
2346 **PFSA** perfluoro sulfonic acid
2347 **PGM** platinum-group metals
2348 **plc** public limited company
2349 **PoC** point of connection
2350 **PPS** polyphenylene sulfide
2351 **PRETZEL** Novel modular stack design for high pressure PEM water electrolyzer technology with wide operation
2352 range and reduced cost
2353 **PROMETH2** Cost-effective PROton Exchange MEmbrane WaTer Electrolyser for Efficient and Sustainable Power-
2354 to-H2 Technology
2355 **PTL** porous transport layer
2356 **PV** photovoltaic
2357 **R&D** research and development
2358 **R&I** research and innovation
2359 **REACH** registration, evaluation, authorisation and restriction of chemicals
2360 **REF** renewable energy factor
2361 **RES** renewable energy source
2362 **RFB** redox flow battery
2363 **RLV** redline version
2364 **RTO** research and technology organisation
2365 **RUL** remaining useful life
2366 **S.L.** Sociedad Limitada
2367 **SA** Société anonyme
2368 **SARL** Société à responsabilité limitée
2369 **SAS** Société par actions simplifiée
2370 **SATP** standard ambient temperature and pressure
2371 **SCADA** supervisory control and data acquisition
2372 **SHE** standard hydrogen electrode
2373 **SI** Système International d'Unités
2374 **SINTEF** Stiftelsen for industriell og teknisk forskning

2375 **SoA** state-of-the-art
2376 **SpA** Società per azioni
2377 **SRIA** strategic research and innovation agenda 2021–2027 of the Clean Hydrogen Partnership for Europe
2378 **TC** Technical Committee
2379 **TEU** Treaty on European Union
2380 **TFEU** Treaty on the Functioning of the European Union
2381 **TIP** test input parameter
2382 **TNO** Nederlandse Organisatie voor Toegepast Natuurwetenschappelijk Onderzoek
2383 **TOP** test output parameter
2384 **TR** Technical Report
2385 **TRL** technology readiness level
2386 **TS** Technical Specification
2387 **UG** Unternehmergesellschaft
2388 **URL** uniform resource locator
2389 **UV** ultraviolet
2390 **VRE** variable renewable energy
2391 **VSCHT** Vysoká Škola chemicko-technologická v Praze
2392 **WE** water electrolyser
2393 **WE system** water electrolyser system
2394 **WEC** water electrolysis cell
2395 **WEL** water electrolysis
2396 **WG** working group
2397 **WT** wind turbine

List of Symbols

Notation	Description
(aq)	subscript denoting aqueous phase
(ed)	subscript denoting electrode
(g)	subscript denoting gaseous phase
(l)	subscript denoting liquid phase
$|Y|$	modulus of electrical admittance
Z^*	modulus of electrical impedance
A_{act}	active electrode area
$a_{\mathrm{H_2O}}$	activity of liquid water
α	power exponent
α_{a}	anodic charge transfer coefficient
α_{a}	cathodic charge transfer coefficient
$\arg(Y)$	argument of electrical admittance
$\arg(Z)$	argument of electrical impedance
C	capacitance
C	carbon
$c_{\mathrm{H_2}}^0$	equilibrium hydrogen concentration
$c_{\mathrm{O_2}}^0$	equilibrium oxygen concentration
Ca	calcium
c_{Ca}	calcium concentration
c_{Cl}	chloride concentration
c_{Cu}	copper concentration
$C_{\mathrm{dl,a}}$	anodic double layer capacitance
$C_{\mathrm{dl,c}}$	cathodic double layer capacitance
c_{F}	fluoride concentration
c_{PAH}	PAH concentration
c_{PFAS}	PFAS concentration
c_{Fe}	iron concentration
$c_{\mathrm{H_2}}$	hydrogen concentration
c_{K}	potassium concentration
Cl$^-$	chloride
c_{Mg}	magnesium concentration
c_{Na}	sodium concentration
c_{Ni}	nickel concentration
Co	cobalt
CO$_2$	carbon dioxide
$c_{\mathrm{O_2}}$	oxygen concentration
CO$_3$	carbonate
c_{p}	specific heat capacity at constant pressure
$c_{\mathrm{p}}^{\mathrm{i}}$	specific heat capacity at constant pressure of fluid i
$c_{\mathrm{p}}^{\mathrm{j}}$	specific heat capacity at constant pressure of fluid j
Cu	copper
$c_{\mathrm{V}}^{\mathrm{j}}$	specific heat capacity at constant volume of fluid j
c_{Zn}	zinc concentration
d_{dl}	double layer length
$\Delta_{q_{\mathrm{m,H_2}}}^{k} E$	total change of energy per unit of mass of hydrogen
$\Delta_{q_{\mathrm{m,H_2}}}^{k} U$	total change of voltage per unit of hydrogen mass flow rate
$\Delta_{q_{\mathrm{V,H_2}}}^{k} U$	total change of energy per unit of volume of hydrogen
$\Delta_{q_{\mathrm{V,H_2}}}^{k} U$	total change of voltage per unit of hydrogen volumetric flow rate
$\Delta_{\mathrm{rel}}^{k} \eta_{\mathrm{HHV,e}}^{0}$	relative rate of change of energy efficiency based on HHV under SATP conditions of hydrogen
$\Delta_{\mathrm{rel}}^{k} \eta_{\mathrm{HHV,el}}^{0}$	relative rate of change of electrical efficiency based on HHV under SATP conditions of hydrogen
$\Delta_{\mathrm{rel}}^{k} \eta_{\mathrm{LHV,e}}^{0}$	relative rate of change of energy efficiency based on LHV under SATP conditions of hydrogen
$\Delta_{\mathrm{rel}}^{k} \eta_{\mathrm{LHV,el}}^{0}$	relative rate of change of electrical efficiency based on LHV under SATP conditions of hydrogen

69

Notation	Description
$\Delta_{\text{rel}}^{k} \text{MAE}\,\overline{U_{\text{cell}}}$	relative rate of change of mean absolute error average cell voltage
$\Delta_{\text{rel}}^{k} P$	relative rate of change of power
$\Delta_{\text{rel}}^{k} R_{\text{ASR}}$	relative rate of change of area-specific resistance
$\Delta_{\text{rel}}^{k} R_{\Omega}$	relative rate of change of ohmic resistance
$\Delta_{\text{rel}}^{k} \text{SD}\,\overline{U_{\text{cell}}}$	relative rate of change of standard deviation of average cell voltage
$\Delta_{\text{rel}}^{k} U$	relative rate of change of voltage
$\Delta_{\text{tot}}^{k} \eta_{\text{HHV, e}}^{0}$	total rate of change of energy efficiency based on HHV under SATP conditions of hydrogen
$\Delta_{\text{tot}}^{k} \eta_{\text{HHV, el}}^{0}$	total rate of change of electrical efficiency based on HHV under SATP conditions of hydrogen
$\Delta_{\text{tot}}^{k} \eta_{\text{LHV, e}}^{0}$	total rate of change of energy efficiency based on LHV under SATP conditions of hydrogen
$\Delta_{\text{tot}}^{k} \eta_{\text{LHV, el}}^{0}$	total rate of change of electrical efficiency based on LHV under SATP conditions of hydrogen
$\Delta_{\text{tot}}^{k} \text{MAE}\,\overline{U_{\text{cell}}}$	total rate of change of mean absolute error average cell voltage
$\Delta_{\text{tot}}^{k} P$	total rate of change of power
$\Delta_{\text{tot}}^{k} R_{\text{ASR}}$	total rate of change of area-specific resistance
$\Delta_{\text{tot}}^{k} R_{\Omega}$	total rate of change of ohmic resistance
$\Delta_{\text{tot}}^{k} \text{SD}\,\overline{U_{\text{cell}}}$	total rate of change of standard deviation of average cell voltage
$\Delta_{\text{tot}}^{k} U$	total rate of change of voltage
E	energy
e^-	electron
E_{compr}	pneumatic energy
E_{el}	electric energy
ε	absolute permittivity
E_{ramp}	ramp energy
U_{rev}	voltage under reversible (equilibrium) conditions
η	efficiency
η_{e}	energy efficiency
$\eta_{\text{HHV, e}}^{0}$	energy efficiency based on HHV under SATP conditions of hydrogen
η_{el}	electrical efficiency
$\eta_{\text{HHV, el}}^{0}$	electrical efficiency based on HHV under SATP conditions of hydrogen
$\eta_{\text{LHV, e}}^{0}$	energy efficiency based on LHV under SATP conditions of hydrogen
$\eta_{\text{LHV, el}}^{0}$	electrical efficiency based on LHV under SATP conditions of hydrogen
E_{th}	thermal energy
F	Faraday constant
F	fluorine
f	frequency
F⁻	fluoride
f_{compr}	compression factor
Fe	iron
f_{max}	maximum frequency
f_{min}	minimum frequency
γ^{j}	isentropic expansion factor of fluid j
H	hydrogen
H^+	proton
H_2	molecular hydrogen or dihydrogen
H_2O	steam
H_3O^+	hydrated proton
HHV_{H_2}	higher heating value of hydrogen
I	current
$\imath$	imaginary unit
$I_{0,\text{a}}$	anodic exchange current
$I_{0,\text{c}}$	cathodic exchange current
I_{a}	anodic current
I_{c}	cathodic current
I_{dc}	direct current

Notation	Description
I_in	input current
I_max	maximum current
$\mathfrak{Im}Z$	imaginary part of electrical impedance
I_nom	nominal (rated) current
Ir	iridium
IrO_x	iridium oxide
I_stack	stack current
J	current density
J_stack	stack current density
K	potassium
KCl	potassium chloride
KOH	potassium hydroxide
L	inductance
LHV_{H_2}	lower heating value of hydrogen
$MAE_{\overline{U_\text{cell}}}$	mean absolute error average cell voltage
Mg	magnesium
m_{H_2}	molar mass of hydrogen
Na	sodium
N_cell	number of cells
Ni	nickel
O	oxygen
O_2	molecular oxygen or dioxygen
OH^-	hydroxide ion
ω	angular frequency
P	power
p	pressure
p^0	standard ambient pressure
P_compr	power of compression
$P_\text{compr, in}$	input power of compression
P_el	electric power
$P_\text{el, d}$	electric power density
$P_\text{el, dc}$	DC power
$P_\text{el, d, stack}$	stack electric power density
$P_\text{el, in}$	input electric power
$P_\text{el, nom}$	nominal (rated) electric power
p_{H_2}	pressure of hydrogen
p_{H_2}	partial pressure of hydrogen
p_{H_2}	pressure of hydrogen
pH_lye	pH value of lye solution
pH_w	pH value of liquid water
p^j	pressure of fluid j
p_{O_2}	partial pressure of oxygen
P_stack	stack power
Pt	platinum
P_th	thermal power
$P_\text{th, in}$	input thermal power
q	flow rate
Q_C	non-ideal capacitance
Q_L	non-ideal inductance
q_m	mass flow rate
q_{m, H_2}	mass flow rate of hydrogen
q_m^i	mass flow rate of fluid i
q_n	molar flow rate
q_{n, H_2}	molar flow rate of hydrogen
q_n^j	molar flow rate of fluid j
q_{n, O_2}	molar flow rate of oxygen
$q_\text{n, out}$	product gas molar flow rate
$q_{\text{V}, H_2}^\text{theo}$	theoretical volumetric flow rate of hydrogen
q_{V, H_2}	volumetric flow rate of hydrogen

Notation	Description
R	resistance
R_0	zero-frequency resistance
R_{ASR}	area-specific resistance
$R_{\text{ct,a}}$	anodic charge transfer resistance
$R_{\text{ct,c}}$	cathodic charge transfer resistance
$\mathfrak{Re}Z$	real part of electrical impedance
R_{g}	universal gas constant
R_{hf}	high-frequency resistance
R_∞	infinite-frequency resistance
R_{lf}	low-frequency resistance
R_Ω	ohmic resistance
R_{pol}	polarisation resistance
RuO_y	ruthenium oxide
$\text{SD}_{\overline{U_{\text{cell}}}}$	standard deviation of average cell voltage
T	temperature
t	time
T^0	standard ambient temperature
t_0	time at beginning-of-test
$\tan(\mathfrak{Im}Z/\mathfrak{Re}Z)$	tangent of loss angle of electrical impedance
t_{compr}	duration of the compressed operation profile
T_{H_2}	temperature of hydrogen
T^{i}	temperature of fluid i
Ti	titanium
TiO_x	titanium oxide
t_{k}	time at interval k
$T_{\text{in}}^{\text{lye}}$	input temperature of lye
t_{origin}	duration of the original operation profile
t_{resp}	response time
T_{stack}	stack operating temperature
T_{w}	water temperature
T_{in}^{w}	input water temperature
U	voltage
u	standard uncertainty
U_{act}	activation polarisation voltage
u_{c}	combined standard uncertainty
U_{cell}	cell voltage
$\overline{U_{\text{cell}}}$	average cell voltage
$U_{\text{cell,n}}$	voltage of cell n
U_{conc}	concentration polarisation voltage
$U_{\text{cut-off}}$	cut-off voltage
U_{dc}	DC voltage
U_{in}	input voltage
U_{nom}	nominal (rated) voltage
U_{OCP}	open circuit potential
U_{OCV}	open circuit voltage
U_{rev}	reversible voltage
U_{stack}	stack voltage
U_{tn}	thermal-neutral voltage
U_{WEC}	water electrolysis cell voltage
V	volume
$V_{\text{m,H}_2}$	molar volume of hydrogen
X	reactance
$x_{\text{n,H}_2}$	molar concentration of hydrogen
$x_{\text{n,O}_2}$	molar concentration of oxygen
Y	electrical admittance
Y^*	complex conjugate of electrical admittance
Z	electrical impedance
z	number of electrons exchanged
Z^*	complex conjugate of electrical impedance

Notation	Description
$\bar{Z}$	average compressibility factor
$\bar{Z}^j$	average compressibility factor of fluid j
Zn	zinc
σ_{el}	electrical conductivity
$\sigma_{el,lye}$	electrical conductivity of lye solution
$\sigma_{el,w}$	electrical conductivity of liquid water
τ	time constant

List of Figures

List of Tables

Annex A   Test safety

In LTWE stacks, hazards arises from

- generated hydrogen and oxygen gases,

- use of alkaline solution,

- temperature,

- pressure and

- voltage.

During installation, commissioning, operation, quiescence, maintenance and decommissioning, the safety of persons requires due care and vigilance by all parties. Entities carrying out testing and chemical analysis should comply with the occupational health and safety (OHS) requirements of ISO 45001:2018 (ISO, 2018) and good laboratory practice (GLP). Tests on WE stacks shall be conducted in accordance with the applicable legislation, granted licenses and issued permits not to pose harm or unacceptable risk to humans, property and the environment.

IEC published guidance on safety of electrical equipment (IEC, 2021b, IEC, 2018) and alkaline ES devices (IEC, 1996). ISO published guidance on safety considerations for hydrogen systems (ISO, 2015) [44]. These guidances shall be observed when testing WE stacks [45]. IEC also published standards on FC safety (IEC, 2019a, IEC, 2020b), which shall be applied by analogy. Additionally, IEC published guidance on the classification of areas where explosive atmospheres can occur (IEC, 2014a, IEC, 2013, IEC, 2017a, IEC, 2020a), which shall also be observed.

In the European Economic Area (EEA) [46], the ATEX Directives 2014/34/EU (EP and Council, 2014b) and 94/9/EC (EP and Council, 1994) apply [47]. In addition, other EU legislation like the electromagnetic compatibility (EMC) Directive 2014/30/EU (EP and Council, 2014a) [48], the Low-Voltage Directive (LVD) 2014/35/EU (EP and Council, 2014c) [49], the general product safety Directive 2001/95/EC (EP and Council, 2001) [50], the machinery Directive 2006/42/EC (EP and Council, 2006) [51] and the Pressure Equipment Directive (PED) 2014/68/EU (EP and Council, 2014d) [52] apply. In principle, test items which do not conform to EU legislation shall not be used within the EEA.

---

[44]   WG 29 of TC 197 currently reviews ISO/TR 15916:2015.

[45]   WG 34 of TC 197 currently prepares the AWI entitled "ISO 22734-1 Hydrogen generators using water electrolysis – Industrial, commercial, and residential applications — Part 1: General requirements, test protocols and safety requirements".

[46]   It comprises the EU territory according to Article 52 of the Treaty on European Union (TEU) and Article 355 of the Treaty on the Functioning of the European Union (TFEU), Island, Norway and Liechtenstein. It also applies to Switzerland under a mutual recognition agreement and Türkiye under a customs union agreement with the EU.

[47]   The EC publishes guidance online at https://single-market-economy.ec.europa.eu/single-market/european-standards/harmonised-standards/equipment-explosive-atmospheres-atex_en.

[48]   The EC publishes guidance online at https://single-market-economy.ec.europa.eu/sectors/electrical-and-electronic-engineering-industries-eei/electromagnetic-compatibility-emc-directive_en.

[49]   The EC publishes guidance online at https://single-market-economy.ec.europa.eu/sectors/electrical-and-electronic-engineering-industries-eei/low-voltage-directive-lvd_en.

[50]   The EC publishes guidance online at https://single-market-economy.ec.europa.eu/single-market/european-standards/harmonised-standards/general-product-safety_en.

[51]   The EC publishes guidance online at https://single-market-economy.ec.europa.eu/sectors/mechanical-engineering/machinery_en.

[52]   The EC publishes guidance online at https://single-market-economy.ec.europa.eu/sectors/pressure-equipment-and-gas-appliances/pressure-equipment-sector/pressure-equipment-directive_en.

Annex B   Test report

B.1   General

The test report shall accurately, clearly and objectively present all relevant information to demonstrate the purpose(s) and objective(s) of the test. As a minimum requirement, the test report shall contain a title page (section B.2) and a summary (section B.3) with the measured or calculated TIPs and TOPs at least as mean values along with their (combined) standard uncertainties, whether absolute, relative or both. The test plan (section 6.6) forms part of the report. Calibration records or certificates of the measuring instruments shall be documented in the report and shall be available upon request.

B.2   Title page

The titlepage(s) shall present the following information:

(a) Report identification, *i. e.* report number (optional),

(b) Type of report (summary, detailed or full),

(c) A reference to this document,

(d) Author(s) of the report,

(e) Entity issuing the report with name and address,

(f) Date of the report,

(g) Person(s) conducting the test when different from the reporting author(s),

(h) Organisation conducting the test when different from report issuing entity,

(i) Date and time per test run,

(j) Location per test run when different from the address of the report issuing entity,

(k) Descriptive name per test and

(l) Identification (model name, serial number, type and specification) of the WE stack tested (including manufacturer).

The titlepage(s) may be followed by a contents page before the summary report.

B.3   Summary

The summary shall include the following information:

(i) test purpose(s) and objective(s),

(ii) description of the test(s) with sufficient information on the test conduct and measurement set-up with test methods, measurement techniques (section 6.2) and test conditions (section 6.3),

(iii) all relevant test parameters, namely TIPs and TOPs with uncertainties (section 7) and

(iv) conclusion(s) with remark(s) and/or observation(s) as appropriate. Unless a full test report is to be issued where all test results shall also be presented graphically (section 7) and properly discussed, a brief discussion with graphical presentation of the main test results (section 7) supporting the conclusion(s) may be appended to the report.

Science for policy

The Joint Research Centre (JRC) provides independent, evidence-based knowledge and science, supporting EU policies to positively impact society

EU Science Hub
joint-research-centre.ec.europa.eu

@EU_ScienceHub

EU Science Hub – Joint Research Centre

EU Science, Research and Innovation

EU Science Hub

@eu_science

Publications Office
of the European Union